Marine and Petroleum Geology 156 (2023) 106442

Contents lists available at ScienceDirect

Marine and Petroleum Geology

journal homepage: www.elsevier.com/locate/marpetgeo

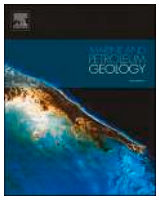

Paleostress analysis and rift kinematics of the petroliferous Barmer rift basin, western Rajasthan, India

Swagato Dasgupta [a], Soumyajit Mukherjee [b,*], Naimisha Vanik [c], Rima Chatterjee [a,1], Sanjit Kumar Pal [a]

[a] Department of Applied Geophysics, Indian Institute of Technology (ISM), Dhanbad, 826004, Jharkhand, India
[b] Department of Earth Sciences, Indian Institute of Technology Bombay, Mumbai, 400 076, Maharashtra, India
[c] Manipal Centre for Natural Sciences, Manipal Academy of Higher Education, Manipal, 576104, Karnataka, India

ARTICLE INFO

Keywords:
Kinematic analysis
Oblique rift
Fault slip
Paleostress regime
Structural inheritance
Neotectonics
Earthquake focal mechanism

ABSTRACT

The NW-trending Barmer rift in western Rajasthan is one of the major petroliferous Indian basins. The basin rifted twice: *(i)* NW – SE extension in Early Cretaceous, and *(ii)* NE – SW extension during Late Maastrichtian to Early Paleogene. We performed structural fieldwork mainly along the rift margins to decipher the rift kinematics through geologic time. We collected ~500 fault-slip data from limited outcrops along the basin's western and eastern margins. Paleostress analysis was performed for the first time in this basin using Win_Tensor, T-Tecto and FaultKin software. The outcome of this analyses shows that a strike-slip stress regime was prevalent in the western rift margin whereas the eastern margin experienced extension to transtension. Four paleostress regimes, D_{Δ}, D_{α}, D_{Φ}, and D_{β}, were identified by inverting the fault-slip data. The two separate extensional regimes, during the Early Cretaceous and in the Late Maastrichtian to Early Paleogene, are confirmed. These are D_{α} (NW – SE extension) and D_{β} (NE – SW extension). The analysis also presents two strike-slip regimes with varying maximum horizontal stress (SHMax) orientation, viz. D_{Δ} and D_{Φ}. Exact age correlation for these strike-slip regimes remains indeterminate. However, we deduced D_{Δ} and D_{Φ} were associated with the first extensional phase (D_{α}) during Early Cretaceous linked to India – Madagascar oblique separation. The Barmer rift extended obliquely guided by pre-existing structures. Remote sensing image analysis indicates that part of the western margin is neotectonically active as inferred from the drainage morphometry. The stress inversion analysis of earthquake focal mechanism data depicts a strike-slip transpressive regime prevailing at present in the NW India along with ~ N-trending SHMax. This is mainly responsible for the neotectonic activities in the basin. We documented several fault gouge zones along moderately-dipping faults in the Cretaceous outcrops at the eastern margin. The lower the fault dips, the thicker the gouge zones associated with the faults. Such thick fault gouge of around 100 cm or more may act as a structural fault bound trap for Cretaceous reservoirs at depth. **(Words: 324)**.

1. Introduction

1.1. Background

Rifted continental margins and intra-continental rift basins have always been a focus of academic and petroleum industrial research to address the nature and significance of lithospheric stretching (e.g. Morgan and Baker, 1983; Gibbs, 1984; Brun, 1999; Merle, 2011; Nemčok, 2016; Cemen, 2023). Rift-basins can either be active: crustal thinning linked to mantle upwelling (e.g., Sengör and Burke, 1978; Condie, 1982; Turcotte and Emerman, 1983; Buck, 1986, 1991; Merle, 2011; Wright et al. 2016), or passive: related to far-field stresses (e.g., Merle, 2011; Koptev et al. 2015). Passive rifting-related lithospheric thinning in extensional stress regimes can result in basaltic magmatism manifested as dykes and sills (e.g., Parsons and Thompson, 1993; Gudmundsson et al., 2008; Koptev et al. 2015; Tibaldi et al. 2020).

Continental rift opening is not always orthogonal; rather in most cases it is oblique (Withjack and Jamison, 1986; Corti, 2008; Brune et al., 2018). Oblique rifting has certain characteristics viz., *(i)* en-echelon faults with relay ramps, which trend at an angle to the rift

* Corresponding author.
E-mail addresses: smukherjee@iitb.ac.in, soumyajitm@gmail.com (S. Mukherjee).
[1] Deceased.

https://doi.org/10.1016/j.marpetgeo.2023.106442
Received 21 December 2022; Received in revised form 20 July 2023; Accepted 31 July 2023
Available online 14 August 2023

axis, and *(ii)* strike-slip associated with transtension/transpression localizes strain and develops pull - apart basins (Fossen and Rotevatn, 2016; Brune et al., 2018; Farangitakis et al., 2021; Dasgupta et al., 2022). Heterogeneity in crustal stress, rheology and pre-existing structurally weak planes promote oblique rifting and slip reorients along faults (Withjack and Jamison, 1986; Schumacher, 2002; Morley et al., 2007; Morley, 2010, 2016; Corti et al., 2013; Philippon et al., 2014; Brune et al., 2018).

Structural inheritance controls rift fault propagation guided by accommodation zones/transfer zones/relay ramps (Gawthorpe and Hurst, 1993; Morley, 1999; Fossen, 2013; Misra and Mukherjee, 2015; Dasgupta, 2019). Such fault planes linked to pre-existing structures do not necessarily obey Andersonian stress regimes, and thus are often identified as non-Andersonian faults (Anderson, 1905; Brune and Autin, 2013; Bonini et al., 2016).

The Barmer intra – cratonic continental rift basin is one of the major sedimentary basins in western Rajasthan, India (Fig. 1). The other two sedimentary basins in western Rajasthan are the Jaisalmer and the Bikaner – Nagaur basins situated NW and NE of Barmer basin, respectively (Dasgupta 1975, 2021; Pandey and Bhadu 2010; Arora et al. 2011; Singh and Tewari 2011; Krishna, 2017; Biswas et al., 2022a). These basins evolved since the Mesozoic having mostly the Malani Igneous Suite (MIS) of Late Proterozoic and Cambrian rocks as the basement (Dasgupta 1975; Misra et al. 1993; Pandit et al., 1999; Biswas 2012; Dwivedi 2016; Dasgupta and Mukherjee, 2017).

The Barmer basin is ~200 km long and ~50 km wide NW-trending rift, which is separated from the northern Jaisalmer basin by a NE-trending structural high-the Devikot-Fatehgarh/Barmer-Devikot-Nachana ridge (Fig. 1; Misra et al., 1993; Compton, 2009; Dolson et al., 2015). A gravity low exists along the rift basin, whereas the rift shoulders show gravity highs (Fig. 1a; Dasgupta and Mukherjee, 2016). The basin deepens towards the S/SE with a sediment thickness of > 6 km. The Devikot – Fatehgarh ridge/Fatehgarh fault trend shows a moderate gravity high, separating the Barmer basin from the gravity low of the Jaisalmer basin (Fig. 1a; Mishra, 2011; Dasgupta and Mukherjee, 2016, 2017). Similar trends are also observed form the residual magnetic anomaly maps (Mishra, 2011). Gravity modelling studies in the Barmer basin depict crustal thinning, presence of magmatic intrusion and mantle upwelling at ~27–28 km depth below the basin. This indicates reactivation during early phase of Deccan volcanism (Mishra, 2011; 2022d; Burley et al., 2023).

The Barmer basin has limited outcrop exposures (Fig. 1a–c). The basin, along with its eastern and western margins, is largely covered by the (longitudinal) sand dunes of the Thar Desert (Dolson et al., 2015; Dasgupta and Mukherjee, 2017). In the eastern margin, Lower Cretaceous Ghaggar-Hakra Formation crops out near the Sarnoo/Sarnu village. Along the western margin, isolated outcrops of Late Proterozoic Malani Igneous Suite (MIS) occur around Barmer town, Dhorimana and north of Gehoon/Gehu village (Pandit et al., 1999; Torsvik et al., 2001; Sharma, 2007; Dasgupta and Mukherjee, 2017). The Paleogene succession from Paleocene Fatehgarh Formation to Eocene Dharvi – Dungar and Akli Formation crops out at N along the uplifted NE trending Devikot-Fatehgarh ridge (Compton 2009; Dasgupta and Mukherjee, 2017). The Bariyada Member of Lower Paleocene is a typical volcanic ash deposit characteristic of K/T impact debris (Sisodia et al., 2005). The seismic-derived fault map depicts transfer zones in the northern part of

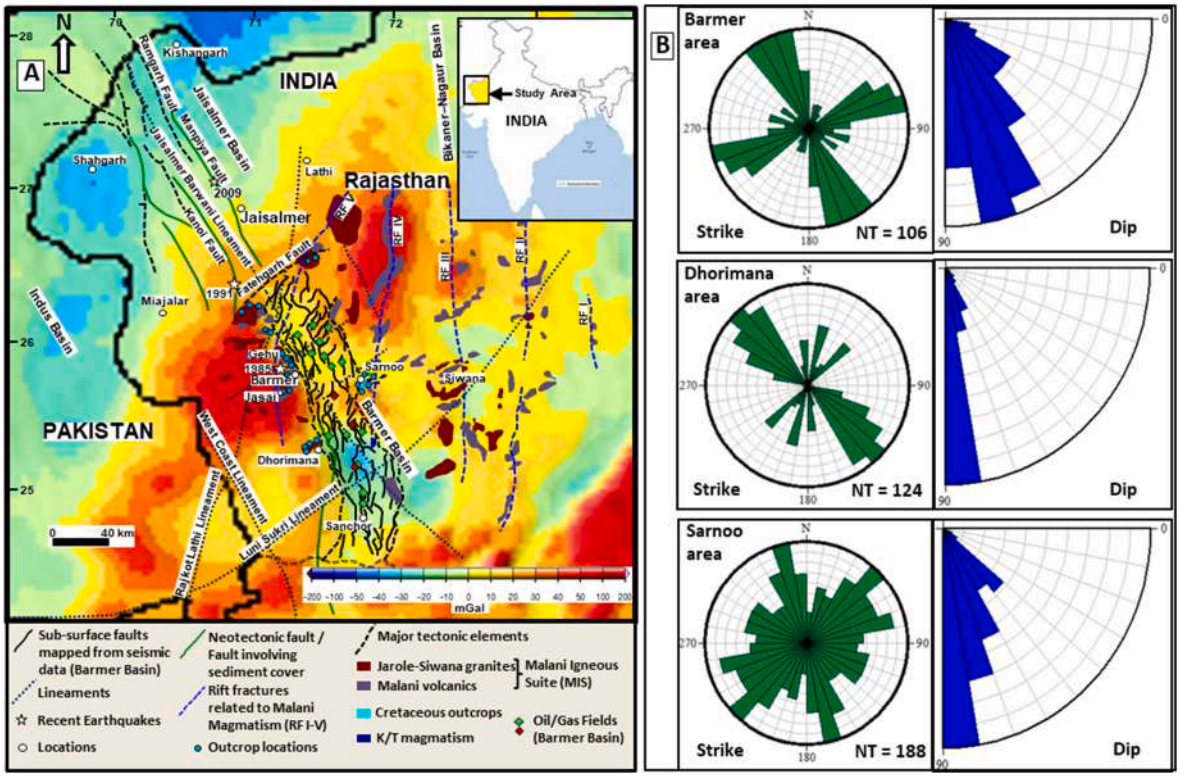

Fig. 1. **(a)** Geological map of western Rajasthan depicting the Barmer basin along with different fault trend including sub-surface faults from seismic data interpretation, neo-tectonic and other lineaments, rift fracture trend of Malani Igneous Suite (MIS) and other major tectonic elements. This has been overlaid on free air gravity map of western India and Pakistan (Compiled and modified from Dasgupta et al., 2000; Dolson et al. 2015; Kothari et al., 2015; Dasgupta and Mukherjee, 2017, URL-3). The field outcrop locations are marked as blue dots along the periphery of the Barmer basin. The major oil and gas field locations are marked within the basin. RF: Rift Fractures of MIS. Recent earthquakes locations which occurred in 1985 and 1991 in western rift shoulder area are plotted on the map (coordinates obtained from website: www.earthquaketract.com). **(b)** Rose diagrams of the strike and dip of fault slip data taken for this analysis. Out of 418 selected dataset; *(i)* 106 fault data are from Barmer and its surroundings, *(ii)* 124 fault data are from Dhorimana hill area, and *(iii)* 188 fault data are from Sarnoo hill area. **(c)** Tectono-stratigraphic chart of Barmer basin (Compiled and modified from Dolson et al. 2015; Kothari et al., 2015; Dasgupta and Mukherjee, 2017), 1-Main Central Thrust, 2-Main Boundary Thrust, 3-Himalayan Frontal Thrust.

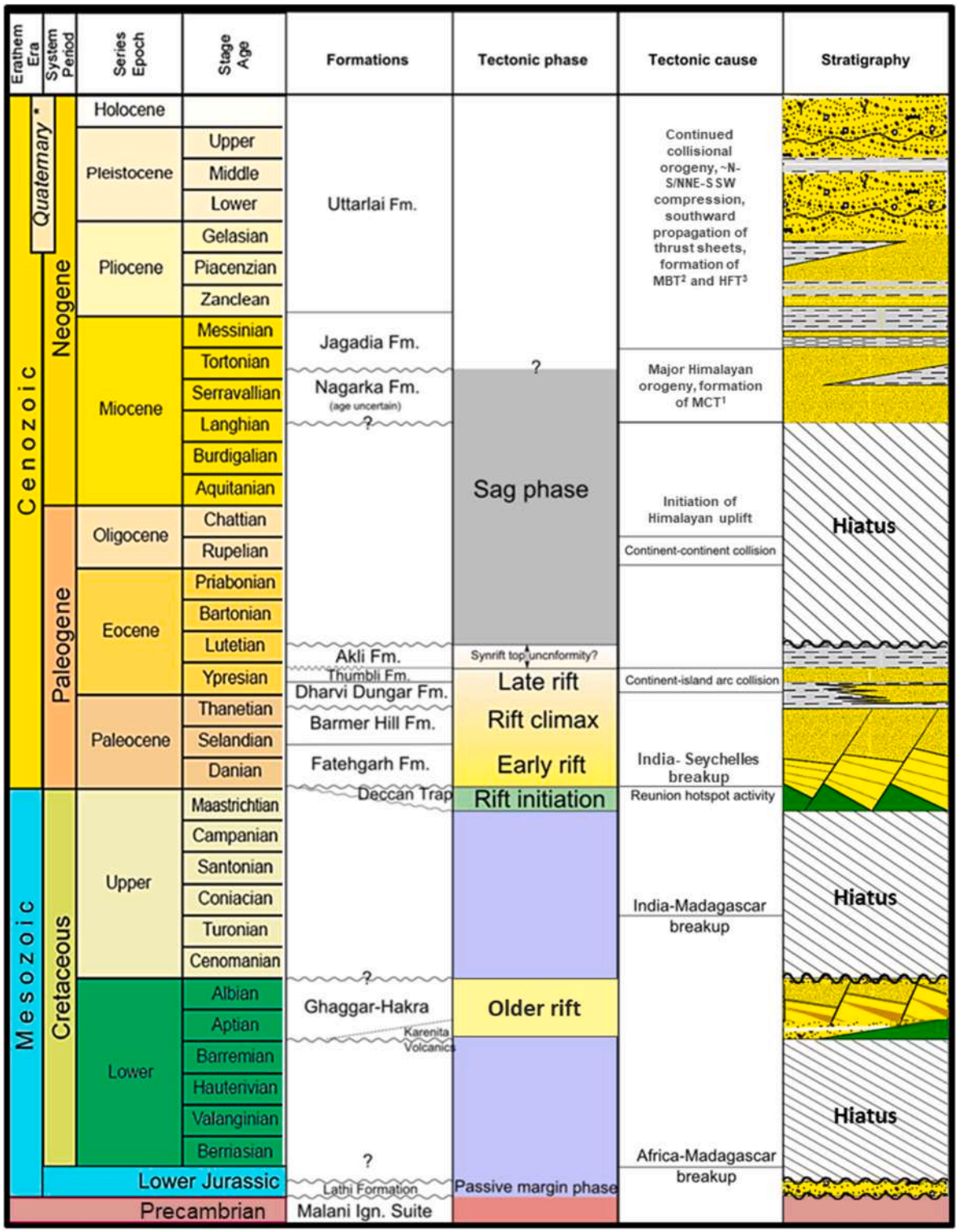

Fig. 1. (*continued*).

the basin (Bladon et al., 2015). Meso-scale transfer zones are also identified from outcrops in the northern boundary along the Fatehgarh fault trend (Dasgupta and Mukherjee, 2017, 2019). The eastern basin margin consists of steep normal faults whereas the western margin uplifted isostatically (Bladon et al., 2014, 2015; Dolson et al., 2015; Dasgupta and Mukherjee, 2017).

The tectonics of the western Rajasthan sedimentary basins, including the Barmer basin, initiated since Rodinia fragmentation in the Late Proterozoic (~751–771 Ma) through anorogenic rifting in the NW portion of the proto Indian plate together with Madagascar and Seychelles (Torsvik et al., 2001; Sharma 2005; Wang et al., 2023). This rifting resulted in bimodal volcanism exceeding 50,000 km^2 extent i.e., the Malani igneous province/MIS/Malani rhyolites (Pareek, 1981; Chawade and Chandrasekaran, 1996; Pandit et al., 1999; Bhushan, 2000; Roy, 2001; Torsvik et al., 2001; Sharma, 2005; Gregory et al., 2009; Sisodia, 2011). The MIS is associated with ~ N-NW linear fracture

trends with volcanic flows, indicating a lineament-controlled magmatism related to intra-cratonic rift zones (Fig. 1a; Sharma, 2005, 2007). A phase of the bimodal volcanism comprises of dolerite and aplite dykes trending ~ NW to NNE (Pooranchandra Rao et al., 2003; Sharma 2005). Intra-cratonic rift related sedimentation occurred during Late Proterozoic to Cambrian in the Punjab rift and the Bikaner – Nagaur basin (Al-Husseini 2000; Mandal et al., 2022). The Bikaner – Nagaur basin is located ~200–300 km NE of Barmer basin. Few small inliers such as the Birmania basin, of Late Proterozoic to Cambrian age, are found in the western Rajasthan, ~100–120 km NW of Barmer (Maheshwari et al., 2002; Hughes et al., 2015). No Late Proterozoic – Cambrian sedimentary unit has been documented till date in the Barmer basin, in rift margin outcrops or in sub-surface stratigraphy (Dasgupta 1975; Dolson et al., 2015; Bladon et al., 2015; Dasgupta and Mukherjee, 2017). However, the older pre-existing rift fractures/weak zones act as sweet spots for the subsequent rifting events that occurred in this area during Mesozoic and Paleogene time.

Rift-related extension in the Barmer basin occurred twice – NW extension in Mesozoic linked to Madagascar separation and NE extension in Paleogene linked to Seychelles micro-continent segregation (Bladon et al., 2015; Dasgupta and Mukherjee, 2017). Pre-existing rift faults and basement fractures of MIS guided the second and the main extension phase during the Paleogene time (Bladon et al., 2015; Dasgupta and Mukherjee, 2017). Thus, it can be well stated that the Barmer rift basin tectonic evolution is complex and structural inheritance played a major role in the basin.

The basin consists of major hydrocarbon producing fields and is termed as a category 1 hydrocarbon producing basin by the Directorate General of Hydrocarbons (DGH), India (Dwivedi 2016, URL-1). Note that category 1, as per DGH, indicates that the basin has proven hydrocarbon presence and is under production. Hydrocarbon exploration, development and production activities are continuing in this basin for last few decades (Dwivedi 2016, URL-1).

Besides hydrocarbon exploration and production, the basin has prospectivity for exploration of rare earth element (REE) in the eastern rift shoulder areas near Sarnoo and Siwana (Fig. 1a; Chandrasekharam et al., 2014; Singh et al., 2014; Aranha et al., 2022; Kumar et al., 2022c; Sinha, 2022). In recent times shallow aquifers of the Barmer basin has been studied which inferred that there is a change in flow dynamics and hydro-chemical equilibrium within the aquifers (Kumar, 2023). Also, the basin is being evaluated for deep geologic repository (in granite and bentonite units) to dispose radioactive waste (Kumar et al., 2022b, 2022d; Kale and Ravi, 2022, 2023; Srivastava et al., 2022). The Barmer basin has higher than average geothermal gradient of ~42–43 °C km^{-1} in north - central part with a further elevated gradient of ~70 °C km^{-1} in northern portion around sub-crop basement high near Uttarlai (Naidu et al., 2017). Present day average heat flow varies between ~40 and 70 m W m^{-2} (Kapoor and Kapoor, 2016; Naidu et al., 2017). Due to this reason the basin has been considered to harness geothermal energy along with hydrocarbon production (URL-2).

Paleostress analyses have been undertaken in the past few decades to decipher the tectonic stress regimes in an area (e.g., Carey and Brunier 1974; Angelier and Mechler, 1977; Armijo and Cisternas, 1978; Etchecopar et al. 1981; Angelier et al. 1982; Angelier, 1984; Angelier et al. 1985; Delvaux et al., 1997; Zain Eldeen et al., 2002; Glorie et al., 2012; Assie et al., 2022; Shaikh et al., 2020; Biswas et al., 2022; Shan et al., 2023). Application of paleostress analyses in sedimentary basins helps in interpreting the direction of stress tensors and variation in stress regimes (Gartrell and Lisk, 2005; Åse et al., 2022; Ping et al., 2022). This may play an important role in understanding the petroleum geology of a basin mainly related to tectonic evolution, hydrocarbon migration direction, fault re-activation and entrapment potentiality. Few examples of paleostress studies from the hydrocarbon-bearing sedimentary basins are: in Oslo graben and northern Bømlo islands, Norway (Sippel et al., 2010; Scheiber and Viola, 2018), paleostress analyses from faults derived from 3D seismic data in Cooper–Eromanga basin and Timor Sea area, Australia (Gartrell and Lisk, 2005; Kulikowski and Amrouch, 2018), from Sichuan basin, China (Ju et al., 2017) and from Central basin of Spitsbergen, northern Norway to infer the subsidence history (Kleinspehn et al., 1989).

1.2. Purpose of this study

The Barmer basin is one of the major hydrocarbon-producing basins of India with >4 billion barrels of in-place oil and considerable amount of gas reserves (Farrimond et al. 2015; Kothari et al. 2015). The majority of the producing hydrocarbon fields of Barmer basin e.g., Mangala, Aishwarya/Aishwariya, Raageshwari, Saraswati, Bhagyam, D-P, and Kameshwari, are from the Early Paleogene successions (Fig. 1a; Compton, 2009; Kothari et al., 2015; Dolson et al., 2015; Saha et al., 2021). Hydrocarbon potential in Cretaceous succession has also been evaluated.

The asymmetric Barmer rift basin consists of half-grabens (Dolson et al., 2015). The sub-crop sediment thickness is non-uniform; the SE part is having much greater sedimentary column than that of W and N portions of the basin (Dolson et al., 2015). The Mesozoic stratigraphic unit is located in the E and SE part of the basin whereas the Paleogene – Neogene sedimentary succession is distributed throughout the basin (Compton, 2009; Bladon et al., 2015; Dolson et al., 2015; Dasgupta and Mukherjee, 2017). The older depocenters are situated alongside the NE-trending faults, whereas the main rift phase depocenters are adjacent to the NW-trending eastern margin rift-parallel faults, as has been observed from the central to eastern part of the basin (Bladon et al., 2015). This indicates that there is variation in subsidence with geologic time, which indirectly can imply that the stress regime varied temporally during the two rifting events that affected the basin. Also, stress regimes seem to vary spatially across the basin.

Hence, in order to understand the temporal and spatial discrepancy of stress field in the Barmer basin, structural fault-slip data were collected from the outcrops of the eastern and western rift margins.

The objectives of this study are to *(i)* reconstruct the paleostress tensors based on structural fault-slip data from field by using standard techniques, *(ii)* determine the major stress regimes acting along the Barmer rift margins, and *(iii)* investigate the inherent relation between continental rift evolutions through geologic time along with variation in stress regime. Recent tectonic changes in the basin are also discussed.

2. Geology

2.1. Stratigraphy

Barmer is a typical continental rift basin with an Early Jurassic to Late Miocene stratigraphic succession along with major hiatuses at Jurassic to Early Cretaceous, Mid- Late Cretaceous, and Late Eocene to Mid-Miocene (Supplementary Table 1; Fig. 1c; Dasgupta, 1975; Beaumont et al. 2015; Dolson et al., 2015; Kothari et al., 2015, Fig. 2 in Dasgupta and Mukherjee, 2017; Beaumont et al. 2019; Chakraborty et al., 2019). Besides the Paleogene hydrocarbon reservoirs, the lacustrine Paleocene - Eocene units consisting of carbonaceous shale and lignite deposits are the prominent source kitchen for the petroliferous Barmer basin (Dolson et al., 2015; Farrimond et al., 2015; Singh et al., 2016; Choudhury and Banerjee, 2022; Kar et al., 2022; Singh et al., 2022; Kumar et al., 2023).

2.2. Tectonics

The Barmer basin sits on the MIS basement rocks. During Mesozoic and Early Paleogene, the basin experienced two non-coaxial extensions- *(i)* NW-SE tension during Early Cretaceous associated with the Ghaggar-Hakra deposition, and *(ii)* NE-SW tension during Maastrichtian to Early Paleogene accompanying with the main rift phase (Bladon et al. 2014, 2015). These are linked to two tectonic episodes viz., the oblique

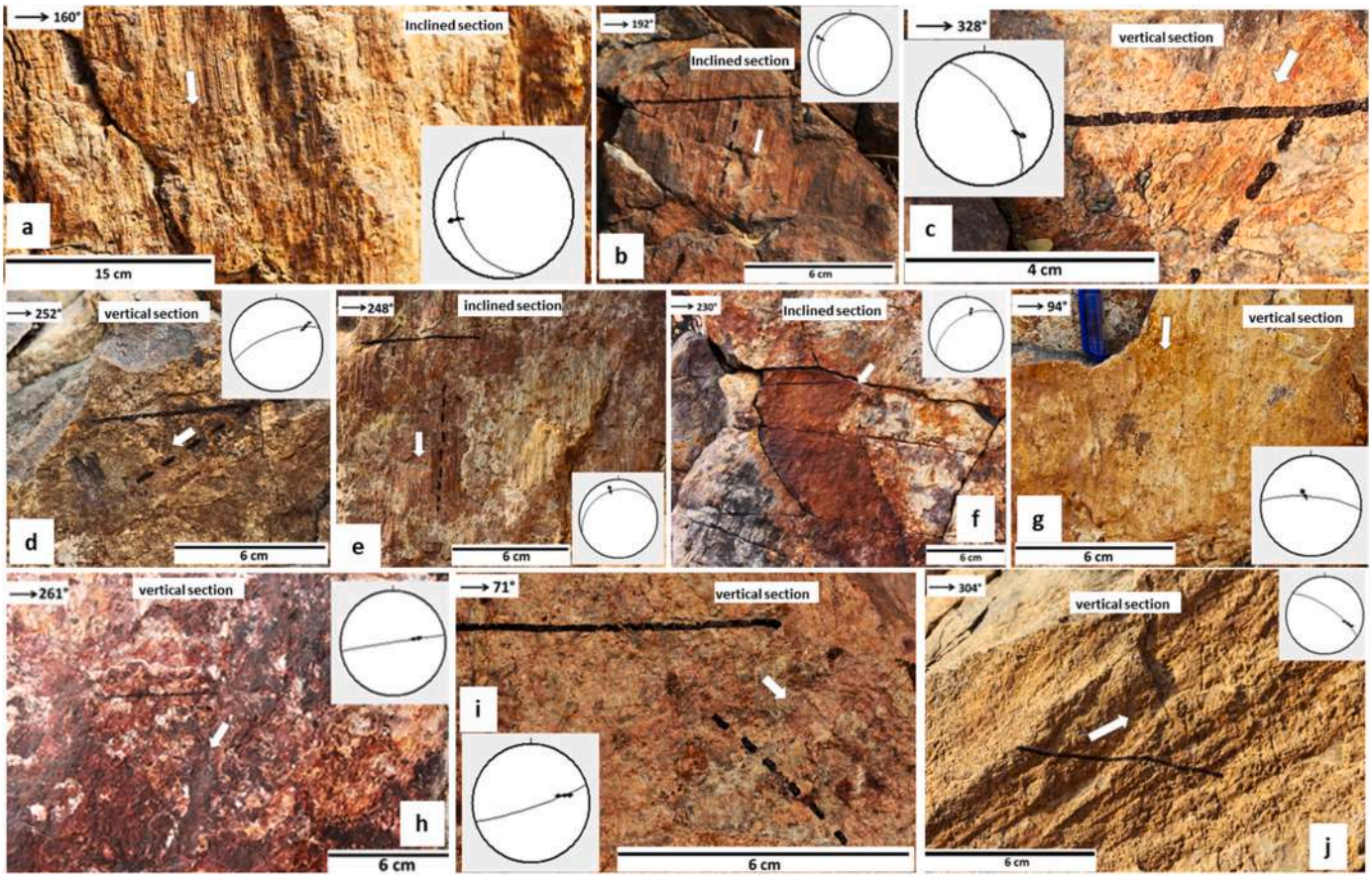

Fig. 2. (a)–(j) Fault slip slickensides collected from Barmer hill area and Gehoon. (**a**) Slickenside feature (crescentic marker) observed on inclined fault plane (strike: 160°, dip 34°, dip direction 250°, rake −96°) missing block moved down. Location: NW of Ratanada temple in Barmer hill area, Barmer town (e.g. from stress tensor 1). (**b**) Slickenside feature (crescentic marker) observed on inclined fault plane (strike: 192°, dip 24°, dip direction 282°, rake −106°) missing block moved down. Location: NW of Ratanada temple in Barmer hill area, Barmer town (e.g. from stress tensor 1). (**c**) Slickenside feature (crescentic marker) observed on inclined fault plane (strike: 148°, dip 63°, dip direction 58°, rake −124°) missing block moved down (left). Location: NW of Ratanada temple in Barmer hill area, Barmer town (e.g. from stress tensor 1). (**d**) Slickenside feature (step and crescentic marker) observed on near vertical fault plane (strike: 248°, dip 71°, dip direction 338°, rake −152°) missing block moved bottom-left. Quartz mineralization seen on the fault surface. Location: NW of Ratanada temple in Barmer hill area, Barmer town (e.g. from stress tensor 2). (**e**) Slickenside feature (crescentic marker) observed on inclined fault plane (strike: 248°, dip 28°, dip direction 338°, rake −95°) missing block moved down. Calcite mineralization is seen on the fault surface associated with slickensides. Location: N of Ratanada temple in Barmer hill area, Barmer town (e.g. from stress tensor 3). (**f**) Slickenside feature (crescentic marker) observed on inclined fault plane (strike: 234°, dip 53°, dip direction 324°, rake −124°) missing block moved bottom left. Quartz mineralization seen on the fault surface associated with slickensides. Location: N of Ratanada temple in Barmer hill area, Barmer town (e.g. from stress tensor 3). **(g)** Slickenside feature (crescentic marker) observed on near vertical fault plane (strike: 275°, dip 75°, dip direction 5°, rake −80°) missing block moved down. Calcite and possibly kaolinite mineralization is seen on the fault surface associated with slickensides. Location: N of Ratanada temple in Barmer hill area, Barmer town (e.g. from stress tensor 4). **(h)** Slickenside feature (step and crescentic marker) observed on vertical fault plane (strike: 261°, dip 89°, dip direction 351°, rake −123°) missing block moved bottom left. Calcite mineralization is seen on the fault surface. Location: Barmer hill area, W of Barmer town (e.g. from stress tensor 4). **(i)** Slickenside feature (step) observed on vertical fault plane (strike: 72°, dip 84°, dip direction 162°, rake −41°) missing block moved bottom right. Quartz mineralization is seen on the fault surface. Location: Barmer hill area, W of Barmer town (e.g. from stress tensor 5). **(j)** Slickenside feature (crescentic marker) observed on near vertical fault plane (strike: 304°, dip 72°, dip direction 34°, rake 38°) missing block moved top right. Location: Roadside exposure towards Gehoon village (e.g. from stress tensor 6).

separation of the Madagascar from India and break-up of Seychelles micro-continent from the Indian plate, respectively (Collier et al., 2008; Mishra, 2011; Torsvik et al., 2013; Bladon et al., 2015; Dasgupta and Mukherjee, 2017). The second and the main rifting phase continued further south in the Cambay basin. Few igneous intrusions occur in the Ghaggar-Hakra Formation in the Sarnoo hill area, which was plausibly fed by precursor of Deccan volcanism and/or Early Aptian Karentia volcanics (Basu et al., 1993; Roy, 2003; Sharma, 2007; Bladon et al., 2015; Vijayan et al., 2015). In Neogene to recent, during the Himalayan orogeny, the basin experienced ~ NNW compression, at shallow (0–10 km) crustal depth. This is recognized from the following field observations:*(i)* uplifted Devikot-Fatehgarh ridge/Fatehgarh Fault associated with fault scarps, and *(ii)* lineament-controlled geomorphic signatures and neotectonic landscape in the eastern and western rift margins (Compton 2009; van Hinsbergenet al., 2012; Kelly et al., 2014; Dasgupta and Mukherjee, 2019; Biswas et al., 2022b).

The present-day maximum horizontal stress (SHMax) orientation in western Indian terrain is along N to NNE with some ~ NNW components (Chatterjee et al., 2013, 2017; Heidbach et al. 2016; Dash et al., 2017; Sen et al., 2019). Recent structural field studies conducted in the basin (as in Dasgupta and Mukherjee, 2017) depicts the key findings: *(i)* faults in the western margin trends mostly NW and NE-trending faults are at places displaced by the NW faults; *(ii)* in the Sarnoo area, NE and NW trending faults co-exists, major displacements are observed along the NE and ~ E-trending faults; *(iii)* the MIS basement rock consists of NW-trending faults parallel to dykes at places, and *(iv)* structural inheritance of older MIS basement fractures occurred during Barmer rifting.

3. Methodology

Structural fieldwork has been carried out to identify brittle shear features and fracture planes from the field exposures. Fault-slip data were acquired from the western and eastern margin of the rift basin (Figs. 1–7) and detail regional structural and paleostress was analysed in order to understand the rift kinematics. Furthermore, some neo-tectonic outcrop features (vertically cut gullies, fault scarp) were documented from the western and northern margin of the basin. A remote sensing analysis, using Shuttle Radar Topography Mission data (SRTM) 30 m Digital Elevation Model (DEM) and Google Earth Pro imagery, was carried out using Arc GIS 10.4 (2016). This was executed to understand the geomorphic changes due to neotectonic activities at the western basin margin near the Barmer town. Also, to understand the present-day stress regime in the W India, stress inversion analysis has been done using earthquake focal mechanism data (source: www.usgs.gov/programs/earthquake-hazards). Supplementary Fig. 1 presents the methodology using a flowchart.

3.1. Brittle shear deformation and slickenside

Brittle shear faults are demarcated by secondary fractures -low angle R and P-planes bound by usually straight Y-planes (Supplementary Fig. 2a; Petit, 1987; Passchier and Trouw, 2005; Mukherjee and Koyi, 2010; Mukherjee, 2012). Due to brittle faulting, slickensides display various geometries of lineation/striation like curved marking, steps, asymmetric elevation etc. (Supplementary Fig. 2b; Doblas, 1998). The movement direction can be inferred from the nature of these striations or grooves**.** Often mineral steps are observed on slickensides consisting of mainly quartz and calcite. Genesis of these steps depends upon the fluid circulation along the fault zones associated with the pressure – temperature conditions (Doblas, 1998; Pascal, 2022).

3.2. Field structural analysis

Around 500 fault-slip data were collected from field (Figs. 2–8). Each of these data consists of fault plane orientation and rake of slickenside observed on the fault planes. The slickenside kinematic indicators include (mineral) steps, crescentic markers and few asymmetric elevations (Supplementary Fig. 2b). The fault plane smoothens towards the direction of missing block movement in many cases. Out of these, only 418 data (Fig. 1b; Supplementary Table 3; 106 from Barmer area, 124 near Dhorimana and 188 in Sarnoo hill area) have moderately to distinctly developed slickensides. Only these data were utilized in the different paleostress techniques.

3.3. Paleostress analysis

Paleostress analysis is commonly applied to decipher the principal stress axes orientations from fault-slip data and thus deduce the different

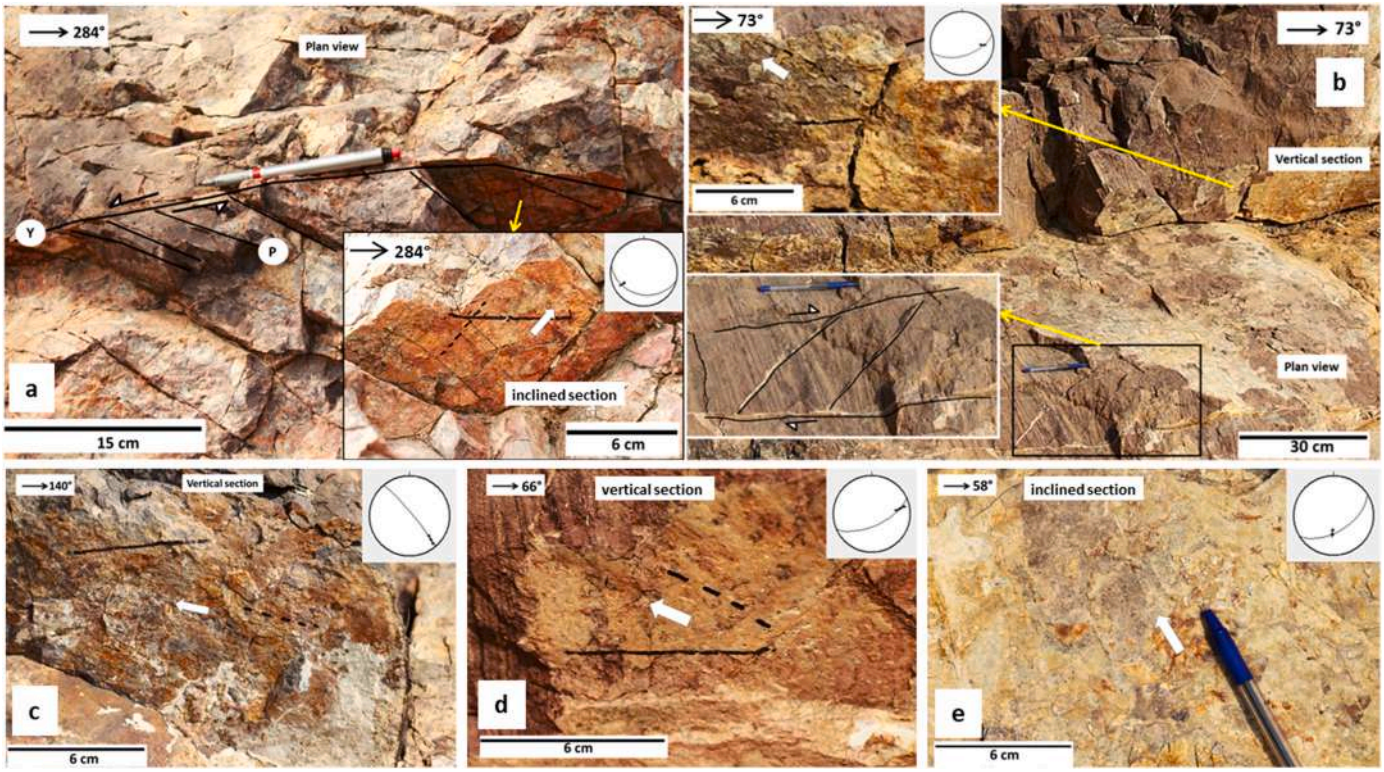

Fig. 3. (a)–(e) Fault slip slickensides collected from Barmer hill area and towards Jasai village. **(a)** Sinistral strike-slip fault observed on plan view, strike of Y plane is 104°. Quartz mineralization on inclined Y plane is observed. Bottom right inset– stepped slickenside feature observed on vertical Y plane (strike: 104°, dip 34°, dip direction 194°, rake 47°) missing block moved top-to-right up connoting the sinistral strike-slip movement. Location: NW of Ratanada temple in Barmer hill area, Barmer town. (e.g. from stress tensor 6). **(b)** Dextral strike-slip fault observed on plan view, strike of Y plane is 72°. Mineralization along Y- and P-planes consists of mainly calcite and secondary quartz. Top left inset– stepped slickenside feature observed on vertical Y plane (strike: 73°, dip 58°, dip direction 163°, rake 144°) missing block moved top-to-left up connoting the dextral strike-slip movement. Location: W of Ratanada temple in Barmer hill area, Barmer town. (e.g. from stress tensor 7). **(c)** Stepped slickenside feature observed on vertical fault plane (strike: 140°, dip 84°, dip direction 50°, rake 21°) missing block moved top-left up. Quartz mineralization seen on the fault surface associated with slickensides. Location: Barmer hill area, W of Barmer town. (e.g. from stress tensor 7). **(d)** Stepped slickenside feature observed on near vertical fault plane (strike: 140°, dip 64°, dip direction 156°, rake 152°) missing block moved top-left up. Quartz mineralization seen on the fault surface associated with slickensides. Location: Barmer hill area, W of Barmer town. (e.g. from stress tensor 7). **(e)** Stepped slickenside feature observed on vertical fault plane (strike: 73°, dip 68°, dip direction 163°, rake 78°) missing block moved top-left up. Calcite mineralization seen on the fault surface. Location: MIS outcrop towards Jasai village, ~15 km W of Barmer town (e.g. from stress tensor 8).

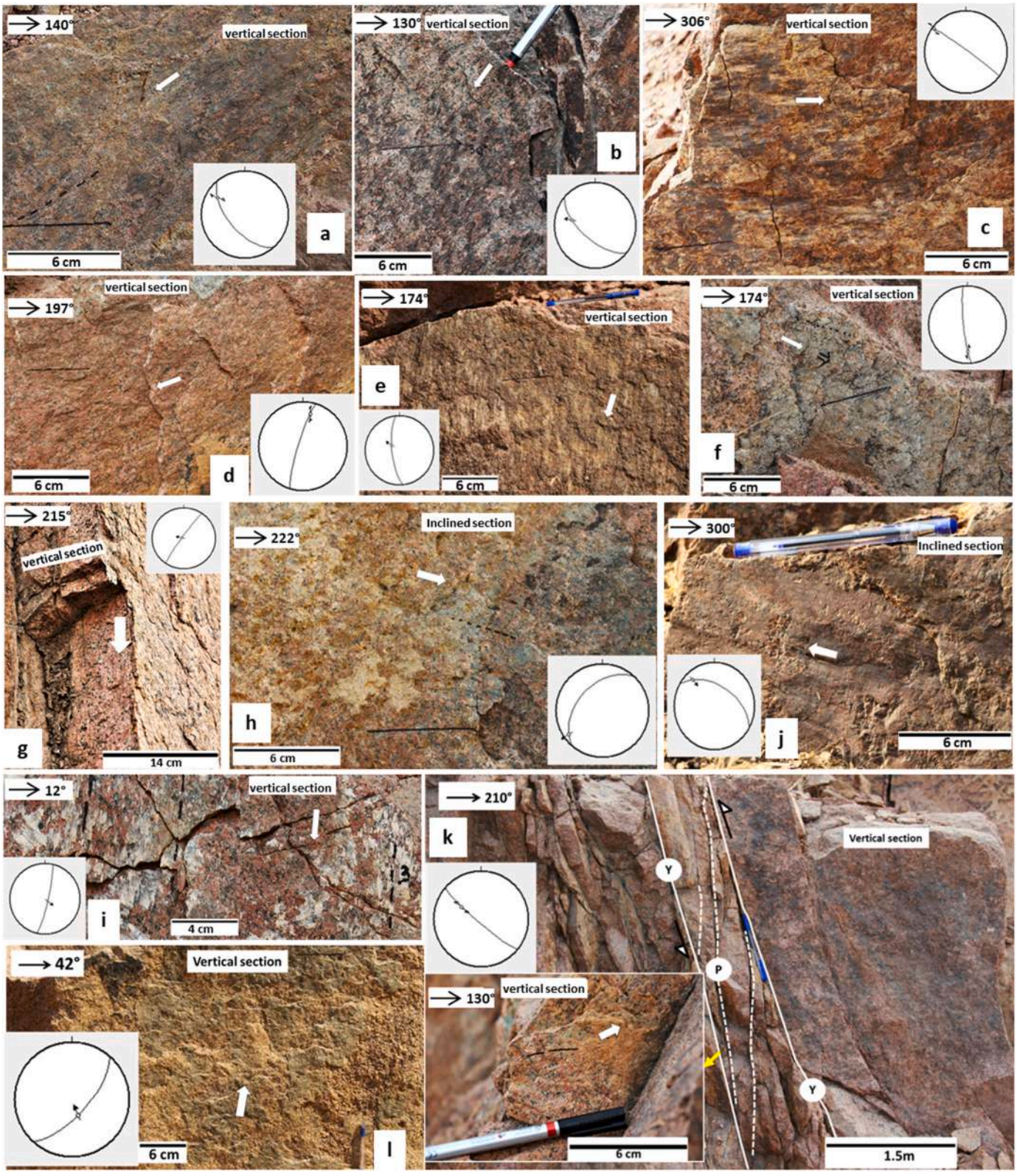

(caption on next page)

Fig. 4. (a)–(k) Fault slip slickensides obtained from Dhorimana hill area, W of Dhorimana village. **(a)** Slickenside feature (step) observed on NW trending inclined fault plane (strike: 140°, dip 55°, dip direction 230°, rake −150°) missing block moved bottom left (e.g. from stress tensor 9). **(b)** Slickenside feature (step) observed on NW trending inclined fault plane (strike: 130°, dip 62°, dip direction 220°, rake −132°) missing block moved bottom left (e.g. from stress tensor 9). **(c)** Slickenside feature (step and crescentic marker) observed on NW trending vertical fault plane (strike: 306°, dip 86°, dip direction 36°, rake −4°) missing block moved right (e.g. from stress tensor 10). **(d)** Slickenside feature (step) observed on NNE trending vertical fault plane (strike: 197°, dip 81°, dip direction 287°, rake −154°) missing block moved bottom left (e.g. from stress tensor 10). **(e)** Slickenside feature (step and crescentic marker and step) observed on ~ N trending inclined fault plane (strike 174°, dip 72°, dip direction 264°, rake −104°) missing block moved down indicated by arrow (e.g. from stress tensor 11). **(f)** Slickenside feature (step) observed on quartz cemented ~ N trending vertical fault plane (strike 174°, dip 82°, dip direction 264°, rake −31°) missing block moved bottom right (e.g. from stress tensor 11). **(g)** Slickenside feature (step) observed on NE trending vertical fault plane (strike 215°, dip 85°, dip direction 305°, rake −88°) missing block moved down indicated by arrow (e.g. from stress tensor 11). **(h)** Slickenside feature (step) observed on NE trending inclined fault plane (strike 222°, dip 44°, dip direction 312°, rake −18°) missing block moved bottom right (e.g. from stress tensor 12). **(i)** Slickenside feature (step and crescentic marker) observed on quartz cemented NNE trending vertical fault plane (strike 13°, dip 82°, dip direction 103°, rake −94°) missing block moved down (e.g. from stress tensor 12). **(j)** Slickenside feature (step) observed on NW trending inclined fault plane (strike 120°, dip 50°, dip direction 30°, rake 153°) missing block moved top left (e.g. from stress tensor 14). **(k)** NW trending brittle shear feature, with a top-to-N (up) slip, observed on sub-vertical section associated with Y (strike 130°) and P planes. Bottom left inset - stepped slickenside feature observed on vertical Y plane (strike 130°, dip 83°, dip direction 220°, rake 51°), missing block moved top-to-right up (e.g. from stress tensor 15). **(l)** Slickenside feature (step) observed on quartz cemented NE trending inclined fault plane (strike 42°, dip 68°, dip direction 132°, rake 79°) missing block moved up indicated by arrow (e.g. from stress tensor 16).

tectonic events (Etchecopar et al. 1981; Angelier, 1984; Angelier et al. 1985; Mercier et al. 1991; Delvaux et al., 1997; Zain Eldeen et al., 2002; Federico et al., 2014; Vanik et al., 2018; Shaikh et al., 2020; Jani et al., 2022; Pascal, 2022). Faults slip along the maximum resolved shear stress direction on the Coulomb fracture surface (Bott, 1959; Delvaux and Sperner, 2003). Slickensides/striations/frictional grooves help in deducing the orientation of the slip movement on the fault surface. Thus, the fault-slip data used for paleostress inversion consists of the strike and dip of the faults, as well as striation orientation (rake) and slip sense along the faults. Paleostress analyses do not usually yield the principal stress magnitudes, but gives their trends. Such structural analyses decipher changes in stress regimes during plate tectonic reconstruction

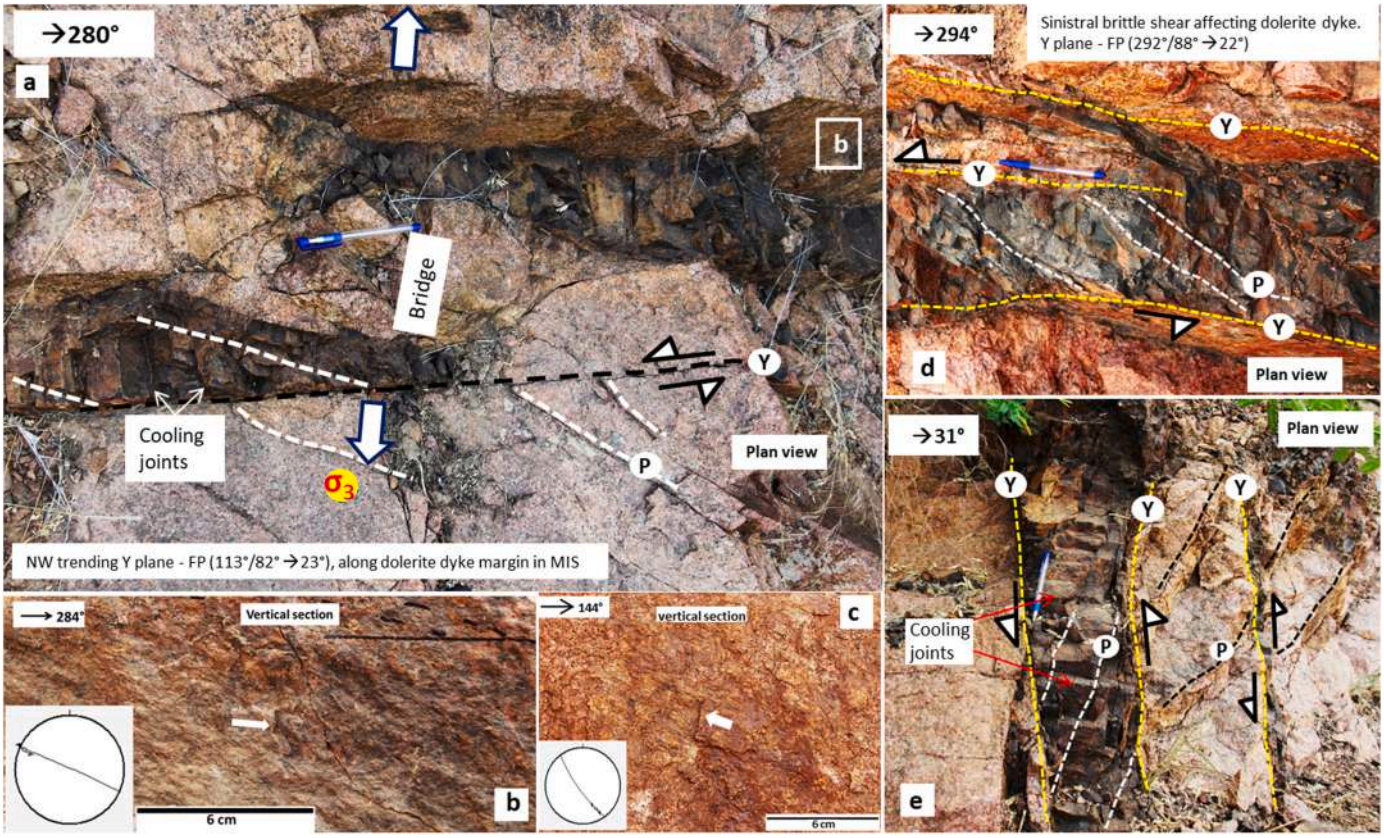

Fig. 5. (a)–(e) Dyke related outcrop pictures from Dhorimana hill area, W of Dhorimana village. **(a)** NW trending brittle shear feature, with a sinistral slip, observed on plan view associated with Y (strike 113°, dip 82°, dip direction 23°) and P planes. Mafic fine grained dolerite dyke body present along Y plane. MIS acts as bridge between continuous ~ 5–16 cm thick dyke segments observed on a sub-horizontal outcrop. σ3 - minimum horizontal stress direction ~ N direction. Parallel joints orthogonal to the dyke margin are present within the dyke that does not extend into the MIS. These are likely to be cooling joints. Few P –planes cut across these cooling joints in the dyke. The 15 cm pen acts as a marker (e.g. from stress tensor 13). **(b)** Slickenside feature (step and crescentic marker) observed on NW trending vertical fault plane (strike 294°, dip 84°, dip direction 24°, rake −10°) along the dyke margin. Missing block moved right (e.g. from stress tensor 13). Location (b) marked in Fig. (a). **(c)** Slickenside feature (step and crescentic marker) observed on NW trending vertical fault plane (strike 144°, dip 80°, dip direction 234°, rake 148°) parallel to dyke margin (not in picture). Missing block moved left top (e.g. from stress tensor 13). **(d)** Sinistral brittle shear affecting dolerite dyke (~18–32 cm thick) observed in a plan view. Y plane (strike 292°, dip 88°, dip direction 22°) oriented along dyke margin, P plane cutting across the dyke. The 15 cm pen acts as a marker. **(e)** Sinistral brittle shear affecting dolerite dyke (~20–27 cm thick) and also host MIS observed in a plan view. Y plane (strike 286°, dip 88°, dip direction 16°) oriented along dyke margin, P plane cuts across the dyke displacing the cooling joints. P plane is also observed in the adjacent host MIS rock. A thin dyke (3–4 cm thick) is seen along Y plane with same shear sense towards right. The 15 cm pen acts as a marker.

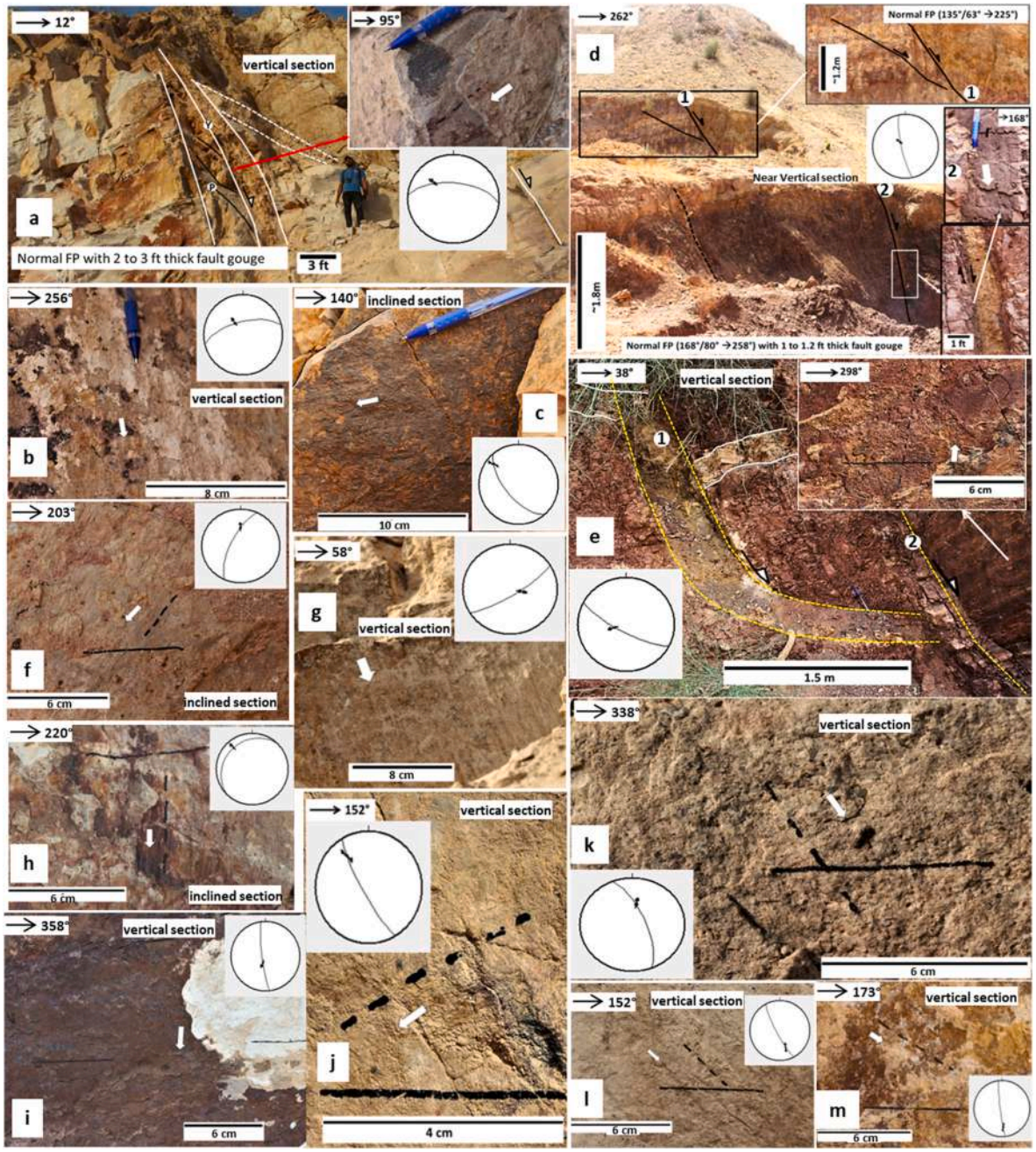

(caption on next page)

Fig. 6. (a)–(m) Fault slip slickensides obtained from W side of Mesozoic outcrop of Sarnoo hill area located E and SE of Sarnoo village. **(a)** Near E trending brittle shear normal fault associated with thick (2–3 ft) fault gouge observed on near vertical section of Upper Ghaggar- Hakra sandstone unit. Top right inset: Slickenside feature (step) observed on the inclined fault plane (strike 275°, dip 60°, dip direction 5°, rake −55°), missing block moved bottom left. There is another smaller fault (dip ~ 45°) towards right which merges with the main normal fault (e.g. from stress tensor 17). Person (height 171 cm) standing as a marker. **(b)** Slickenside feature (step) observed on ENE trending inclined fault plane (strike 256°, dip 63°, dip direction 346°, rake −80°), missing block moved down (e.g. from stress tensor 17). Kaolinite and probable calcite cementation seen on fault surface. **(c)** Slickenside feature (crescentic marker) observed on NW trending inclined fault plane (strike 140°, dip 62°, dip direction 230°, rake −158°), missing block moved left (e.g. from stress tensor 18). **(d)** NW trending normal faulting observed on a near vertical section on one side of a hillock. Top right inset 1: NW trending Normal faulting (strike 135°, dip 63°, dip direction 225°) in the upper part of the hillock. Right inset 2: Prominent slickenside feature (step) observed on NNW trending vertical fault plane (strike 168°, dip 80°, dip direction 258°, rake −102°) in the lower section of the hillock, missing block moved down. Bottom right inset: Fault gouge (1–1.2 ft thickness) seen along this near vertical fault in the lower section of the hillock (e.g. from stress tensor 18). **(e)** 1 - NW trending listric normal fault associated with thick (~34 cm) fault gouge. This fault has displaced a yellow colour sandstone bed in the upper part. The fault terminates at another NW trending fault (2) towards right. 2 - Fault plane surface seen on hangingwall. Top right inset: Slickenside feature (step) observed on hangingwall side of NW trending near vertical normal fault plane 2 (strike 118°, dip 76°, dip direction 208°, rake −104°), missing block (footwall) moved top right (e.g. from stress tensor 18). The truncation of fault plane 1 against fault plane 2 indicates that fault plane 2 is younger. **(f)** Slickenside feature (step) observed on NE trending inclined fault plane (strike 205°, dip 69°, dip direction 295°, rake −126°), missing block moved bottom left. Kaolinite cementation seen on fault surface (e.g. from stress tensor 19). **(g)** Slickenside feature (step and crescentic marker) observed on NE trending near vertical fault plane (strike 58°, dip 78°, dip direction 148°, rake −78°), missing block moved down (e.g. from stress tensor 20). **(h)** Slickenside feature (crescentic marker) observed on NE trending inclined fault plane (strike 225°, dip 22°, dip direction 315°, rake −94°), missing block moved down (e.g. from stress tensor 20). Kaolinite and probable calcite cementation seen on fault surface. **(i)** Slickenside feature (step) observed on NNW trending vertical fault plane (strike 173°, dip 82°, dip direction 263°, rake −76°), missing block moved down (e.g. from stress tensor 21). Kaolinite cementation seen on right side of the fault surface. **(j)** Slickenside feature (crescentic marker) observed on NW trending vertical fault plane (strike 150°, dip 80°, dip direction 240°, rake −148°), missing block moved bottom left (e.g. from stress tensor 21). **(k)** Slickenside feature (step) observed on NW trending near vertical fault plane (strike 158°, dip 69°, dip direction 68°, rake −60°), missing block moved bottom right (e.g. from stress tensor 22). **(l)** Slickenside feature (step and crescentic marker) observed on NW trending near vertical fault plane (strike 152°, dip 80°, dip direction 242°, rake −41°), missing block moved bottom right (e.g. from stress tensor 24). **(m)** Slickenside feature (step and crescentic marker) observed on NNW trending near vertical fault plane (strike 173°, dip 85°, dip direction 263°, rake −34°), missing block moved bottom right (e.g. from stress tensor 24). Kaolinite cementation seen on fault surface.

at different geologic times.

Paleostress analysis using different software was carried out on fault-slip data from outcrops. The analysis considers mutually perpendicular three principal stress axes (σ1, σ2 and σ3). Here σ1 and σ3 are the maximum and the minimum principal stress axes, respectively, thus σ1 > σ2 > σ3 (Angelier, 1994). The plunge of σ1, σ2 and σ3 defines the three end member tectonic stress regimes: extensional (vertical σ1), strike-slip (vertical σ2) and compressional (vertical σ3). The shape of the stress ellipsoid is defined by the unit-less stress ratio parameter R or D (Delvaux et al., 1997; Žalohar and Vrabec, 2007) = [(σ2- σ3)/(σ1- σ3)] and ranges from 0 to 1 (Angelier, 1990, 1994; Delvaux et al., 1997). In between this there are three end member tectonic stress regimes. There can be other subordinate stress regimes defined by the function of $R^{/}$ (stress regime index) that ranges between 0 and 3 (Delvaux et al., 1997). Extensive regime ($R^{/}$ = R) varies from radial extensive (0< $R^{/}$< 0.25), pure extensive (0.25 < $R^{/}$<0.75) to partly transtensive (0.75 < $R^{/}$<1). The strike-slip regime [$R^{/}$ = (2-R)] is defined by transtensive (1 < $R^{/}$<1.25), pure strike-slip (1.25 < $R^{/}$<1.75) and transpressive (1.75 < $R^{/}$ < 2). While compressional regime [$R^{/}$ = (2 + R)] can be partly transpressive (2 < $R^{/}$< 2.25), pure compressive (2.25 < $R^{/}$ < 2.75) to radial compressive (2.75 < $R^{/}$ < 3).

The trend of fault-slip on a pre-existing weak plane, oblique to the principal stress directions: σi (i = 1, 2, 3), is governed by *(i)* the applied shear stress, *(ii)* the R value, and *(iii)* the orientation of the fault plane with respect to σi (Angelier, 1990, 1994).

Several assumptions exist for fault-slip inversion and to deduce paleostress (Wallace, 1951; Bott, 1959; Pollard et al., 1993; Nemčok and Lisle, 1995; Žalohar and Vrabec, 2007; Žalohar 2018; Pascal, 2022). *(i)* The rock is isotropic and the stress field is homogeneous; *(ii)* The same stress field govern the movements along the faults; *(iii)* fault-slip parallels the maximum resolved shear stress direction on the Coulomb fracture surface, as deduced from the regional stress tensors; *(iv)* the slip/displacement is translational; and *(v)* faults do not interact/link up. Paleostress analyses in this work mostly follow these assumptions. In particular, since the rock type is uniform devoid of veins and secondary mineralization as seen in naked eyes around Barmer, Dhorimana and Sarnoo (Figs. 3–4, 6), and majorly devoid of any marker/lineation, point *(i)* is almost followed. Second, faults documented in this study are all translational as indicated by the straight slickenlines developed on the fault planes. Third, interlinked faults/fault scarps do occur at the northern basin margin (Section 4.1.4; Fig. 8). However, we picked up only discrete faults from field from the eastern and the western margins for the paleostress analysis. These faults do not interact.

The aim of paleostress analyses is to find out information on stress regime, and secondly to identify stress regimes that changed temporally. The stress inversion process used in paleostress analyses, are the Right Dihedron, iterative rotational optimization and the Gaussian method (Delvaux and Sperner, 2003; Žalohar and Vrabec, 2007; Pascal, 2022). Fault data depicting spatial variation of stress tensors are termed as heterogeneous fault-slip data (e.g. Zain Eldeen et al., 2002; Biswas et al. 2022). Such data can only be explained in terms of different stress orientations and regimes. On other hand, homogeneous fault-slip data connotes a single stress regime. To initiate stress inversion, the entire heterogeneous dataset needs to be separated into homogeneous subsets based on the degree/amount of misfit (of fault-slip data group) determined with respect to the calculated stress regime at every step (Yamaji, 2003; Yamaji et al., 2006). Each of these subsets consists of homogeneous fault-slip data related to specific tectonic event.

We used three open-source software applications for the standard paleostress calculations -Win_Tensor (v.5.9.2; Delvaux and Sperner, 2003), T-Tecto studio X5 (Žalohar and Vrabec, 2007) and FaultKin (v.8.1; Marrett and Allmendinger, 1990; Allmendinger et al., 2012). Paleostress analysis results may vary for different applied methods, therefore several techniques are recommended on the same data set (e.g., Simón, 2019 and as adapted in Shaikh et al., 2020, 2022; Maurya et al., 2021; Biswas et al., 2022; Goswami et al., 2022).

Win_Tensor applies the Right Dihedron Method (RDM), while Gaussian weighted RDM is used in T- Tecto studio X5 for inverse analyses of fault planes to get the paleostress tensors (Delvaux and Sperner, 2003; Žalohar and Vrabec, 2007). Linked Bingham statistical method is utilized in FaultKin (Allmendinger et al., 2012). All the homogeneous subsets of the fault-slip data have angular misfit ≤30°, which is reasonably acceptable (Delvaux and Sperner, 2003). All these three software applications provide stress axes trend and plunge for each stress tensors. Win_Tensor and T-Tecto also provides stress ratio R and D respectively. These varied applications were used to precisely calculate the paleostress tensors linked to unique tectonic events, thereby minimizing the level of uncertainties**. Supplementary text** details these software.

Relative timing of activation of the obtained paleostress tensors can

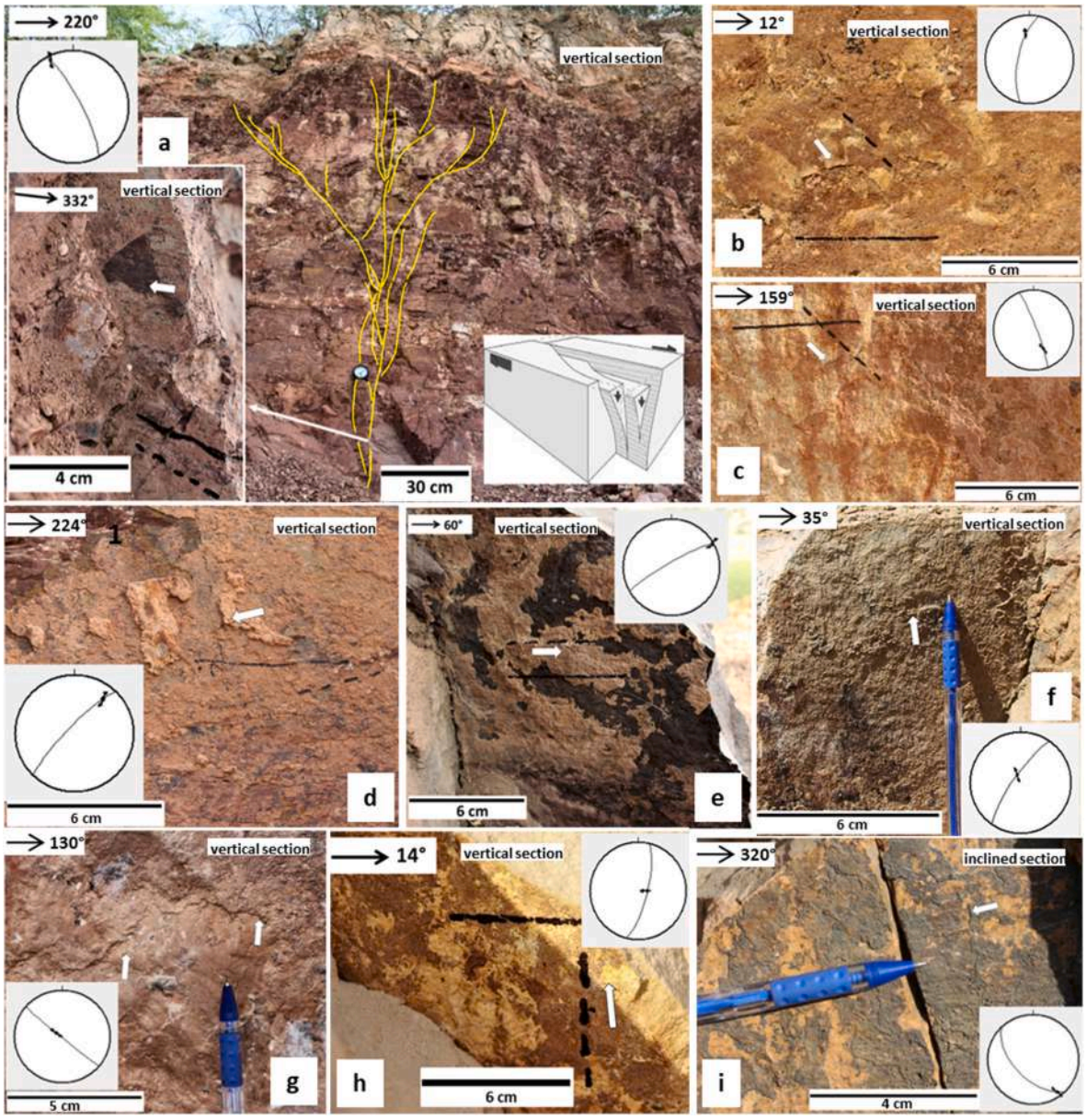

Fig. 7. (a)–(i) Faults and slickensides obtained from W side of Sarnoo hill area located E of Sarnoo village. **(a)** Vertical cross-sections of NW trending strike slip brittle shear observed in the Cretaceous sandstone. The P – and the Y planes together depict a flower structure. Bottom left inset: Slickenside feature (crescentic marker) observed on NW trending vertical Y plane (strike 152°, dip 78°, dip direction 62°, rake −8°) on the right side block (e.g. from stress tensor 23). Missing block moved left thus inferred a dextral sense of shear. Bottom right inset: schematic 3D block diagram of a dextral strike slip fault. **(b)** Slickenside feature (step) observed on NNE trending near vertical fault plane (strike 192°, dip 69°, dip direction 282°, rake −133°), missing block moved bottom right (e.g. from stress tensor 25). Kaolinite cementation seen on fault surface. **(c)** Slickenside feature (step) observed on NNW trending vertical fault plane (strike 159°, dip 83°, dip direction 69°, rake −134°), missing block moved bottom right (e.g. from stress tensor 26). Kaolinite cementation seen on fault surface. **(d)** Slickenside feature (step) observed on NE trending vertical fault plane (strike 224°, dip 80°, dip direction 314°, rake −155°), missing block moved left (e.g. from stress tensor 27). **(e)** Slickenside feature (step and crescentic marker) observed on NE trending vertical fault plane (strike 240°, dip 82°, dip direction 330°, rake −178°), missing block moved right (e.g. from stress tensor 27). Calcite and kaolinite cementation seen on fault surface. **(f)** Slickenside feature (step and crescentic marker) observed on NE trending near vertical fault plane (strike 215°, dip 68°, dip direction 305°, rake 83°), missing block moved upward (e.g. from stress tensor 28). Kaolinitic and probably calcite cementation seen on fault surface. **(g)** Slickenside feature (step) observed on NW trending vertical fault plane (strike 130°, dip 88°, dip direction 220°, rake 78°), missing block moved up (e.g. from stress tensor 29). **(h)** Slickenside feature (step) observed on NW trending near vertical fault plane (strike 14°, dip 74°, dip direction 104°, rake 94°), missing block moved up (e.g. from stress tensor 30). **(i)** Slickenside feature (step) observed on NW trending inclined fault plane (strike 136°, dip 55°, dip direction 226°, rake 167°), missing block moved left (e.g. from stress tensor 31).

be deduced from the direct field-based observations of the faults slip data taken as inputs. These are *(i)* cross-cut relation amongst faults, *(ii)* known stratigraphic age of the faulted (host) rock, and *(iii)* mineralization on the faults and associated slickensides – striations on the mineralized/cemented or non-mineralized faults.

3.4. Drainage morphometry analysis around Barmer

We analysed the drainage morphology quantitatively along the western margin around Barmer and Jasai areas, in order to understand the neotectonic activeness and its impact on landscape. The terrain is devoid of major rivers and is covered by ~ NE-trending longitudinal

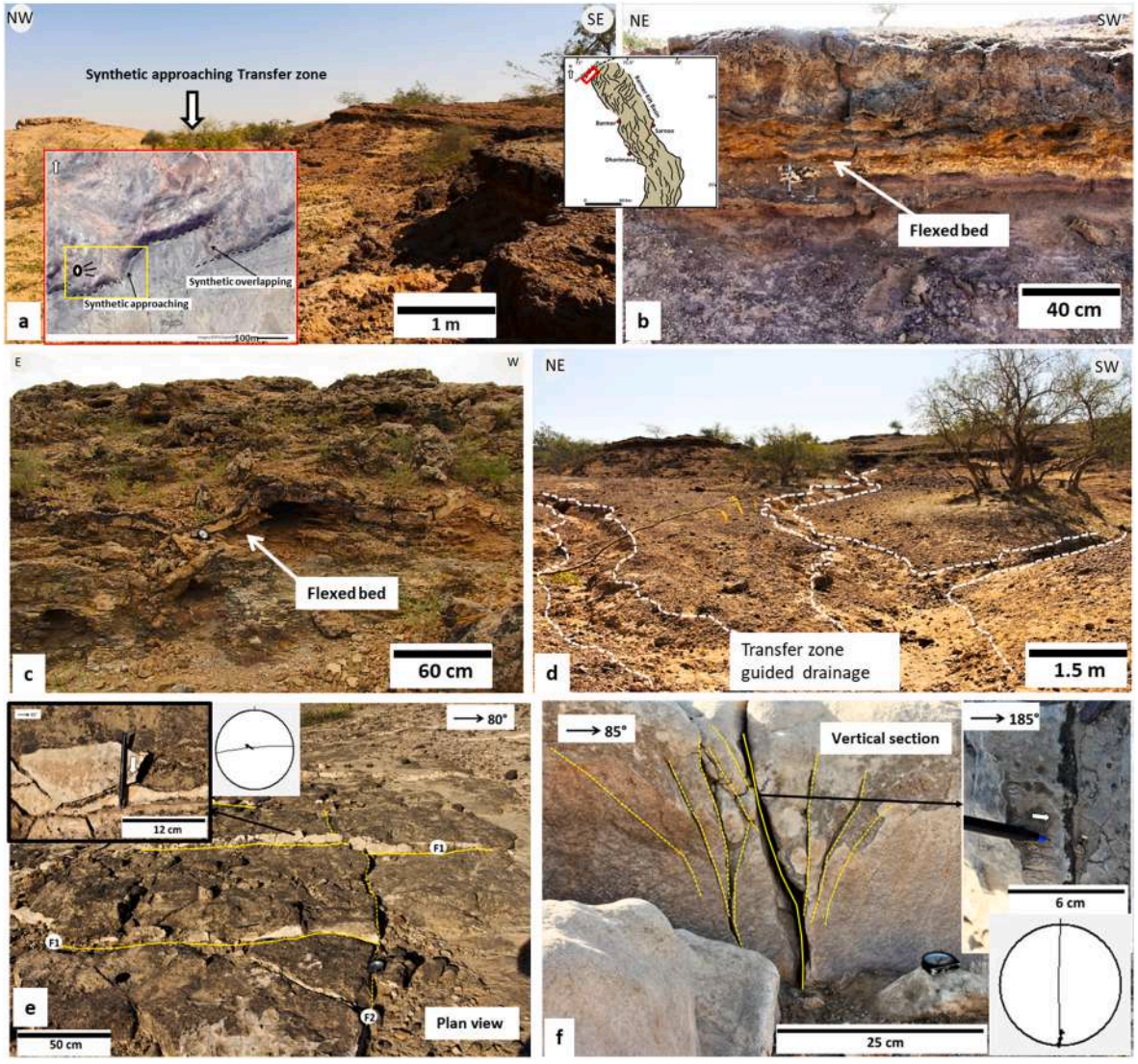

Fig. 8. (a)–(f) Outcrop observations from Fatehgarh fault area in the N margin. Location: Along Fatehgarh fault trend, ~14–15 km SW of Bariyada village. **(a)** Outcrop view of large scale transfer zone (synthetic approaching) along Fatehgarh fault. Bottom left inset: Satellite imagery from Google Earth Pro of the same area. The yellow box and observation point highlights the exact location. Right inset: location area marked in red box on the Barmer basin fault map. **(b)** and **(c)** Flexed beds consisting of calcareous unit and volcanic ash bed likely to be of Barmer Hill Formation and/or Bariyada Member. **(d)** Transfer zone guided seasonal drainage sourced from the Fatehgarh fault, observed on the NW side of the fault zone. **(e)** Interlinked fault planes in Fatehgarh sandstone near Fatehgarh fault observed on planer surface. The ~ E trending F1 faults are having normal throw. The F2 fault has laterally displaced the F1 fault. Top left inset: Slickenside feature (crescentic marker) observed on E trending vertical fault plane (strike 265°, dip 85°, dip direction 355°, rake −82°), missing block moved down. **(f)** Vertical cross section of the F2 fault observed on Fatehgarh sandstone depicting a flower type of structure. There is a small lateral displacement of one block with respect to the other. Right inset: Slickenside feature (crescentic marker) observed on N trending vertical fault plane on the left fault block (strike 180°, dip 88°, dip direction 270°, rake −12°), missing block moved right, indicating sinistral displacement. Note: These faults (F1 & F2 and others along the Fatehgarh fault trend) have not been considered for paleo-stress analysis.

sand dunes (Ghose, 1964). Google Earth pro satellite imagery, SRTM digital elevation model (DEM) with 30 m resolution and ArcGIS (10.4) have been used to identify seasonal drainage basins.

These images of the dry channels are compared with that of the base map, toposheets NG 42-12 series U502 of Barmer (India) and Pakistan of 1:250,000 scale. The unclassified streams on this map have been traced on the DEM in ArcGIS for the present study and for drainage basin analysis. The basic geomorphologic parameters including the area, length, stream number, stream frequency, drainage density, basin relief, relief ratio and hypsometric integral have been calculated to understand the basin area with respect to the basin slope (Supplementary Table 2). Details in **Supplementary text**.

3.5. Earthquake focal mechanism

Ten recent earthquake focal mechanism data, between 1990 and 2010, with moment of magnitude (Mw) above 5 from USGS (www.usgs.gov/programs/earthquake-hazards) were taken for this study (Supplementary Table 3). Two are from Jaisalmer basin area while the remaining eight are from the Kutch (Kachchh) basin. Also, among these nine focal mechanism data are of magnitude between 5 and 5.8 Mw while only one (near Bhuj, Gujarat, India) is having a magnitude of 7.7 Mw. The earthquake focal depths are within 10–45 km below the surface. Stress inversion analysis was performed using earthquake focal mechanism data in order to deduce the present-day stress regime in the NW India using Right Dihedron and Rotational Optimization methods in Win_Tensor (v.5.9.2; Delvaux and Sperner, 2003).

4. Results

4.1. Fault-slip analysis

All the fault-slip data collected from the western and eastern margin outcrops depict overall NW, NE, ~E and ~N striking faults (Supplementary Table 3). The individual extents of the outcrop faults are short (< 10 m) and discrete. In the western margin, around Barmer and Dhorimana area, the faults are observed in MIS basement rock. In the eastern margin, Sarnoo hill area, the sandstones of fluvial Lower Cretaceous Ghaggar-Hakra Formation are brittle deformed. At few places the MIS basement crops out alongside the Ghaggar-Hakra Formation. Both these units are brittle deformed. All the outcrops faults are identified based on the presence of brittle shear Y and P planes, and/or slickensides on brittle planes. At many places, Y-planes consist of the slickenside kinematic indicator, which enables to decipher the slip senses. Fault-slip data with reliable slickenside slip sense were considered for paleostress analysis. The fault planes were interpreted on sub-vertical and inclined sections and also on sub-horizontal outcrops. In the northern boundary of the Barmer basin, near Devikot- Fatehgarh ridge, quality fault-slip data is scanty (<10) also, many of them are interlinked and so those were not incorporated in the paleostress analysis.

In the present analysis, all the 31 fault-slip groups from 418 fault-slip data were analysed. The faults in the western margin (Figs. 2–5) are dominantly normal dip-slip to oblique slip and strike-slip. Some reverse dip-slip faults also exist. At eastern margin the faults (Figs. 6 and 7) are majorly normal dip-slip to oblique-slip with lesser strike-slip movements. Each of the obtained 31 stress tensors from western and eastern basin margins consists of a stress regime index value (R') and a maximum horizontal stress (SHMax) orientation (Figs. 9–11, Table 1).

In the western margin, both in Barmer and Dhorimana areas, cross-cut relation has been recognized in our field study, the NE faults are cut by NW faults (Supplementary Figs. 3 and 4). This indicates that the NW-trending faults are younger. Besides, we have also noticed quartz, calcite and possible kaolinite mineralization on several faults in Barmer area and also locally around Dhorimana and Sarnoo. Slickenside – striations do occur on many of these mineralized/cemented fault surfaces (Fig. 2d–i; 3a-e; 4f, i, l; 6b, f, h, i, m; 7b, c, e, f), thus indicating fluid flow along fracture planes.

The outcrop specific results are presented below.

4.1.1. Around Barmer hill area, western margin

The outcrops near Barmer town are *(i)* hill area west of Barmer, *(ii)* Gehoon village area NW of Barmer, and *(iii)* hilly outcrops towards Jasai village SW of Barmer. These outcrops consist of faulted Malani rhyolite basement rocks. Faults dip moderate to steep (50–85°; Fig. 1b). Slickensides are either present directly on the faults or in many cases observed on the cements, quartz or calcite, associated with faults (Figs. 2 and 3). Mineralization along brittle shear planes is quite common in these outcrops. The slip sense is deduced from the slickenside kinematic indicators. NW-trending faults cut NE-trending faults at three places, enabling determination of relative time of those deformations (e.g. Supplementary Fig. 3). These faults are mostly oblique-slip and strike-slip (Figs. 2 and 3). Near dip-slip to oblique-slip occurs mainly for the NW-trending faults. Normal, reverse and strike-slip faults have been identified from outcrops, out of which normal oblique-slip faults are more numerous. Eight paleostress tensors were obtained from these outcrops consisting of 106 fault-slip data. Out of these, three tensors belongs to extensive to transtensive regime (Fig. 9 no. 1, 3–4; Supplementary Figs. 8 and 9; Table 1; also see field photos Fig. 2a–c, e-h), three in strike-slip regime (Fig. 9 no. 2, 5, 7; Supplementary Figs. 8 and 9; Table 1; also see field photos Fig. 2d, i, 3b-d) while two are of compressive regime (Fig. 9 no. 6, 8; Supplementary Figs. 8 and 9; Table 1; also see field photos Fig. 2j and 3a, e).

4.1.2. Around Dhorimana hill area, western margin

The Malani granites crop out in the hilly terrain adjacent to the

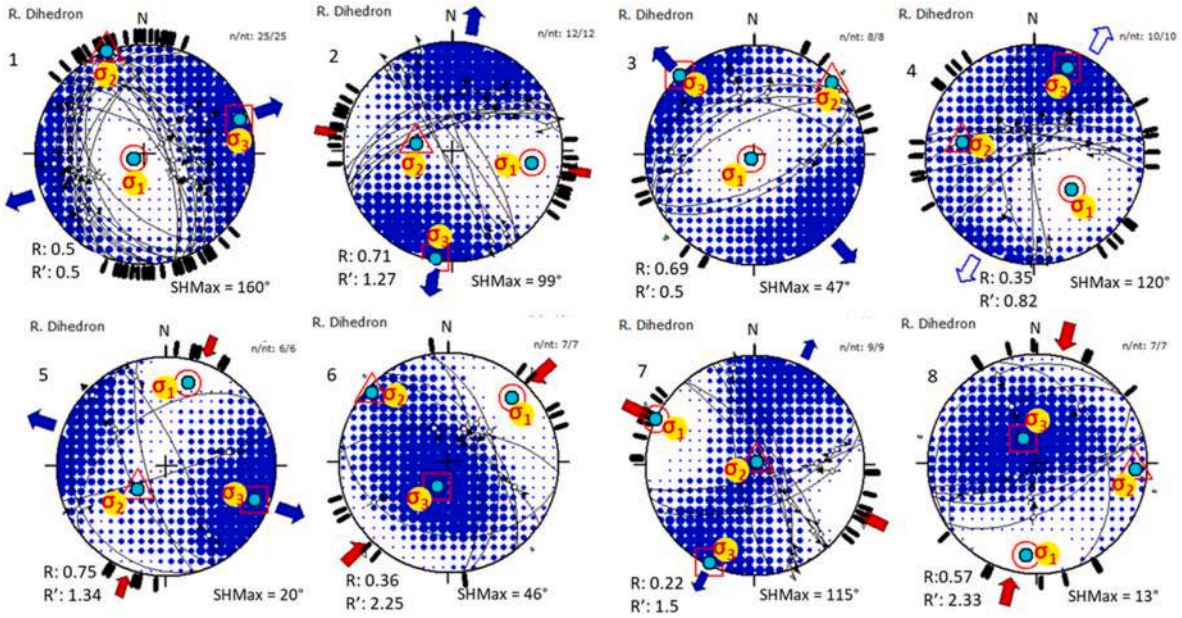

Fig. 9. 8 Stress tensors (Schmidt net, lower hemisphere), obtained from different sites of Barmer and its surrounding areas in western margin, deduced from Win_Tensor Right Dihedral Method (RDM) of stress inversion output (Delvaux and Sperner, 2003). Fault planes are shown by black lines associated with slip vectors (marked by hollow circle with arrow). Red inward pointed double arrow: orientation of maximum horizontal principal stress (SHmax). Blue outward pointed double arrow: orientation of minimum horizontal principal stress (Shmin). Red circle, triangle and square with smaller cyan circle inside: orientation of maximum (σ1), intermediate (σ2) and minimum (σ3) stress axes respectively (σ1 ≥ σ2 ≥ σ3). Solid black small lines at the periphery of stress tensors: SHmax orientation for individual fault-slip data. n/nt: number of fault-slip data used in paleostress analysis with respect to the total number of fault-slip data collected from the particular location. R and R′: stress ratio and stress index respectively (Delvaux et al., 1997). The blue and white gridded quadrant of the stereoplots corresponds to regions of tension and compression respectively.

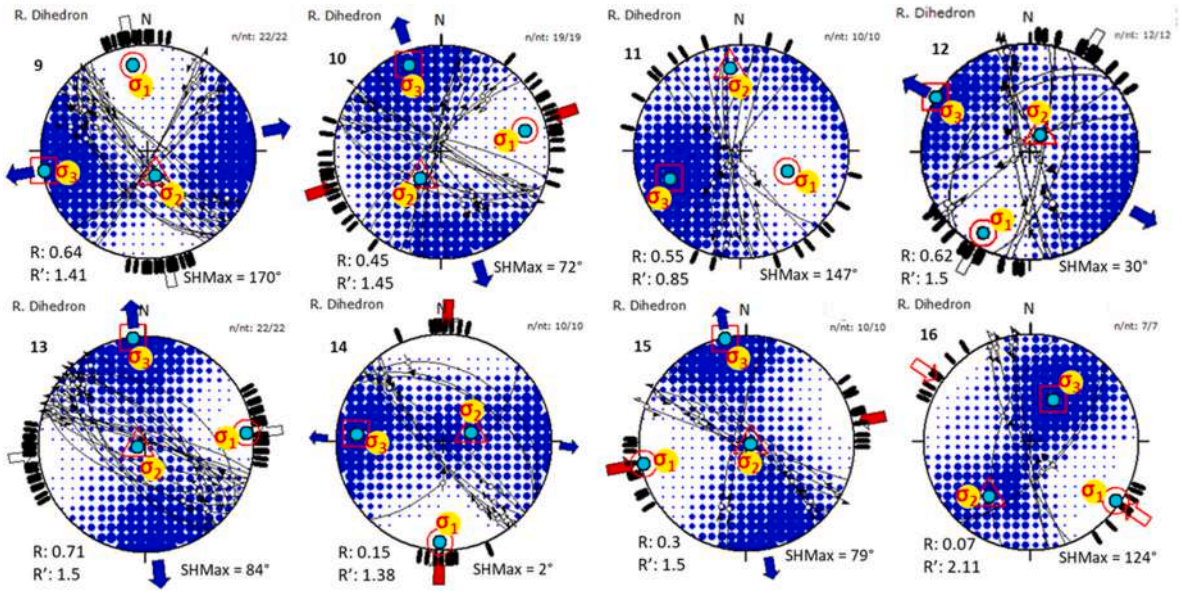

Fig. 10. 8 Stress tensors (9–16), obtained from different sites of Dhorimana hill area W of Dhorimana village in western margin, deduced from Win_Tensor (Delvaux and Sperner, 2003). Refer to Fig. 9 caption for details of the legends.

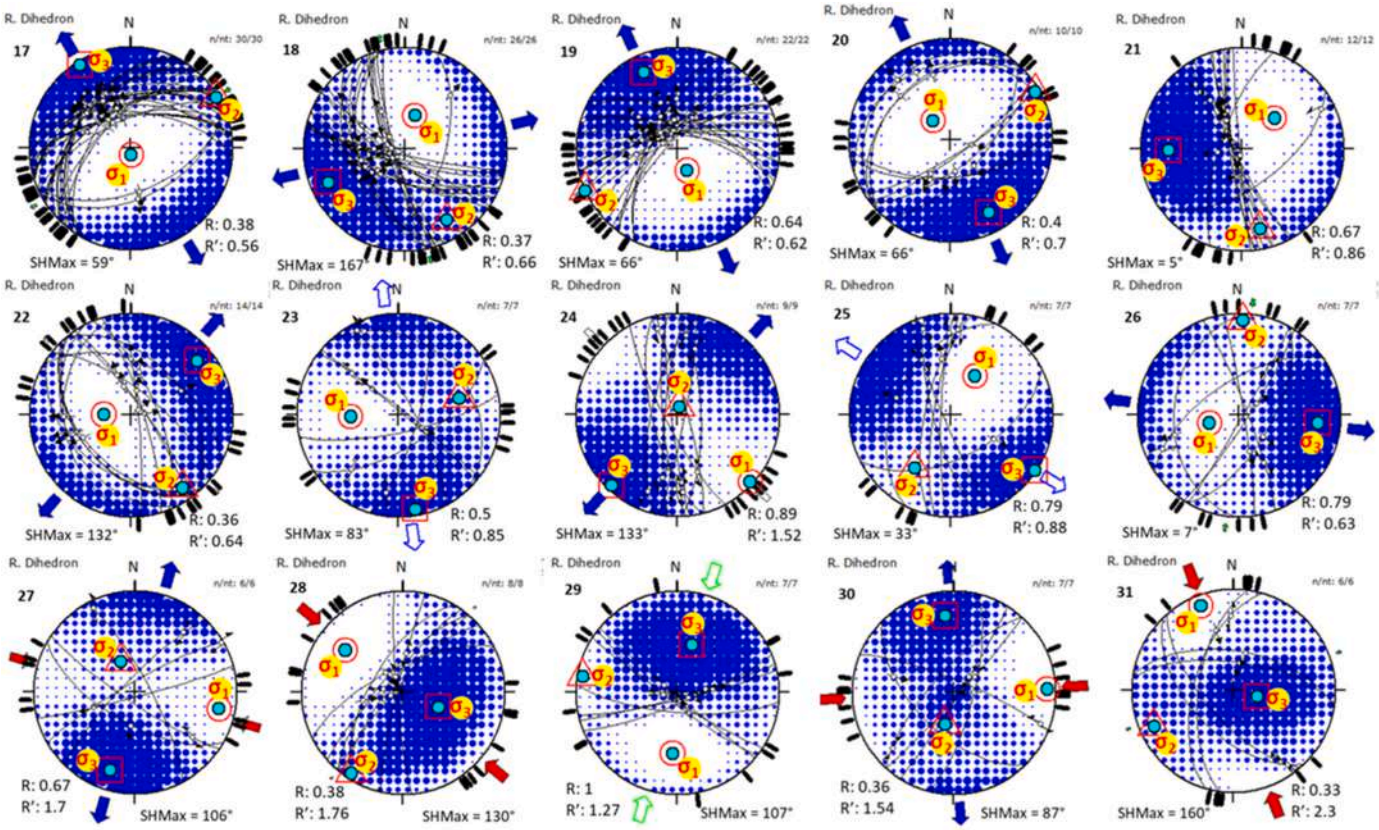

Fig. 11. 15 Stress tensors (17–31), obtained from different sites of Sarnoo hill area S & N of Sarnoo village in eastern margin, deduced from Win_Tensor (Delvaux and Sperner, 2003). Refer to Fig. 9 caption for details of the legends.

Dhorimana village. Faults in this granitic outcrop exhibit brittle shears. The NW and NE major lineament trends are well-observed in Google Earth Pro imageries (as in Dasgupta and Mukherjee, 2017). The observed small-scale fault trends in the outcrop matches well with the larger lineament trends in the Dhorimana hill area. Faults trend dominantly NW but several trend NE. Here also the NW-trending faults cut the NE-trending faults as observed at four places at the Dhorimana hill area (Supplementary Fig. 4), thereby indicating the relative timing of deformation. Faults dip steeply (>60°; Fig. 1b). The dominant fault types are oblique-slip normal, strike-slip and reverse faults (Figs. 4 and 5). Cement along the fault surfaces is infrequent (Fig. 4). Brittle shear and slickenside kinematic indicators are observed along near-vertical

Table 1
Paleostress analyses results as obtained from fault slip data of western (Barmer and Dhorimana) and eastern (Sarnoo) margins.

Area	No.	Sense of Slip	Dominant Rock Type	Number of Fault Slip data	Software and Method used									Stress Ratios (unitless)		Stress Regime (unitless)		SHMax (Win Tensor, in °)	SHMax (T-Tecto, in °)
					Win Tensor - RDM			T-Tecto - Gauss weighted RDM			FaultKin - Linked Bingham Statistics								
					σ1 (trend/ plunge, in °)	σ2 (trend/ plunge, in °)	σ3 (trend/ plunge, in °)	σ1 (trend/ plunge, in °)	σ2 (trend/ plunge, in °)	σ3 (trend/ plunge, in °)	σ1 (trend/ plunge, in °)	σ2 (trend/ plunge, in °)	σ3 (trend/ plunge, in °)	D	R	R′	Inference		
W Margin - around Barmer	1	Normal	MIS	25	249/82	340/0	70/8	194/77	348/11	79/5	218/75	343/9	75/12	0.4	0.5	0.5	Pure Extensive	160	170
	2	Normal	MIS	12	98/28	283/62	189/2	105/24	291/66	22/0	106/20	282/70	15/1	0.7	0.71	1.27	Pure Strike Slip	99	105
	3	Normal	MIS	8	220/86	47/4	317/0	353/84	229/3	138/4	337/84	228/2	138/6	0.5	0.69	0.5	Pure Extensive	47	55
	4	Normal	MIS	10	133/52	279/33	21/17	132/44	277/40	24/20	135/48	270/32	16/24	0.4	0.35	0.82	Extensive to Transtensive	120	113
	5	Normal	MIS	6	15/22	232/63	111/15	27/28	210/62	113/3	13/26	224/61	235/4	0.5	0.75	1.34	Pure Strike Slip	20	26
	6	Reverse	MIS	7	45/18	312/6	205/70	63/12	154/6	267/75	53/16	144/4	246/74	0.6	0.36	2.25	Pure Compressive	46	57
	7	Reverse	MIS	9	295/0	28/87	205/3	110/0	200/85	32/5	113/1	224/86	22/4	0.2	0.22	1.5	Strike Slip to Transpressive	115	113
	8	Reverse	MIS	7	187/18	93/12	332/69	165/19	75/0	345/73	179/21	84/12	327/66	0.7	0.57	2.33	Pure Compressive	13	10
W Margin - around Dhorimana	9	Normal	MIS	22	350/19	163/71	259/2	7/30	181/60	90/0	356/26	169/64	265/3	0.6	0.64	1.41	Pure Strike Slip	170	177
	10	Normal	MIS	19	75/21	218/64	340/14	82/35	273/55	172/8	78/34	243/56	343/7	0.2	0.45	1.45	Pure Strike Slip	72	68
	11	Normal	MIS	10	113/51	353/22	249/30	117/40	347/37	230/31	113/49	347/27	242/28	0.4	0.55	0.85	Extensive to Transtensive	147	136
	12	Normal	MIS	12	210/15	31/75	300/0	163/69	37/31	302/18	210/33	28/57	119/1	0.3	0.62	1.5	Pure Strike Slip	30	15
	13	Dyke Parallel*	MIS	22	83/6	252/83	353/1	75/1	264/89	162/0	261/1	35/89	171/1	1	0.71	1.5	Strike Slip to Transtensive	84	87
	14	Reverse	MIS	10	182/8	71/68	275/20	169/12	66/47	273/39	180/10	48/76	272/10	0.2	0.15	1.38	Strike Slip to Transpressive	2	336
	15	Reverse	MIS	10	259/3	103/87	349/1	81/0	0/90	163/0	256/7	35/81	165/6	0.2	0.3	1.5	Strike Slip to Transpressive	79	80
	16	Reverse	MIS	7	124/4	218/36	28/53	303/11	193/60	39/27	123/6	224/61	30/28	0.4	0.07	2.11	Transpressive to Compressive	124	129
E Margin - around Sarnoo	17	Normal	Sandstone	30	176/85	59/2	329/5	138/80	234/1	144/0	183/83	60/4	330/6	0.3	0.38	0.56	Pure Extensive	59	63
	18	Normal	Sandstone	26	16/62	149/20	247/19	32/61	136/8	230/27	17/61	140/17	237/23	0.2	0.37	0.66	Pure Extensive	167	160
	19	Normal	Sandstone	22	156/71	246/0	336/19	160/61	255/2	346/29	169/64	68/5	336/25	0.2	0.64	0.62	Pure Extensive	66	60
	20	Normal	Sandstone	10	318/69	60/5	152/20	323/74	59/2	150/14	317/71	64/6	156/18	0.2	0.4	0.7	Pure Extensive	66	86
	21	Normal	Sandstone	12	46/54	167/21	269/28	60/46	168/16	271/39	45/46	165/26	273/32	0.7	0.67	0.86	Extensive to Transtensive	5	360
	22	Normal	Sandstone	14	272/68	145/14	50/17	267/77	153/5	62/12	273/73	146/11	54/14	0	0.36	0.64	Extensive	132	120
	23	Normal	Sandstone	7	269/51	74/38	170/7	283/55	65/29	163/15	268/36	95/54	0/3	1	0.5	0.85	Extensive to Transtensive	83	80
	24	Normal	Sandstone	9	133/3	12/84	223/6	126/7	311/83	43/0	133/16	335/73	224/6	0.7	0.89	1.52	Strike Slip to Transtensive	133	129
	25	Normal	Sandstone	7	31/53	215/37	123/2	45/43	212/46	122/0	40/41	213/49	307/4	0.4	0.79	0.88	Extensive to Transtensive	33	25
	26	Normal	Sandstone	7	255/65	2/8	96/23	239/70	9/13	102/13	247/63	4/13	100/24	0.5	0.79	0.63	Extensive to Transtensive	7	15
	27	Normal	Sandstone	6	101/17	334/63	198/21	96/17	303/71	180/11	97/13	326/70	191/15	0.5	0.67	1.7	Pure Strike Slip	106	90
	28	Reverse	Sandstone	8	306/30	213/6	112/59	311/28	219/4	123/57	306/31	215/2	122/59	0.7	0.38	1.76	Transpressive to Strike-slip	130	125
	29	Reverse	Sandstone	7	184/40	280/6	17/49	186/39	286/13	32/50	184/40	279/5	14/49	0.9	1	1.27	Transtensive to Strike Slip	107	105
	30	Reverse	Sandstone	7	88/9	196/63	354/25	113/19	226/48	13/37	80/14	189/52	340/34	0	0.36	1.54	Strike Slip to Transpressive	87	114
	31	Reverse	Sandstone	6	339/11	246/15	104/71	172/0	262/39	99/49	349/10	255/24	99/64	0.1	0.33	2.3	Compressive to Transpressive	160	183

Note: Software applications used for this analysis are Win_Tensor (v.5.9.2; Delvaux and Sperner, 2003), T- Tecto studio X5 (Žalohar and Vrabec, 2007) and FaultKin (v.8.1; Marrett and Allmendinger, 1990; Allmendinger et al., 2012). RDM: Right Dihedral Method; σ1 – maximum principal stress axes; σ2 – intermediate principal stress axes; σ3 – minimum principal stress axes (σ1> σ2> σ3). Trend and plunge measured in degree. Stress ratio (unitless) R obtained from Win_Tensor and D from T-Tecto. Stress regime index - R′ (unitless) is obtained from Win_Tensor.

and inclined fault surfaces. The near-vertical fault planes at places crop out for tens of m high; Supplementary Fig. 5). The NW-striking faults are parallel to some dolerite dyke margins (Fig. 5) in the western side outcrops of the Dhorimana hill area. These NW–striking faults depict strike-slip movement (Fig. 5a–c). The dolerite dykes are fine-grained and 8–~90 cm thick (Fig. 5). Transverse fractures, most likely cooling joints (Budkewitsch and Robin 1994; Misra and Mukherjee, 2017), are present at many places within these dykes (Fig. 5a). Dyke bridges and dyke-lets occur locally (Fig. 5a). Such features provide good indicators of the σ3 direction (trending ~ N). These dykes most likely relate to the last and final phase of the Malani magmatism in the Late Proterozoic, as deciphered from elsewhere from western Rajasthan, India (Pandit et al., 1999; Pooranchandra Rao et al., 2003; Sharma 2005).

The brittle shear fractures have cut across the host MIS and the dolerite dyke, with the NW trending Y – plane oriented along the boundary of the dyke and host MIS contact surface while the P- planes cutting across the dyke and MIS (Fig. 5a, d and e). This indicates that the NW-trending faults are of later origin after emplacement of the dykes and the weak planes along the dyke margins possibly favoured the next phase of brittle deformation.

Relation of these dykes with precursor of Deccan magmatism is unlikely since *(i)* no Deccan volcanic-related outcrops occur in the western rift shoulder of Barmer basin associated with MIS, *(ii)* the texture of these dykes differs from that of Deccan volcanic outcrops in Sarnoo area, and *(iii)* brittle shear cut across the dyke and host MIS, indicating that the dykes are of older age equivalent to MIS of Late Proterozoic. However, radiometric dating of these dykes can reveal the precise age relations.

Overall most of the NW and NE faults exhibit oblique-slip and near strike-slip movement. In the entire Dhorimana hill area, a total of 124 fault-slip data were considered for paleostress analysis. Eight paleostress tensors were obtained from these outcrops (Fig. 10; Supplementary Figs. 10 and 11; Table 1). These falls under strike-slip to transtensive (Fig. 10 no. 9–15; Supplementary Figs. 10 and 11; Table 1; also see field photos Fig. 4a–k and 5) and transpressive regime (Fig. 10 no. 16; Supplementary Figs. 10 and 11; Table 1; also see field **photo** Fig. 4l).

4.1.3. Around Sarnoo hill area, eastern margin

The outcrops near Sarnoo/Sarnu village in eastern margin consist of Lower Cretaceous fluvial clastic exposures as hillocks on the either sides of the road (State Highway16). The MIS basement rock crops out locally adjacent to the clastic outcrops on the northern side of the road. In two outcrops, basaltic rocks appear in the basal part of the Lower Cretaceous succession. These could probably be the Karentia volcanic event of Aptian age (**~122–113 Ma**; Compton, 2009; Bladon et al., 2014). Faults in the Sarnoo hill outcrops dip between ~60 and 85° (Fig. 1b). Most of the faults extend for a short distance (1 to < 10 m). The Sarnoo hillock outcrops have abundant NE-trending faults, though there are good proportions of the NW faults. The trend of the NE faults ranges from ~ E to NNE (Figs. 6 and 7). The ~ E and NE-trending faults have dm-**s**cale throw and are mostly present in the upper unit of the Ghaggar-Hakra Formation (Supplementary Figs. 6 and 7). NE to ENE trending faults associated with syn-sedimentary growth (Supplementary Figs. 6 and 7) have been identified in the Early Cretaceous sandstones of Sarnoo hill area in eastern margin. These points to the first rifting event in the basin. Majority of the faults in the Sarnoo outcrops are dip-slip to oblique-slip, with few having strike-slip movement (Figs. 6 and 7). Normal faulting is predominant in this area.

Slickenside kinematic indicators include mainly steps and few curved marker**s.** 10–100 cm thick fault gouge is seen mainly associated with moderate to steep-dipping faults (Fig. 6a, d, e; Supplementary Fig. 7a). Paleostress analysis includes a total of 188 fault-slip data from the Sarnoo hill outcrops. Fifteen stress tensors were deduced. Out of these, nine tensors depicts extensive to transtensive regime (Fig. 11**, no. 17–23, 25–26;** Table 1; Supplementary Figs. 12 and 13**;** also see field photos Figs. 6a–k, 7a-c), four falls under strike-slip category (Fig. 11, no. 24, 27 and 29–30; Table 1; Supplementary Figs. 12 and 13; also see field photos Fig. 6l-m, 7d-e, g-h), and the remainder two denotes transpression to compression (Fig. 11, no. 28 and 31; Table 1; Supplementary Figs. 12 and 13; also see field photos Fig. 7f, i).

4.1.4. Along Devikot - Fatehgarh ridge, northern margin

Paleocene – Eocene sequence**s** crop out along the uplifted Devikot – Fatehgarh ridge/Fatehgarh Fault. It consists of the Paleocene Fatehgarh and Barmer Hill Formations, and Eocene Bariyada Member and Dharvi Dungar Formation. Erosion and neotectonic activeness (Dasgupta and Mukherjee, 2019; Biswas et al., 2022b) are higher in this area. Thus, too few (<10) quality data on fault-slip are available from here. Out of these many are interconnected and thus are avoided in the paleostress analysis. The uplifted Fatehgarh Fault (reverse) scarp displays mega-scale relay structures, observed in Google Earth imagery and identified from field (Fig. 8a). The transfer zones constitute both approaching and overlapping relay ramps (Morley et al., 2007; Dasgupta and Mukherjee, 2017; 2019; Dasgupta, 2019). The approaching relays are connected by transfer fault scarps at places. Eocene Bariyada Member is flexed locally along the uplifted hangingwall block between the two consecutive transfer zones/faults (Fig. 8b and c). Local lateral compression produced between two transfer faults probably created this flexure. The transfer zones guide the seasonal drainage system down slope through deep channel cuts and gorges (Fig. 8d).

The Fatehgarh sandstone outcrop along the Fatehgarh Fault trend are locally faulted and fractured. Two sets of faults and/or joints occur – one along ENE to ~E and the other ~ N (Fig. 8e and f). The ~ E trending faults are dip-slip normal while the ~ N-trending faults are commonly strike-slip (Fig. 8e and f). The fault surfaces are cemented with calcite and kaolinitic mineral. As mentioned earlier, the slickenside kinematic indicators observed on these cemented fault surfaces, and are not considered for paleostress analyses. The ~ N trending strike-slip faults are essentially related to the transfer faults, near orthogonal to the Fatehgarh Fault trend. These observations indicate that the fractures in the Fatehgarh Formation (sandstone) and subsequent cementation and faulting (~N and ~E), along the northern margin of the basin occurred much later, presumably in Neogene to Quaternary. This was probably linked with the Himalayan orogeny (Kelly et al., 2014).

4.2. Outcome of drainage morphometric analysis around Barmer

The maximum elevation of the terrain around Barmer is ~640 m with distinct slope break from hilly areas of MIS to flat desert plain (Fig. 12). Three seasonal drainage basins originate in the hilly terrains, west of Barmer and flows down towards E/SE and ultimately disappears into the desert plains (Fig. 12). The geomorphic parameters - hypsometric integral (Hi) and hypsometric curve are commonly used to recognize the landscape evolution stages and associated erosional processes. This is a key element to analyse tectonic activeness, lithologic and/or climatic effects on a terrain (Keller and Pinter, 2002; Siddiqui and Soldati, 2014). Accordingly, three drainage basins have been identified around Barmer and Jasai in the western rift shoulder (Figs. 12 and 13). Hi has been calculated (Strahler, 1952; Keller and Pinter, 2002) using elevation of the individual drainage basins, which defines the area of interest. Hi is defined as follows:

$$\text{Hi} = (\text{Mean elevation} - \text{minimum elevation}) \,/\, (\text{maximum elevation} - \text{minimum elevation})$$

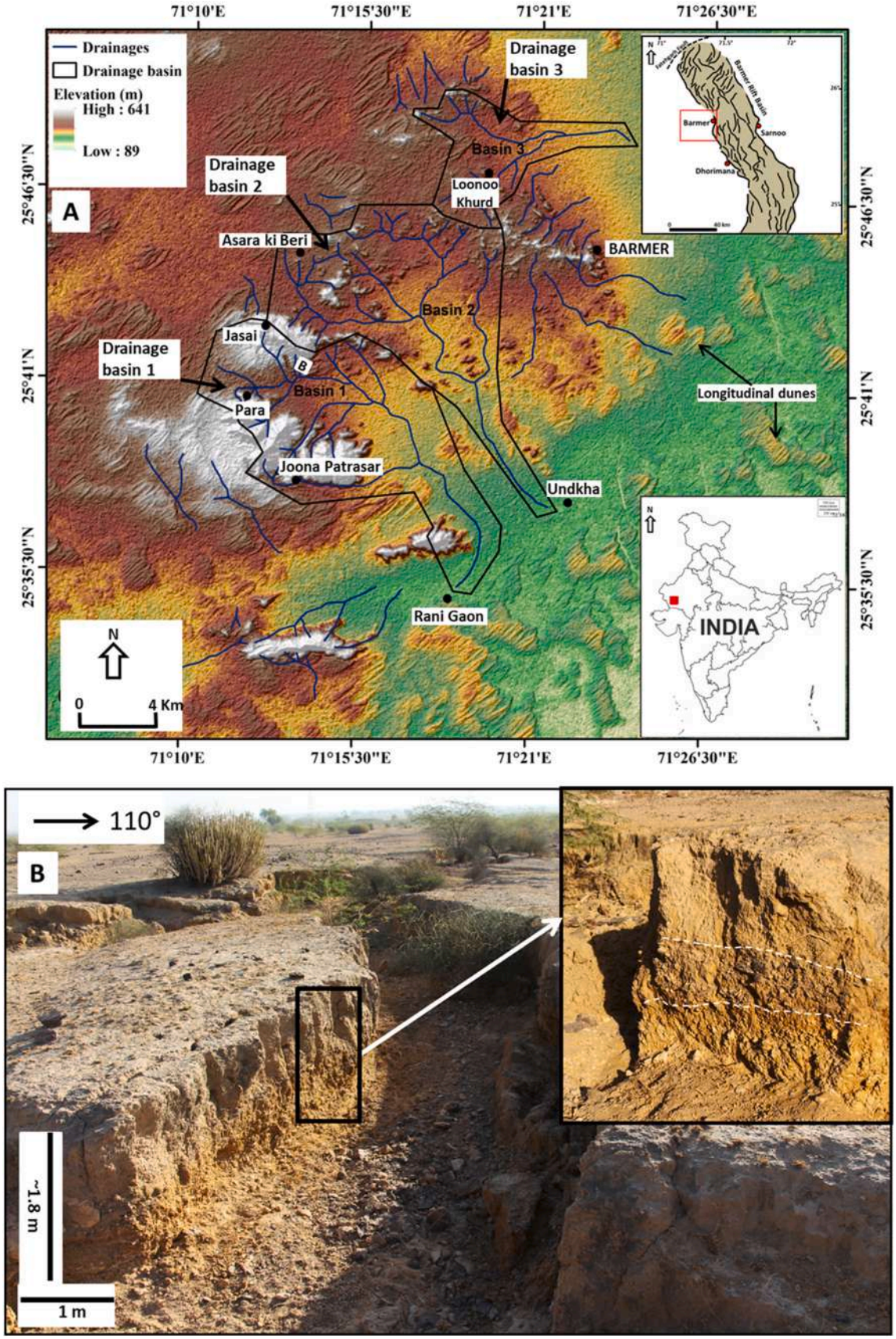

Fig. 12. **(a)** SRTM digital elevation model (DEM) image of the study area. Blue line indicates river traced from the base map (ng-42-12). Black polygons are the drainage basin/watershed. Top right inset: location of the drainage morphometry study area with respect to Barmer basin structure map. Bottom right inset: location marked in map of India. **(b)** Dry channel gully with deep vertical cut observed SE of Jasai village, location (b) marked in Fig. 12a, indicate tectonically controlled geomorphic terrain. Top right inset: 3 cycles of fining upward recent deposition is observed on the vertical channel cut section.

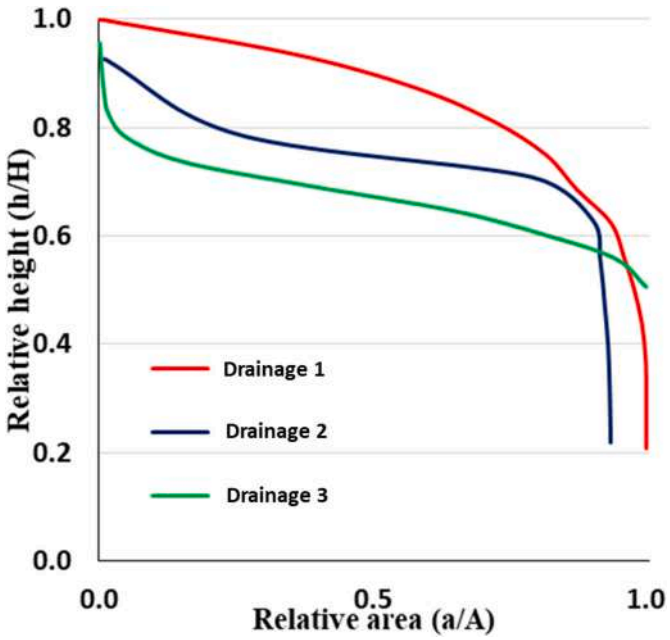

Fig. 13. Hypsometric curves of all the three drainage basins near Barmer region as shown in Fig. 12a.

The Hi values for drainage basins 1, 2 and 3 are 0.32, 0.29 and 0.33, respectively. In the present study, all the three drainage basins show different types of hypsometric curves (Fig. 13) even though the area is small and with very less difference in Hi values. Within ~600 km^2 area, the channels selected for the study shows three stages of landscape evolution. Drainage 1 shows convex-up geometry. This indicates a youthful landscape. Drainages 2 and 3 are characterized by sigmoid hypsometric curves. This indicates that the landscape is relatively older and at the mature stage of development. The above parameters and geomorphic indices calculated for the three small drainage basins indicate that some parts (e.g., drainage 1) of the western margin of Barmer basin can be considered as tectonically active region.

4.3. *Inference from stress inversion of earthquake focal mechanism data*

Stress inversion analysis using Right Dihedron and Rotational Optimization methods in Win_Tensor **(v.5.9.2;** Delvaux and Sperner, 2003**)** precisely identifies the stress ratio and stress axes positions **(e.g.,** Irmak, 2013; Mishra et al. 2020; Ali et al. 2021**).** The Rotational Optimization method reduces the misfit angle/function of the stress tensors. The best fit focal planes are considered for a decisive inversion and deduction of principal stress ratio for a consistent stress field (Gephart and Forsyth, 1984).

In the present study the results from both these methods resemble. The average misfit function derived from the Right Dihedron method is 21.7, whereas for Rotational Optimization method it is 7.5. Both the methods depict a strike-slip transpressive stress regime (Fig. 14) prevailing in the NW Indian basins. The obtained present day SHMax from the stress inversion analysis is trending towards N. This transpressive stress regime is responsible for the neotectonic deformations and activeness as observed in the N - NW part of the basin and in the W rift shoulder area near Barmer. It is to be noted that few stress tensors derived from the fault slip analysis depicts a transpressive to partly compressive stress regime with SHMax trending NW to NE **(no. 8** in

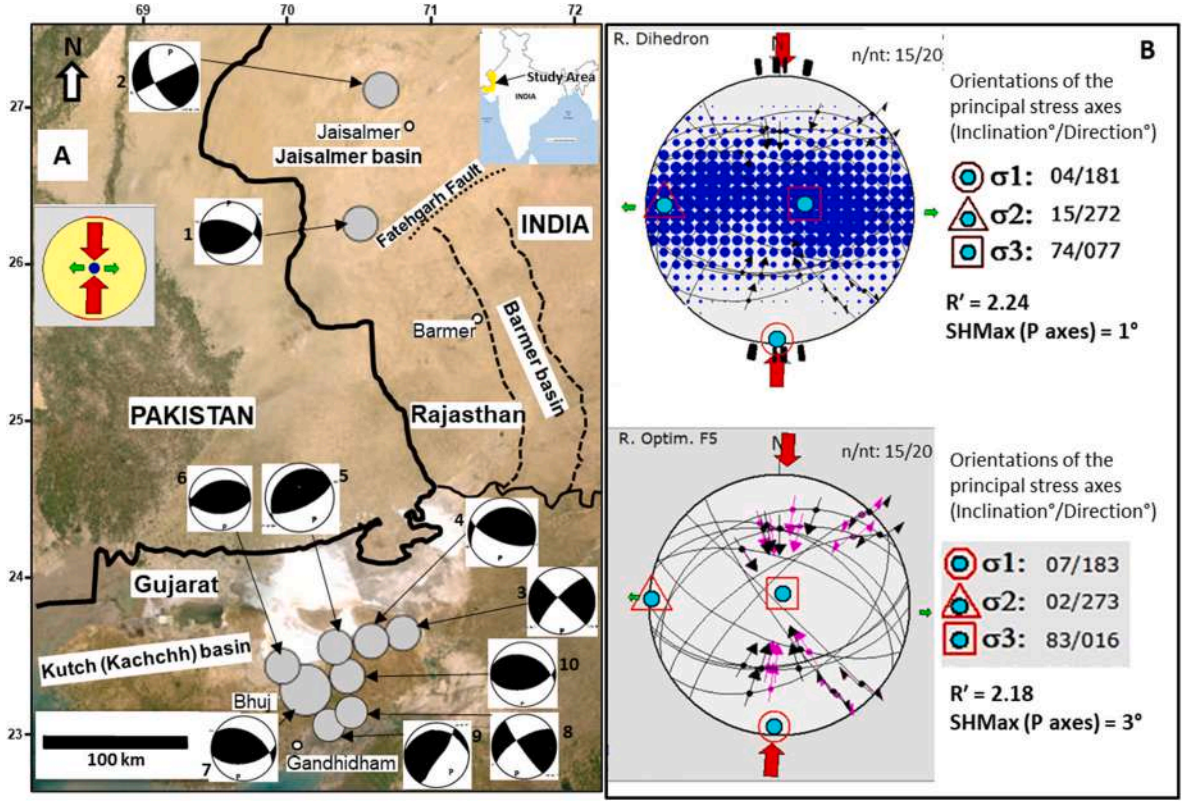

Fig. 14. (a) Earthquake focal mechanism in the NW Indian basins as derived from USGS website (earthquake.usgs.gov). The black and white areas in the beach balls represents compressional and tensional quadrants, respectively. Refer to Supplementary Table 3 for parameter details of the respective beach balls. Left inset – red arrow represents σ1 (P axis) direction while green arrow represents σ2 intermediate axis. **(b)** Stress inversion analysis results performed with the earthquake focal mechanism data. Top – Right Dihedron method with misfit function of 21.7. Bottom - Rotational Optimization method with misfit function of 7.5.

Fig. 9; **no. 16** in Fig. 10; **no. 28** and **31** in Fig. 11**).** However, these were not considered for the final outcome of the paleostress analyses since the number of fault slip data in each of these stress tensors were less than 10.

5. Discussions

The interpretation of the fault-slip data and the stress tensors obtained from paleostress analyses from the western and the eastern margins of the Barmer basin indicates: *(i)* normal faulting is dominant on both eastern and western margins, *(ii)* dip-slip normal faults are more numerous in the eastern margin-the Sarnoo hill area, whereas oblique-slip predominates in the western margin, *(iii)* strike-slip to transtensional and transperssional regimes are dominant in the western margin with limited extension and compressional regime, and *(iv)* pure extensional to transtensive regime mostly in the eastern rift margin. A relationship between the number of fault-slip data used for the paleostress analysis and corresponding stress regime index (R') value (majority between 0.5 and 1.5, with a few between 2 and 2.3) depicts that the governing stress regimes in the Barmer basin in its evolution is dominantly extensional and strike-slip (Fig. 15).

Overall, the W margin is governed by strike-slip regime whereas the E margin is dominated by extensional to transtensional regime. The reason for such structural mechanical differences on either side of the rift margin remains an open question. Probable causes are *(i)* variation in rheology of the rock types, *(ii)* presence of pre-existing fractures, *(iii)* oblique extension and *(iv)* variation in magmatic intrusion related to precursor of Deccan volcanism during rift evolution.

Outcrop-based structural analysis also infers the relative age correlation of the brittle deformation events considering the cross-cut relation between two faults and the rock type or stratigraphic unit affected by the deformation.

Paleostress regimes and relative timing: The computed stress tensors from the paleostress inversion analysis of total fault-slip data were correlated considering the orientation of maximum and minimum horizontal stress axes (SHMax and Shmin, respectively), stress ratio (D and R) and stress regime index - R' (Angelier, 1984; Delvaux et al., 1997; Zain Eldeen et al., 2002; Delvaux and Sperner, 2003; Tripathy and Saha, 2013; Dutta et al., 2019; Köküm and İnceöz, 2020; Hossain et al., 2022; Kumar et al., 2022a). Note that even for a particular tectonic/stress stage the stress field may change, i.e. the relative magnitudes of the stress axes can vary (Zain Eldeen et al., 2002; Kaymakci, 2006; Bubniak et al., 2021; Åse et al., 2022; Assie et al., 2022). Along with R', the maximum horizontal stress (SHMax) provides clues regarding prevailing stress conditions and orientation. Paleostress analyses from both Win-Tensor and T-Tecto software applications provide the SHMax orientation value for each of the stress tensors (Table 1). SHMax can be σ1 if the stress regime is transpressive to compressive, σ3 (sub)vertical while σ1 and σ2 are (sub)horizontal. In case of strike-slip regime σ2 is vertical and σ1 and σ3 horizontal; SHMax is defined by σ1. While SHMax can be σ2 if the stress regime is extensive to transtensive, i.e. when σ1 is (sub)vertical while σ2 and σ3 are horizontal (to sub-horizontal). Among the 31 stress tensors obtained from the analysis, 16 tensors having fault slip data more than 10 for each stress tensors are considered for rift kinematic study. These tensors are no. 1, 2, and 4 from Barmer area; no. 9–15 from Dhorimana area; and no. 17–22 from Sarnoo area. These 16 stress tensors have been segregated into four groups: D_{Δ}, D_{α}, D_{Φ} and D_{β}, considering the stress regime index (R') and orientation of the stress axes. We avoid numbers in subscripts in order to exclude any relative chronological implications. Detail discussions are provided in the following paragraphs.

Listric faults with dm scale throw and syn-sedimentary growth along the fault plane (Fig. 6a, e; Supplementary Figs. 6 and 7) have been identified in the Lower Cretaceous outcrops of E margin. Also, as stated earlier, cross-cutting relationship between NW and NE-trending faults indicates that the NE faults are of older age. These faults, trending NE to ~ E, exist in the stress tensors no. 17, 19 and 20 (Fig. 11) and present a NW-SE extensional stress regime with a NE-oriented SHMax. There is another similar tensor showing same behaviour: no. 3 from Barmer area (W margin), dominated by NE to ~E (Fig. 9), however not considered in

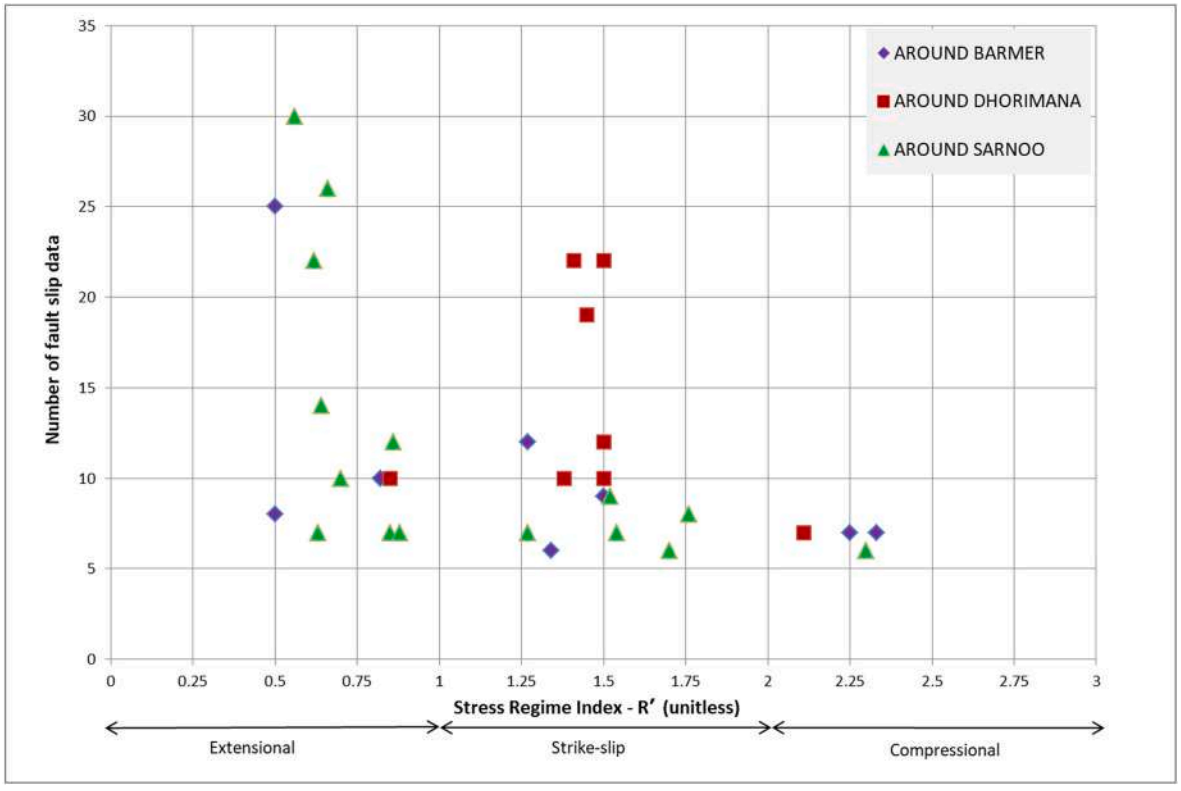

Fig. 15. Plot of stress regime index R' (Delvaux et al., 1997) versus number of fault slip data groups of respective locations from western (Barmer & Dhorimana) and eastern margins (Sarnoo) taken for the paleostress analysis. Plot shows extensional and strike-slip stress regimes were predominant during Barmer rift evolution.

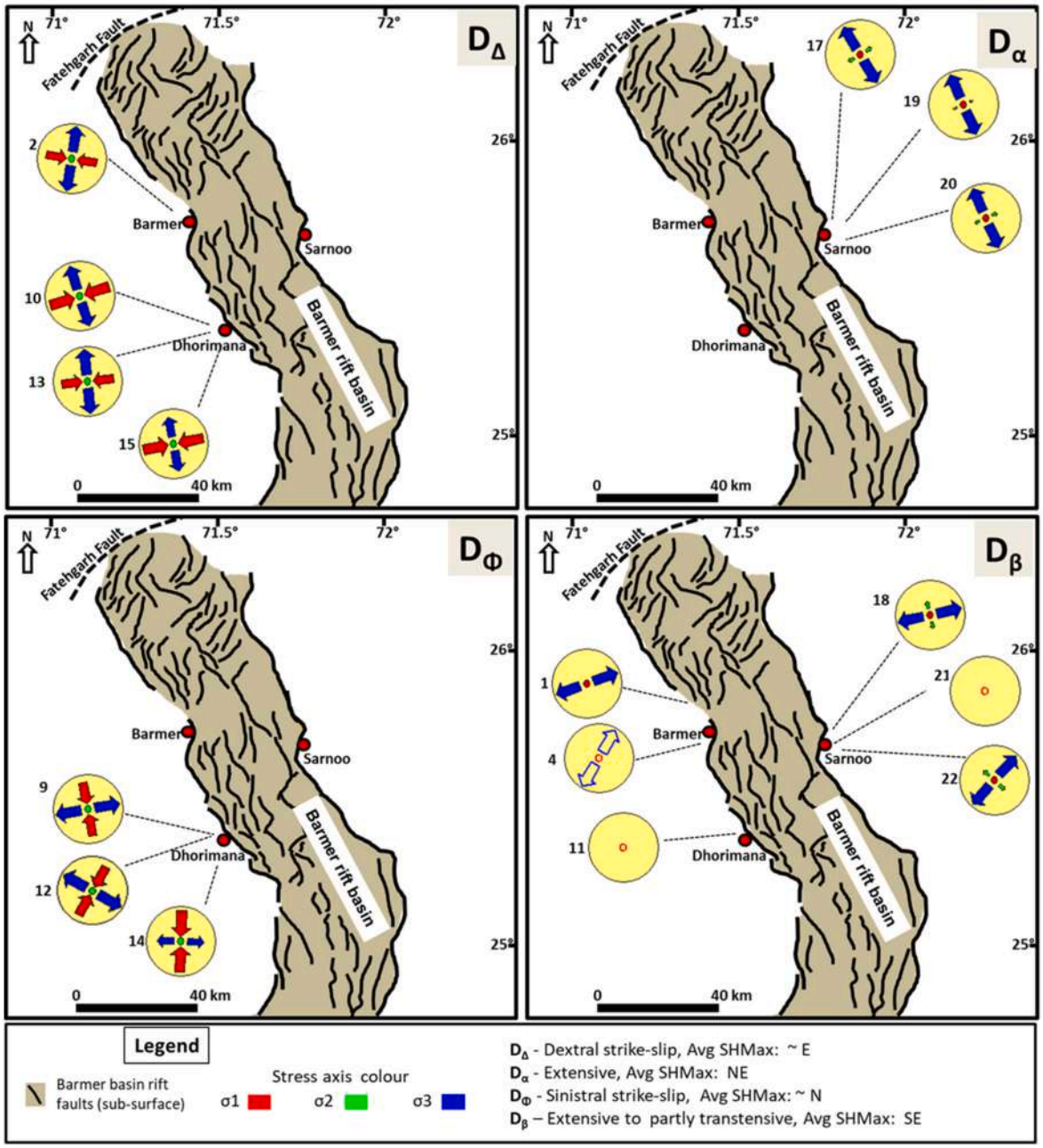

Fig. 16. Paleostress tensors of each group plotted on the structural fault map of Barmer basin. D_Δ group having four stress tensors with average SHMax = 84° (rounded off to nearest whole number). D_α group having three stress tensors with average SHMax = 64° (rounded off to nearest whole number). D_Φ group having three stress tensors with average SHMax = 7° (rounded off to nearest whole number). D_β group having six stress tensors with average SHMax = 152° (rounded off to nearest whole number). Red double arrow: orientation of σ1 principal stress (maximum). Blue double arrow: orientation of σ3 principal stress (minimum). Green double arrow: orientation of intermediate principal stress σ2.

the group because of a smaller number of faults. Such tensors belong to one particular tectonic stress regime, which underwent NW – SE trending extensional brittle deformation in the Early Cretaceous unit. This group is termed as 'D_α' in Fig. 16 with average SHMax trending 64°.

Another set of tensors are dominated by NW-trending normal faults that depicts NE-SW extension and belongs to extensional stress regime having SE-trending SHMax. These dip-slip to oblique slip normal faults occur in Barmer, Dhorimana (W margin) and in Cretaceous outcrops of Sarnoo area (E margin). The stress tensors showing such behaviours are – no. 1 and 4 from Barmer, no. 18, 21 and 22 from Sarnoo and no. 11 from Dhorimana (Figs. 9–11; 16). These faults have deformed the MIS at W margin and also affected the Cretaceous outcrops at E margin. Unfortunately, there are no Paleogene outcrops in W or E margins with brittle faults and slickensides. However, numerous NW-trending subsurface faults display slips and syn-sedimentary growth structures in the blind Paleogene Fatehgarh and Barmer Hill Formations as identified from seismic interpretation (Bladon et al., 2015; Dolson et al., 2015). Taking this into account we can infer that the stress tensors, no. 1, 4, 11, 18, 21 and 22 belong to a single tectonic stress regime depicting an overall NE – SW extension in the basin. This can be correlated to the Early Paleogene extension. This stress regime is depicted as 'D_β' in Fig. 16 with ~SE (152°) oriented SHMax. Point to note is that the extension direction (Shmin) of the above-mentioned tensors is not always orthogonal to the rift margin.

Several strike-slip to oblique-slip faults were identified from fieldwork. Strike-slip and transfer faults were also documented from seismic

data interpretation of sub-surface stratigraphy by the previous authors (Bladon et al., 2015; Dolson et al., 2015). Fig. 15 presents the tensors, which indicate a strike-slip regime (Figs. 9–11). Fig. 16 segregates this strike-slip to transpressive stress tensors into **two** groups as per the stress regime index (R') and the relative orientations of the stress axes (σ2 remains close to vertical in all cases). These tectonic stress regime groups are 'D_{Δ}' **and** 'D_{Φ}' (Fig. 16).

The stress regime group D_{Δ} depicts a dextral strike-slip regime with average SHMax ~ E (84°). There are four tensors from W margin (MIS outcrops), no. 2 from Barmer, while no. 10, 13 and 15 from Dhorimana. The majority of the faults are strike-slip. Under dextral transtension regime, the NW-trending faults depicts sinistral shear while NE-trending faults depicts dextral shear (e.g. Fig. 3b, 4k, 5a-c). The NW-trending faults depict reverse slip on a near vertical plane (e.g. Fig. 4k, 5c and 7g). σ1 is near-horizontal for most of the tensors with ~ E-W trend with <25° variation. The axis σ3 is also sub-horizontal, trending ~ N–S with <25° variation while σ2 is near vertical. A set of the strike-slip faults trending NW (tensor no. 13) are parallel to the dolerite dyke trend in MIS as identified in the Dhorimana area. Many of these NW-trending brittle shear has affected both the dolerite dyke and the host MIS rock (Fig. 5). We can infer that these faults are re-activated and pre-existing Late Proterozoic fractures/weak zones of MIS has guided this transtensive strike-slip movement.

The stress regime group D_{Φ} depicts a sinistral strike-slip regime with average SHMax ~ N (7°). All the three sensors are from Dhorimana area in W margin, **no. 9, 12 and 14** (Fig. 10; 16). Several faults are strike-slip, while there are also some normal and reverse oblique slip faults. Here the NW-trending strike-slip faults have dextral shear while the NE-trending ones have sinistral shear. The faults have affected only the MIS basement rock. σ1 is sub-horizontal for all the tensors and near vertical σ2 depicting pure sinistral strike-slip.

Assigning a geologic age to a particular stress regime (group) is always challenging, especially in areas affected by multiple tectonic deformations. In the present case, the two extensional stress regimes D_{α} and D_{β} are very distinct. D_{α} consists of NE to ~E trending fault planes and associated with syn-sedimentary deformation in the Early Cretaceous outcrop of E margin. Field observation of cross-cutting relation between NW and NE trending faults further confirms these two separate extensions. Thus, D_{α} can be linked to the first phase of extension during Early Cretaceous that affected the Barmer basin. This has an association with the initiation of separation of Madagascar from W Indian plate margin through strike-slip movement (Gombos et al., 1995; Reeves, 2013; Bladon et al., 2015; Gaina et al., 2015). The stress regime D_{β}, as mentioned in previous paragraph, depicts a NE-SW extension and such an extension happened during the main phase of Barmer rifting in Late Maastrichtian to Early Paleogene (Dolson et al., 2015; Bladon et al., 2015). Therefore, it can be linked to this tectonic episode.

The dextral and sinistral strike-slip stress regimes D_{Δ} and D_{Φ} have SHMax orientations of ~ E and ~ N, respectively. Assigning geological ages to D_{Δ} and D_{Φ} would be difficult since the faults/fault-slip data are present in the MIS rocks at the W margin. However, as per Fig. 16, D_{Δ} and D_{Φ} can be the two end members of stress regime D_{α}. This means there is a considerable rotation of horizontal stress axis from ~ E to ~ N or vice-verse i.e., either a dextral strike-slip regime followed by extension to transtension and then another sinistral strike-slip regime, or a sinsitral strike-slip regime followed by extension and then a dextral strike-slip regime. The group D_{Φ} can also be linked to progressive deformation after the main Barmer rifting event linked to India -Seychelles separation, considering the overall ~ N trending SHMax orientation. In other words, D_{Φ} can be a consequence of the north-ward movement of Indian plate after separation from Seychelles. In the present work we cannot conclude anything beyond this.

None of the stress regimes have been linked to Late Proterozoic to Cambrian extension. This is because *(i)* the rift developed in Late Proterozoic is presently far away, >200 km NE of Barmer basin, known as the Bikaner-Nagaur/Marwar basin, *(ii)* the fault-slips were collected from outcrops located just at the Barmer basin margin, the further outboard rift shoulder areas were not considered so that only the Barmer basin related tectonic events can be captured, and *(iii)* the pre-existing Late Proterozoic fractures gets inherited into the subsequent extensional episodes during Mesozoic and Early Paleogene time. Nevertheless, there can be subtle possibility that some of the strike-slip related tensors may be associated with the older Proterozoic deformation phase.

The obtained paleostress tensor results from the three applications depicts that: *(i)* the stress tensors derived from Win_Tensor and FaultKin analyses match, and *(ii)* there is relatively very less variation (≤25°) in the orientation of the three principal stress axes for the tensors derived from Win_Tensor and T-Tecto (Figs. 9–11; Supplementary Figs. 8–13; Table 1). The stress ratio 'R' derived from Win_Tensor and 'D' from T-Tecto, come very close, except for ~10 cases where the variation is slightly more (between 0.2 and 0.5). Several stress tensors depict steep plunge for one of the principal stress axes, rather than being vertical. The other two stress axes are near-horizontal. Also, the presence of pre-existing fractures and variation in rock property can result in rock anisotropy. These indicate non-Andersonian faulting within the Barmer rift basin (Anderson, 1905; Sibson et al., 1988; Yin and Ranalli, 1992; Yin and Taylor, 2008; Bonini et al., 2016; Pascal, 2022).

The MIS rock in the W margin and fluvial sandstone in E margin are largely non-foliated and homogeneous as observed in naked eyes (Figs. 2–4, 6-7). There are some dolerite dyke intrusions in the MIS in W part of Dhorimana outcrop (Fig. 5). Yet, the stress tensor (no. 13 in Fig. 10) obtained from the fault slip data along the dyke margins is similar to those where there are no intrusions (**no. 10 and 15 in** Fig. 10), as observed from Dhorimana location. Moreover, paleostress analyses have been executed in similar outcrops elsewhere (e.g., Lisle, 1989; Tripathy and Saha, 2013).

In areas where the sedimentary rocks are highly tilted, the paleostress inversion analysis becomes difficult to apply. In such cases a tilt correction is necessary for fault planes older or synchronous to the tilting event (Yamaji et al. 2005; Tripathy and Saha, 2013). No tilt correction is necessary for faults that postdates the tilting (Yamaji et al. 2005). In Sarnoo hill area, E margin, the Cretaceous fluvial sandstone bedding planes are observed at some places distributed irregularly. Also, due to large scale rock quarrying activity in this area, within the desert terrain, observations of continuity of bedding planes are difficult. The average bedding dip is between 8° and 20° dipping towards S to SE (**e.g.**, Supplementary Fig. 16; Beaumont et al. 2015). Since the dip is gentle, tilt correction was not required in this area (as in Yamaji et al. 2010).

Nevertheless, in order to minimise the uncertainties in the rift kinematics and structural evolution of the Barmer narrow continental rift basin, it is better to perform a structural restoration of seismic/geological cross section across the basin along with the rift shoulder areas. This will decipher the amount of isostatic uplift of the rift shoulders. Note that the rift shoulder uplift will have an impact on the pre-existing bedding dip and orientation. Thus, proper structural restoration will justify both these cases. Paleostress analysis performed with all such structural restorations can better define the rift kinematics and stress orientations. This can be the future scope of research in this basin.

Paleostress analysis from Barmer basin can in further lead to better structural interpretation of seismic profiles. Paleostress interpretation from faults derived from 3D seismic data (e.g., Gartrell and Lisk, 2005; Lacazette 2009; Ping et al., 2022) can narrow down the uncertainty related to assigning an age to a particular stress regime. It will also further improve the rift kinematic understanding and exploration to field development strategies. The paleostress regimes will have impact on sediment dispersal pattern and also on paleo fluid flow during different stages of basin formation (e.g. Dasgupta et al., 2022).

Tectonics of West Indian margin: Several researchers have documented and reviewed the tectonic framework of the western Indian plate margin (Biswas, 1987; Gombos et al., 1995; Pandey and Agrawal, 2000; Chatterjee et al., 2013; Reeves, 2013; Gaina et al., 2015; Bhattacharya and Yatheesh, 2015; Yatheesh, 2019; Mukherjee et al., 2020). The

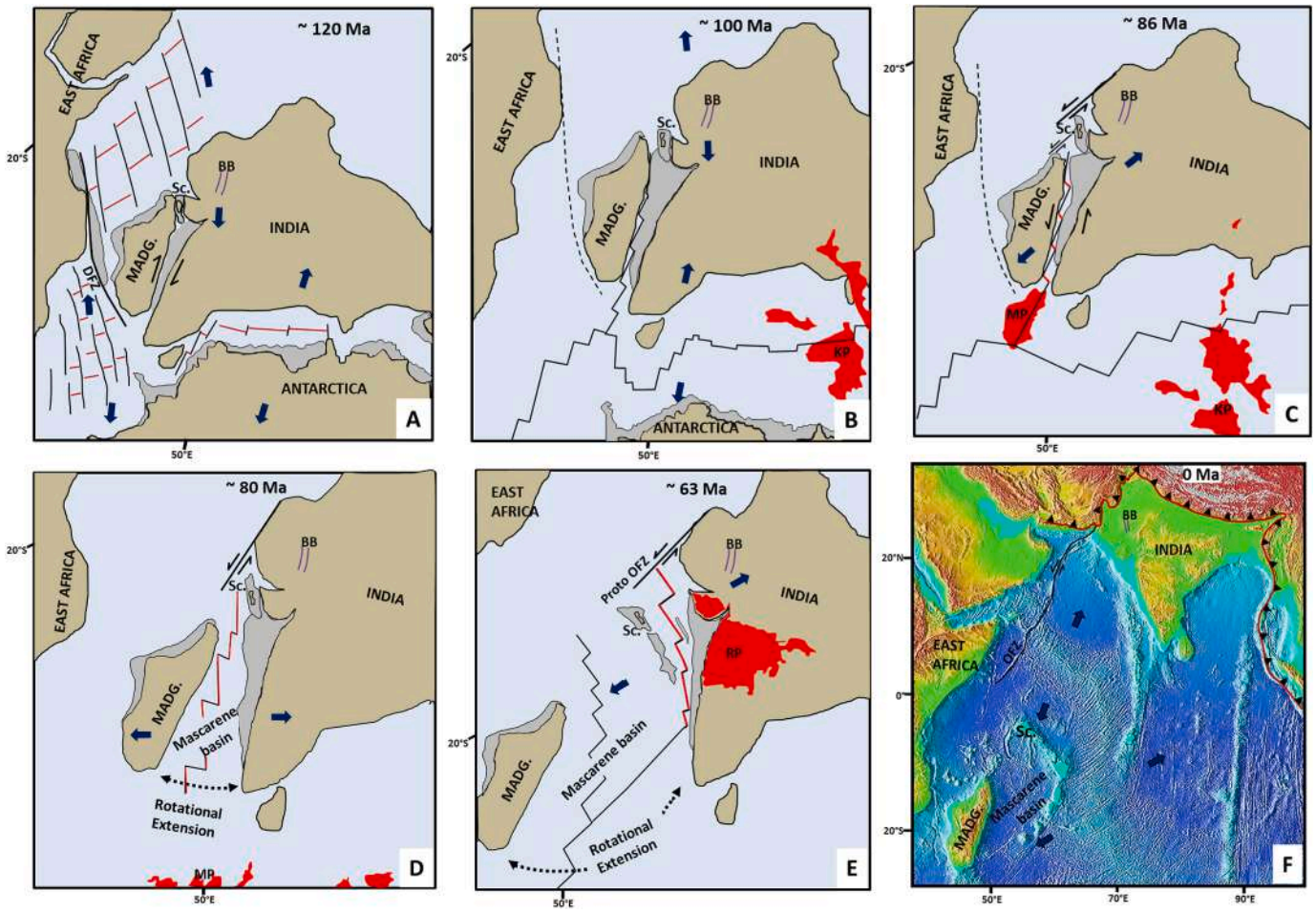

Fig. 17. (a–e) Schematic plate tectonic model of greater India, Antarctica, East Africa, Madagascar and Seychelles constructed at different geological time (adapted from Smith and Sandwell, 1997; Chatterjee et al., 2013; Gibbons et al., 2013; Reeves, 2014, 2018; Reeves et al., 2016; Pandey et al., 2019). **(a)** Accelerated separation of Africa from Antarctica and India at ~ 120 Ma. Extension between India and Antarctica is in continuation, the rate is slower compared to Africa and Antarctica separation thereby resulting in dextral strike-slip along Davie Fracture Zone (DFZ). The combined effect also initiated dextral movement between India and Madagascar. **(b)** The oblique extension between India and Madagascar continued till Albian time (~100 Ma). The strike-slip movement along DFZ have ceased by this time. **(c)** Continued oblique separation between India and Madagascar occurred during ~88 to 84 Ma. through sinistral strike slip. The Marion plume activity further helped this oblique extension. **(d)** Opening of Mascarene basin initiated due to rotational extension between India and Madagascar during Late Cretaceous (~80 Ma) guided by the Marion plume activity. The rotational extension between India and Madagascar developed a sinistral strike-slip movement along the NW margin of India and Seychelles during Late Cretaceous. The combined effect produced a transpressive regime in the NW part of Indian plate with includes the Barmer basin. **(e)** The asymmetric separation of Seychelles from Indian plate initiated during Maastrichtian and continued in Paleocene time. Réunion plume activity and related Deccan volcanism developed during this time (~68–63 Ma). The sinistral strike-slip movement along the NW to W margin of Indian plate continued during this time. It has been termed as Proto Owen Fracture Zone (Chatterjee et al., 2013; Pandey et al., 2019). **(f)** Present day position and plate tectonic boundaries around Indian plate depicted over Indian Ocean topographical map (URL-4). BB - Barmer basin; DFZ – Davie Fracture Zone; KP – Kerguelen plume; MADG. - Madagascar; MP – Marion plume; OFZ – Owen Fracture Zone; RP - Réunion plume; Sc. – Seychelles microcontinent. Blue arrows indicate the extension direction.

present paleostress analyses from the Barmer rift basin lead to the following synthesis. The basin has been largely affected by change in stress regime during its tectonics evolution related to different stages of plate movement from Jurassic to Recent (Fig. 17).

The paleostress outcome depicts that there are spatial and temporal changes in stress regime (Figs. 15 and 16). At west India, Jaisalmer – Indus and Kutch basins started evolving as Africa separated from India – Madagascar – Antarctica and formed Somali basin between west India and east Africa in Jurassic. This produced a broad shelf slope system in the present-day western Rajasthan (India) and east Pakistan. The Lathi Formation of Jaisalmer basin deposited during this earliest phase of extension documented in western Rajasthan – Jaisalmer and parts of N Barmer basin. However, the intensity was insufficient to produce any significant extension in the Barmer basin.

The opening of Somali basin and continued oblique separation of Africa from India – Madagascar and Antarctica produced a dextral strike-slip along the Davie Fracture Zone (DFZ, Fig. 17a), which continued till the Mid Aptian (~120 Ma, Reeves et al., 2016; Reeves, 2018). Movement between India and Madagascar initiated since Barremian – Aptian time which was initially a dextral strike-slip transtension. This transtension between Madagascar and India continued until about Late Albian (~100 Ma, Reeves et al., 2016).

The first significant brittle deformation and related sediment deposition occurred in the Barmer basin during Early Cretaceous linked to the initiation of the dextral transtension and oblique extension between India and Madagascar (Bladon et al., 2015; Dasgupta and Mukherjee, 2017). Such oblique extension during a strike-slip movement essentially produces pull-apart basin having normal faults with syn-sedimentary growth (e.g. Farangitakis et al., 2021; Dasgupta et al., 2022). The deformation in Sarnoo hill area, in eastern basin margin, typically shows similar structure. Even though the India-Madagascar separation is oblique, associated with strike-slip movement, in Barmer basin area it can produce local extension associated with pull-apart type basin formation. It did not produce a mature rift basin in the Barmer region. The

SHMax orientation varies from ~E to ~N, from D_{Δ} to D_{Φ} (Fig. 16), pointing to considerable stress axes rotation during the entire episode of India – Madagascar transtensional strike-slip separation.

India obliquely separated from Madagascar finally at ~88- 84 Ma by sinistral transtension (Storey et al., 1995; Reeves, 2013, 2018). This accelerated northward movement of Indian plate from Madagascar following onset of Marion plume activity (Fig. 16b–d; Storey et al., 1995; Chand and Subrahmanyam, 2013; Reeves, 2013, 2014, 2018; Pandey et al., 2019).

There is another school of thought for India – Madagascar separation: an initial sinistral strike-slip up to ~100 Ma followed by a dextral diachronous transtension (Fig. 9 in Gibbons et al., 2013, also see Gaina et al., 2007). Considering this model, the ordering of the stress regimes in the Barmer basin would be– initial sinistral strike-slip followed by oblique extension and finally a dextral strike-slip transtension. However, the later model does not properly consider the relative movement between *(i)* Africa and Antarctica and *(ii)* India and Antarctica during East Gondwana fragmentation. This is further strengthened by the plate tectonic model proposed by Reeves (2013, 2014, 2018), which explains the relative plate movements across the Davie Fracture Zone (DFZ, Fig. 17a). Nevertheless, largely it can be said that India - Madagascar separation was associated with strike-slip transtension and oblique extension. Out of the two possible models of India – Madagascar separation, one by **Reeves**, and the other by **Gibbons et al.** and **Gaina et al.,** the present work cannot specify which one is more accurate for the Barmer rift.

The transtension between India and Madagascar during Late Cretaceous produced rotational extension thereby generating Mascarene basin (Fig. 17c and d). The Marion plume activity further assisted this extension and separation of Madagascar (Pandey et al., 2019; van Hinsbergen et al., 2021). Overall, the Indian plate rotated counter-clockwise from Early to Late Cretaceous (Figs. 17a-d**).** This tectonic change also generated local/small-scale compression along the NW Indian plate margin, associated with strike-slip (Fig. 17c and d; Pandey et al., 2019). Such a tectonic episode also acted as a sweet spot to generate the next rifting phase between India and Seychelles. The Seychelles micro-continent extensional separation from NW India started to initiate in Maastrichtian and continued in Paleocene, the Réunion plume activity and related Deccan volcanism further aided the separation of Seychelles micro-continent from India (~68.5–63 Ma; Plummer, 1996; Collier et al. 2008; Ganerød et al., 2011; Torsvik et al. 2013; review in Misra et al. 2014; Pandey et al., 2019).

The asymmetric spreading and associated ridge jump between India and Seychelles initiated in the NW segment of Indian plate (Fig. 17e; Yatheesh, 2019; Pandey et al., 2019). The relative extension was greater in the NW part than in the SE, between W India and Seychelles. This resulted in anti-clockwise rotation of Seychelles micro-continent (Chatterjee et al., 2013; Pandey et al., 2019). This also formed the proto-Owen Fracture Zone (OFZ) with a sinistral slip (Fig. 17e). The Barmer basin evolved during this time into an elongated matured rift basin. The paleostress regime D_{β} likely to be related to this event. As mentioned earlier and from the above discussion it is evident that the extension direction need not be orthogonal to the rift axis. The pre-existing ~ NNW basement fractures and ~NE faults further guided the rift fault propagation and obliquity.

Continued northward movement of Indian plate followed by soft and hard collisional tectonics associated with Himalayan orogeny (e.g. Chatterjee et al., 2013; Mukherjee et al., 2013; Mukherjee, 2015) resulted in neotectonic events in the Barmer basin area. The present-day stress regime in NW India is strike-slip transpressive with SHMax trending N as derived from the earthquake focal mechanism data (Fig. 14). Also, the SHMax orientation observed from borehole breakout and image data and earthquake focal mechanism in the sedimentary basins of NW India is ~ NE to NNE and ~ N (Fig. 17f; Chandra, 1977; Chung and Gao, 1995; Chatterjee et al., 2013; Abdelaziz et al., 2016; Chatterjee et al., 2017; Dash et al., 2017; Sen et al., 2019; Singh and Ghosh, 2019).

The recent tectonic changes are indicated by: *(i)* the uplifted Fatehgarh fault trend along northern margin of the basin, *(ii)* ~ NW and ~ ENE trending fault-slip observed on cemented fractures of Fatehgarh Sandstone, *(iii)* transfer zone guided seasonal drainage and *(iv)* active lineaments along the western margin (Figs. 1 and 8). Neotectonic activeness has been additionally recorded from the morpho-tectonic analysis along the eastern and western basin margin (Styron and Pagani, 2020; Biswas et al., 2022b). The remote sensing analyses around Barmer also suggest that parts of the western margin area are tectonically active. Outcrop-based spot study of the dry channel cuts and gullies indicate tectonically controlled geomorphic terrain (Fig. 12b). Furthermore, compressional structures and fault reactivation have been reported from the N part of the Barmer basin based on interpreted seismic data (Dolson et al. 2015). All these events are probably linked to a transpressive to partly compressive stress regime with ~ N trending SHMax, prevailing in the NW part of India.

Brittle deformation and fault gouge: Brittle faulted sedimentary, igneous and metamorphic rocks can result in different types of fault rocks-mylonite to fault gouge. Upper crustal deformation is dominated by cataclasis resulting in fault gouge and breccia whereas lower crustal brittle deformation produces mylonite zones (Scholz, 1987, 2002). A typical fault gouge zone consists of mixtures of fine-grained quartz, clay minerals e.g., kaolinites and phylosilicates (Crawford et al., 2008). In a rock body under high effective stress, increase in fault gouge thickness and associated fine-grained clay mineral content tend to decrease the permeability and frictional strength of the fault zone (Crawford et al., 2002, 2008; Ikari et al., 2009; Torabi et al., 2019). Thus, fluid flow across and along a fault zone depends upon the complexity, thickness and mineral compositional variation of the fault gouge (Shipton et al., 2005).

Also, in many cases, an overall linear relation exists between the fault gouge thickness and fault-slip, i.e., with increase in slip the gouge thickness increases (Scholz, 1987; Marrett and Allmendinger, 1990; van der Zee and Urai 2005; Torabi et al., 2019). However, this linear relationship may not justify in some cases where there is influence of per-existing fractures on the fault plane (van der Zee et al., 2008).

Field observations from Barmer basin show more numerous occurrences of fault gouge in the Cretaceous sandstone outcrops of Sarnoo hill area, eastern basin margin (Fig. 6a, d, e; Supplementary Fig. 7a), than in western margin. The average fault gouge thickness when plotted against fault dip depicts an approximate increase in the thickness with decrease in dip (Fig. 18). The variation is more in the Cretaceous outcrops of Sarnoo hill area. Thus, taking this observation into account, it can be predicted that the relatively gentler sub-surface faults with dip 40–60° at depths in Cretaceous unit towards eastern margin probably have thicker fault gouge.

These faults/fault zones can act as good fault-bound structural traps in sub-surface. The Mesozoic stratigraphy is much less explored in the Barmer basin. Such field observations in the Mesozoic unit can be useful for future explorations of deeper targets. Nevertheless, detail fault geometry study and fault seal analysis from 3D seismic data along with well information are required to identify potential target reservoirs.

Oblique rifting: The strike-slip transtension during Late Cretaceous and Early Paleogene generated oblique extension in the Barmer basin. The rotation of SHMax with varying stress regime (D_{Δ} to D_{α} to D_{Φ}) during Cretaceous to Paleogene is one of the prime factors for the rift obliquity of the Barmer basin. The other two factors, which favoured the oblique rifting are: *(i)* structural inheritance of pre-existing, ~N/NNW trending MIS basement fracture during the two rifting phases in Cretaceous and in Maastrichtian to Paleocene, and *(ii)* asymmetric extension during India-Seychelles separation. The subsurface fault map of the Barmer basin (Fig. 1a) also portrays rift obliquity, especially in the N part of the basin associated with NE cross faults and relay structures at a higher angle to the rift axis trend. Also, the paleostress tensor group D_{β} depicts that the extension direction is not necessarily orthogonal to the

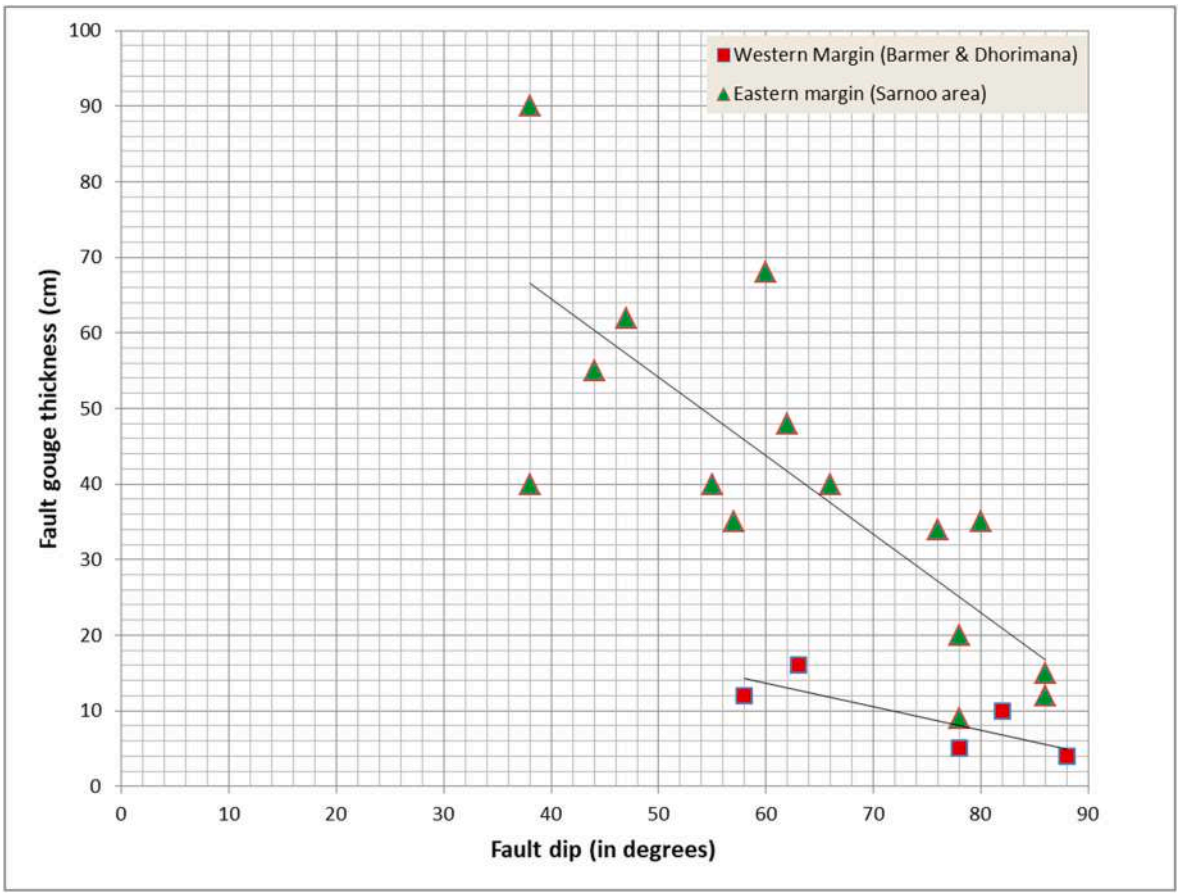

Fig. 18. Plot of fault gouge thickness versus corresponding fault dip. Majority of the faults with gouge are from Sarnoo hill area in eastern basin margin, only a few are from the western margin.

rift margin/axis for all the tensors (Fig. 16).

Similar examples for rift obliquity can be found from various basins worldwide, e.g. central Norway (Titus et al., 2002), Ethiopian rift (Bonini et al., 1997; Corti et al., 2013; Philippon et al., 2014), East African rift system (Morley, 2010), Baikal rift (Philippon et al., 2014), Palar-Pennar basin, Indian east coast (Dasgupta et al., 2022), Gulf of California and the Gulf of Aden (Withjack and Jamison 1986; Withjack et al., 1998; Brune and Autin, 2013; Brune et al., 2018). As a result of such oblique rifting, there would be modification in fault dip and slip due to change in stress regime and the fault-controlled sediment depocenters will vary across the basin. This has been observed in Barmer rift basin.

Crustal thinning and magma under-plating in extensional regimes such as intracratonic rift basins have been recognized worldwide, e.g. Iberia/Newfoundland margins (Lavier and Manatschal, 2006), Baikal rift in Siberia (Thybo and Nielsen, 2009) and Vøring basin, Norway (van Wijk et al., 2004). Narrow rifts are more prone to such crustal thinning and magma upwelling, especially when they are affected by multiple deformation events (e.g., Gulf of Suez and Rhine Graben, Buck, 1991; Corti et al. 2003). The Barmer oblique rift basin and Cambay basin towards south exhibit similar characteristics, i.e. magma upwelling towards E to SE side of the basin and also in parts of basin centre. This has been identified from gravity modelling, seismic interpretation and radioactive age dating of the volcanic rocks (Mishra, 2011; Dasgupta and Mukherjee, 2016; Chouhan et al., 2020; Burley et al., 2023). Such crustal thinning and magma upwelling generate heat influx within a rift basin. These play key roles in rift evolution and crustal deformation (Buck 1986, 1991; Watts, 2001; Ziegler and Cloetingh, 2004; Whitney et al., 2013; Cunha et al., 2021).

6. Conclusions

The Barmer intra-continental oblique rift basin has evolved though different tectonic phases guided by structural inheritance of MIS basement fractures. This is the first work on paleostress analysis based on fault-slip data from this basin. The key conclusions are:

1. Paleostress analysis depicts that the western margin of the basin was dominated by strike-slip regime whereas the eastern margin is governed by extensional to transtensional regime during its tectonic evolution from Cretaceous to Paleogene.
2. Paleostress analysis work also portrays that *(i)* the basin has undergone two main extensional – transtensional events i.e. NW oblique extension in Early Cretaceous followed by NE extension in Late Maastrichtian to Early Paleogene, supporting earlier works, *(ii)* Strike-slip to oblique extension associated with an anticlockwise rotation of stress axes during Madagascar's separation from India, and *(iii)* asymmetric extension happened during Late Maastrichtian and Paleocene. This is the main rifting event in the Barmer basin linked to India – Seychelles separation. Anticlock-wise rotation of Indian plate has been agreed by previous workers (**e.g.,** Keary et al., 2013**).**
3. Structural inheritance, linked to MIS basement fractures and early ~ NE extensional fractures, play important roles in the basin as has been observed from variation in stress regime and extension type during different tectonic phases. These kinematic changes led to obliquity of the Barmer rift. The overall basin geometry also portrays this oblique nature of the Barmer basin.
4. Remote sensing image and outcrop analyses indicate that parts of the western margin of the Barmer basin is neotectonically active. Stress

inversion analysis from earthquake focal mechanism data depicts that transpression has been prevailing in NW India with a ~ N-trending SHMax orientation. This is responsible for the neotectonic activities observed in the basin surrounding. Also, this transpression event results in fault reactivation and inversion of subsurface structures.

5. A number of dipping faults trending NE to E in Lower Cretaceous sandstone, Sarnoo hill area consist of thick fault gouge having fine-grained clay minerals, associated with syn-sedimentary growth. Moderately dipping faults tend to have thicker fault gouge. Presence of such faults in sub-surface Cretaceous units can act as potential structural traps.

Author contributions

SDG – data gathering from field outcrops, paleostress analysis, tectonic model building, manuscript writing and finalization. **SM –** Supervision, conceptualization and finalization of the manuscript. **NV –** Geomorphologic work related to neo-tectonic activeness in the western basin margin. **RC –** Supervision and finalization of the manuscript. **SKP –** Supervision.

Declaration of competing interest

Authors express no conflict of interest with anyone regarding this ms.

Data availability

Data will be made available on request.

Acknowledgements

The work was initiated as self-funded work by SDG and SM. In later phase, SM was funded from the Center of Excellence in Oil, Gas and Energy, IIT Bombay (grant number RD/0120-PSUCE19-001). We dedicate this article to Prof. P.K. Saraswati (retired from IIT Bombay). We thank the three anonymous reviewers and Dr. Chris Elders for constructive detail review in two rounds, also acknowledge Profs. Alexander L. Peace and Massimo Zecchin for punctual editorial support.

Appendix A. Supplementary data

Supplementary data to this article can be found online at https://doi.org/10.1016/j.marpetgeo.2023.106442.

References

Abdelaziz, S., Leem, J., Praptono, A.S., Shankar, P., Mund, B., Gupta, A.K., Goyal, R., Sidharth, P., 2016. An integrated workflow to the Success of complex tight-gas reservoirs development north of India: case study. In: Paper Presented at the IADC/Society of Petroleum Engineers Asia Pacific Drilling Technology Conference. Singapore, SPE-180586-MS.

Al-Husseini, M.I., 2000. Origin of the arabian plate structures: amar collision and najd rift. GeoArabia 5, 527–542.

Ali, S.M., Abdelrahman, K., Al-Otaibi, N., 2021. Tectonic stress regime and stress patterns from the inversion of earthquake focal mechanisms in NW Himalaya and surrounding regions. J. King Saud Univ. Sci. 33, 101351.

Allmendinger, R.W., Cardozo, N.C., Fisher, D., 2012. Structural Geology Algorithms: Vectors & Tensors. Cambridge University Press, Cambridge.

Anderson, E.M., 1905. The dynamics of faulting. Trans. Edinb. Geol. Soc. 8, 387–402.

Angelier, J., Mechler, P., 1977. Sur une méthode graphique de recherche des contraintes principales également utilisable en tectonique et en séismologie: la méthode des dièdres droits. Bull. Soc. Geol. Fr. 19, 1309–1318.

Angelier, J., Tarantola, A., Valette, B., Manoussis, S., 1982. Inversion of field data in fault tectonics to obtain the regional stress. I. Single phase fault populations: a new method of computing the stress tensor. Geophys. J. Roy. Astron. Soc. 69, 607–621.

Angelier, J., 1984. Tectonic analysis of fault slip data sets. J. Geophys. Res. 89, 5835–5848.

Angelier, J., Colletta, B., Anderson, R.E., 1985. Neogene paleostress changes in the basin and range: a case study at hoover dam, Nevada-Arizona. Geol. Soc. Am. Bull. 96, 347–361.

Angelier, J., 1990. Inversion of field data in fault tectonics to obtain the regional stress. A new rapid direct inversion method by analytical means. Geophys. J. Int. 103, 363–376. https://doi.org/10.1111/j.1365-246X.1990.tb01777.x.

Angelier, J., 1994. Fault-slip analysis and paleostress reconstruction. In: Hancock, P.L. (Ed.), Continental Deformation. Pergamon Press, Oxford, pp. 53–101.

Aranha, M., Porwal, A., Sundaralingam, M., González-Álvarez, I., Markan, A., Rao, K., 2022. Rare earth elements associated with carbonatite–alkaline complexes in western Rajasthan, India: exploration targeting at regional scale. Solid Earth 13, 497–518. https://doi.org/10.5194/se-13-497-2022.

Armijo, R., Cisternas, A., 1978. Un problème inverse en microtectonique cassante. Comptes Rendus Hebdomadaires de L'Académie des Sciences France, Série D 287, 595–598.

Arora, K., Suman, K., Dixit, M.M., Sarkar, D., 2011. Jaisalmer basin of western Rajasthan: a gravity perspective. In: Geo India: South Asian Geoscience Conference and Exhibition, 2nd. Greater Noida, New Delhi, India. 2011. http://www.apgindia.org/pdf/475.pdf.

Assie, K.R., Wang, Y., Tranos, M.D., Ma, H., Kouamelan, K.S., Brantson, E.T., Zhou, L., Ketchaya, Y.B., 2022. Late Cenozoic faulting deformation of the Fanshi Basin (northern Shanxi rift, China), inferred from palaeostress analysis of mesoscale fault-slip data. Geol. Mag. https://doi.org/10.1017/S0016756822000085.

Åse, H., Deta, G., Thomas, S., Joachim, J., Roelant, V.D.L., Jasmin, Schö, Ksienzyk, A.K., 2022. The brittle evolution of Western Norway – a space-time model based on fault mineralizations, K–Ar fault gouge dating and paleostress analysis. J. Struct. Geol. 160, 104621.

Basu, A.R., Renne, P.R., Dasgupta, D.K., Teichmann, F., Poreda, R.J., 1993. Early and late alkali igneous pulses and a high 3He plume origin for the Deccan flood basalts. Science 261, 902–906.

Beaumont, H., Clarke, S.M., Burley, S.D., Taylor, A., Gould, T., Mohapatra, P., 2015. Deciphering tectonic controls on fluvial sedimentation within the Barmer basin, India: the lower cretaceous Ghaggar- Hakra Formation. Search Discov 2015, 51100.

Beaumont, H., Clarke, S.M., Burley, S.D., Taylor, A., Mohapatra, P., 2019. Sedimentology and the facies architecture of the Ghaggar-Hakra Formation, Barmer basin, India: implications for early cretaceous deposition on the north-western Indian plate margin. Depositional Record 5, 53–83.

Bhattacharya, G.C., Yatheesh, V., 2015. Plate-Tectonic evolution of the deep ocean basins adjoining the western continental margin of India - a proposed model for the early opening scenario. In: Mukherjee, S. (Ed.), Petroleum Geosciences: Indian Contexts. Springer Geology, ISBN 978-3-319-03119-4.

Bhushan, S.K., 2000. Malani rhyolites - a review. Gondwana Res. 3, 65–77.

Biswas, S.K., 1987. Regional tectonic framework, structure and evolution of the western marginal basins of India. Tectonophysics 135, 307–327.

Biswas, S.K., 2012. Status of petroleum exploration in India. Proc. Indian Natl. Sci. Acad. Spec. Issue 78, 475–494.

Biswas, M., Gogoi, M.P., Mondal, B., Sivasankar, T., Mukherjee, S., Dasgupta, S., 2022a. Geomorphic assessment of active tectonics in Jaisalmer basin (western Rajasthan, India). Geocarto Int. https://doi.org/10.1080/10106049.2022.2066726.

Biswas, M., Puniya, M.K., Gogoi, M.P., Dasgupta, S., Mukherjee, M., Kar, N.R., 2022b. Morphotectonic analysis of petroliferous Barmer rift basin (Rajasthan, India). J. Earth Syst. Sci. 131, 140.

Biswas, T., Bose, N., Dutta, D., Mukherjee, S., 2022. Arc-parallel shears in collisional orogens: global review and paleostress analyses from the NW Lesser Himalayan Sequence (Garhwal region, Uttarakhand, India). Mar. Petrol. Geol. 138, 105530.

Bladon, A.J., Burley, S.D., Clarke, S.M., Beaumont, H., 2014. Geology and regional significance of the Sarnoo Hills, eastern rift margin of Barmer Basin, NW India. Basin Res. 27, 636–655.

Bladon, A.J., Clarke, S.M., Burley, S.D., 2015. Complex rift geometries resulting from inheritance of pre-existing structures: insights and regional implications from the Barmer Basin rift. J. Struct. Geol. 71, 136–154.

Bonini, L., Basili, R., Toscani, G., Burrato, P., Seno, S., Valensise, G., 2016. The effects of pre-existing discontinuities on the surface expression of normal faults: insights from wet-clay analogue modeling. Tectonophysics 684, 157–175.

Bonini, M., Souriot, T., Boccaletti, M., Brun, J.P., 1997. Successive orthogonal and oblique extension episodes in a rift zone: laboratory experiments with application to the Ethiopian rift. Tectonics 16, 347–362.

Bott, M.H.P., 1959. The mechanisms of oblique slip faulting. Geol. Mag. 96, 109–117.

Brun, J.P., 1999. Narrow rifts versus wide rifts: inferences for the mechanics of rifting from laboratory experiments. Philos. Trans. R. Soc. London, Ser. A 357, 695–712.

Brune, S., Autin, J., 2013. The rift to break-up evolution of the Gulf of Aden: insights from 3D numerical lithospheric-scale modelling. Tectonophysics 607, 65–79.

Brune, S., Williams, S.E., Müller, R.D., 2018. Oblique rifting: the rule, not the exception. Solid Earth 9, 1187–1206.

Burley, S.D., Gould, T., Taylor, A., Mishra, P., 2023. Syn-rift volcanism in Barmer Basin: an intra-basin extrusive complex at the northern limit of the Deccan volcanic province in India. Geol. J. 58 (3), 1256–1292.

Bubniak, I., Tranos, M.D., Andrew Bubniak, A., 2021. Paleostress reconstruction of the southeast Ukrainian outer carpathians. Int. Geol. Rev. https://doi.org/10.1080/00206814.2021.1986679.

Buck, W.R., 1986. Small-scale convection induced by passive rifting: the cause for uplift of rift shoulders. Earth Planet Sci. Lett. 77, 362–372.

Buck, W.R., 1991. Modes of continental lithospheric extension. J. Geophys. Res. Solid Earth 96 (20), 178, 161–20.

Budkewitsch, P., Robin, P.Y., 1994. Modelling the evolution of columnar joints. J. Volcanol. Geoth. Res. 59, 219–239.

Carey, E., Brunier, B., 1974. Analyse the'orique et nume'rique d'une mode'le me'chanique e'le'mentaire applique' a l'e'tude d'une population de failles. C.R. Acad. Sci., Paris. Ser. D 279, 891–894.

Cemen, I., 2023. Extensional Tectonics - Continental Breakup to Formation of Oceanic Basins. John Wiley & Sons Inc.. ISBN:9781119773740.
Chakraborty, P.P., Tandon, S.K., Saha, S., 2019. Development of Phanerozoic sedimentary basins of India. J. Asian Earth Sci. 184, 103991.
Chand, S., Subrahmanyam, C., 2013. Rifting between India and Madagascar- mechanism and isostasy. Earth Planet Sci. Lett. 210, 317–333.
Chandra, U., 1977. Earthquakes of Peninsula India–a seismotectonic study. Bull. Seismol. Soc. Am. 67, 1387–1413.
Chandrasekharam, D., Varun, C., Garg, G., Singh, H.K., Trupti, G., 2014. High heat generating granites of Siwana, Rajasthan. GRC Transactions 38, 625–628.
Chatterjee, S., Goswami, A., Scotese, C.R., 2013. The longest voyage: tectonic, magmatic, and paleoclimatic evolution of the Indian plate during its northward flight from Gondwana to Asia. Gondwana Res. 23, 238–267.
Chatterjee, R., Dutta Gupta, S., Mandal, P.P., 2017. Fracture and stress orientation from borehole image logs: a case study from Cambay basin, India. J. Geol. Soc. India 89, 573–580.
Chawade, M.P., Chandrasekaran, V., 1996. Petrology and geochemistry of anorthosite, Jiwan Singh Ki Beri, Barmer district, Rajasthan. J. Geol. Soc. India 47, 747–750.
Chouhan, A.K., Choudhury, P., Pal, S.K., 2020. New evidence for a thin crust and magmatic underplating beneath the Cambay rift basin, Western India through modelling of EIGEN-6C4 gravity data. J. Earth Syst. Sci. 129, 64.
Choudhury, T.R., Banerjee, S., 2022. Khanolkar S., the geochemical affinity of Paleogene glauconites in paleo-tethyan deposits of India. In: Armstrong-Altrin, J.S., et al. (Eds.), Geochemical Treasures and Petrogenetic Processes, pp. 22–29. https://doi.org/10.1007/978-981-19-4782-7_10.
Chung, W.Y., Gao, H., 1995. Source parameters of the Anjar earthquake of July 21, 1956, India, and its seismotectonic implications for the Kutch rift basin. Tectonophysics 242, 281–292.
Collier, J.S., Sansom, V., Ishizuka, O., Taylor, R.N., Minshull, T.N., Whitmarsh, R.B., 2008. Age of Seychelles-India break-up. Earth Planet Sci. Lett. 272, 264–277.
Compton, P.M., 2009. The geology of the Barmer Basin, Rajasthan, India, and the origins of its major oil reservoir, the Fatehgarh Formation. Petrol. Geosci. 15, 117–130.
Condie, K.C., 1982. Plate Tectonics and Continental Drifts. Pergamon Press, Oxford.
Corti, G., Bonini, M., Conticelli, S., Innocenti, F., Manetti, P., Sokoutis, D., 2003. Analogue modelling of continental extension: a review focused on the relations between the patterns of deformation and the presence of magma. Earth Sci. Rev. 63, 169–247.
Corti, G., 2008. Control of rift obliquity on the evolution and segmentation of the main Ethiopian rift. Nat. Geosci. 1, 258–262.
Corti, G., Philippon, M., Sani, F., Keir, D., Kidane, T., 2013. Stress re-orientation and pure extensional faulting at oblique rift margins: comparison between the Main Ethiopian Rift and laboratory experiments. Terra Nova 25, 396–404.
Crawford, B.R., Myers, R.D., Woronow, A., Faulkner, D.R., Rutter, E.H., 2002. Porosity-permeability relationships in clay-bearing fault gouge. In: Rock Mechanics Conference, Rep. 78214. Soc. of Petrol. Eng./Int. Soc. for Rock Mech., Dallas, Texas.
Crawford, B.R., Faulkner, D.R., Rutter, E.H., 2008. Strength, porosity, and permeability development during hydrostatic and shear loading of synthetic quartz-clay fault gouge. J. Geophys. Res. 113, B03207.
Cunha, T.A., Rasmussen, H., Villinger, H., Akinwumiju, A.A., 2021. Burial and heat flux modelling along a southern Vøring basin transect: implications for the petroleum systems and thermal regimes in the deep mid-Norwegian Sea. Geosciences 11, 190.
Dasgupta, S., Pande, P., Ganguli, D., Iqbal, Z., Sanyal, K., Venkatraman, N.V., Dasgupta, S., et al., 2000. Thar Desert and plains of Jaisalmer-Barmer area. In: Narula, P.L., Acharyya, S.K., Banerjee, J. (Eds.), Seismotectonicatlas of India and its Environs. Geol. Surv. India, Calcutta, p. 17.
Dasgupta, S.K., 1975. A revision of the mesozoic-tertiary stratigraphy of the Jaisalmer basin, Rajasthan. Indian J. Earth Sci. 2, 77–94.
Dasgupta, S., Mukherjee, S., 2016. Review on Tectonics of Barmer Rift Basin, Rajasthan, India (Abstract). Tectonic Studies Group Annual Meeting - TSG 2016, London, p. 73. https://tsg2016.wordpress.com/.
Dasgupta, S., Mukherjee, S., 2017. Brittle shear tectonics in a narrow continental rift: asymmetric non-volcanic Barmer basin (Rajasthan, India). J. Geol. 125, 561–591.
Dasgupta, S., Mukherjee, S., 2019. Remote sensing in lineament identification: examples from western India. In: Billi, A., Fagereng, A. (Eds.), Problems and Solutions in Structural Geology and Tectonics, Developments in Structural Geology and Tectonics Book Series, vol. 5. Mukherjee S. Elsevier, Series. ISBN 9780128140482, pp. 205–221. ISSN: 2542-9000.
Dasgupta, S., 2019. Implication of transfer zones in rift fault propagation: example from Cauvery basin, Indian east coast. In: Mukherjee, S. (Ed.), Tectonics and Structural Geology: Indian Context. Springer Geology. Springer, Cham. https://doi.org/10.1007/978-3-319-99341-6_10.
Dasgupta, S., 2021. A review of stratigraphy, depositional setting and paleoclimate of the different Mesozoic basins of India. In: Mesozoic Stratigraphy of India. Springer, Cham, Switzerland, pp. 1–37.
Dasgupta, S., Biswas, M., Mukherjee, S., Chatterjee, R., 2022. Structural evolution and sediment depositional system along the transform margin- Palar–Pennar basin, Indian east coast. J. Petrol. Sci. Eng. 211, 110155.
Dash, S., Konar, S., Kuila, U., Bora, A.K., Mishra, P., Mohapatra, P., 2017. Maximizing Productivity and Establishing Additional Reserves in Low Permeability Rocks through Improved Understanding of in Situ Stress State: A Case Study from Barmer Basin, Rajasthan, India. In: AAPG Technical Symposium, Hidden Potential in Mature Basins: Play Analogs and Best Practices, Indonesia. https://www.searchanddiscovery.com/pdfz/documents/2017/11033dash/dash_poster.pdf.html.
Delvaux, D., Moeys, R., Stapel, G., Petit, C., Levi, K., Miroshnichenko, A., Ruzhich, V., San'kov, V., 1997. Paleostress reconstructions and geodynamics of the Baikal region, central asia, Part 2. Cenozoic rifting, Tectonophys. 282, 1–38.
Delvaux, D., Sperner, B., 2003. Stress tensor inversion from fault kinematic indicators and focal mechanism data: the TENSOR program. In: Nieuwland, D. (Ed.), New Insights into Structural Interpretation and Modelling, vol. 212. Geological Society, London, Special Publications, pp. 75–100.
Doblas, M., 1998. Slickenside kinematic indicators. Tectonophysics 295, 187–197.
Dolson, J., Burley, S.D., Sunder, V.R., Kothari, V., Naidu, B., Whiteley, N.P., Farrimond, P., Taylor, A., Direen, N., Ananthakrishnan, B., 2015. The discovery of the Barmer Basin, Rajasthan, India, and its petroleum geology. Am. Assoc. Petrol. Geol. Bull. 99, 433–465.
Dwivedi, A.K., 2016. Petroleum exploration in India —a perspective and endeavours. Proc. Indian Natl. Sci. Acad. 82, 881–903.
Dutta, D., Biswas, T., Mukherjee, S., 2019. Arc-parallel compression in the NW Himalaya: evidence from structural and palaeostress studies of brittle deformation from the clasts of the Upper Siwalik, Uttarakhand, India. J. Earth Syst. Sci. 128, 125.
Etchecopar, A., Vasseur, G., Daignieres, M., 1981. An inverse problem in microtectonics for the determination of stress tensors from fault striation analysis. J. Struct. Geol. 3, 51–65.
Farangitakis, G., McCaffrey, K.J.W., Willingshofer, E., et al., 2021. The structural evolution of pull-apart basins in response to changes in plate motion. Basin Res. 33, 1603–1625.
Farrimond, P., Naidu, B.S., Burley, S.D., Dolson, J., Whiteley, N., Kothari, V., 2015. Geochemical characterization of oils and their source rocks in the Barmer Basin, Rajasthan, India. Petrol. Geosci. 21, 301–321.
Federico, L., Crispini, L., Vigo, A., Capponi, G., 2014. Unravelling polyphase brittle tectonics through multi-software fault-slip analysis: the case of the Voltri Unit, Western Alps (Italy). J. Struct. Geol. 68, 175–193.
Fossen, H., 2013. The role of pre-existing structures during extension of Caledonian crust and formation of the northern North Sea rift. Geol. Soc. Am. Abstr. Program 45, 522.
Fossen, H., Rotevatn, A., 2016. Fault linkage and relay structures in extensional settings – a review. Earth Sci. Rev. 154, 14–28.
Gaina, C., Müller, R.D., Brown, B., Ishihara, T., Ivanov, S., 2007. Breakup and early seafloor spreading between India and Antarctica. J Geophys. International 170, 151–170.
Gaina, C., van Hinsbergen, D.J.J., Spakman, W., 2015. Tectonic interactions between India and Arabia since the Jurassic reconstructed from marine geophysics, ophiolite geology, and seismic tomography. Tectonics 34, 875–906.
Ganerød, M., Torsvik, T.H., van Hinsbergen, D.J.J., Gaina, C., et al., 2011. Palaeoposition of the Seychelles microcontinent in relation to the deccan traps and the plume generation zone in late cretaceous-early palaeogene time. Geol. Soc. London Spec. Publ. 357, 229–252.
Gartrell, A.P., Lisk, M., 2005. Potential new method for paleostress estimationby combining three-dimensional fault restoration and fault-slip inversion techniques: first test on the Skua field, Timor Sea. In: Boult, P., Kaldi, J. (Eds.), Evaluating Fault and Cap Rock Seals: AAPG Hedberg Series, No. 2, pp. 23–36.
Gawthorpe, R.L., Hurst, J.M., 1993. Transfer zones in extensional basins: their structural style and influence on drainage development and stratigraphy. J. Geol. Soc. Lond. 150, 1137–1152.
Gephart, J.W., Forsyth, D., 1984. An improved method for determining the regional stress tensor using earthquake focal mechanism data: application to the San Fernando earthquake sequence. J. Geophys. Res. 89, 9305–9320.
Ghose, B., 1964. Geomorphological aspects of the formation of salt basins in western Rajasthan. In: Proc. Symp.Problems of Indian Arid Zone, Minist. Educ. Gov. India and UNESCO, CAZRI, Jodhpur, pp. 79–83.
Gibbons, A.D., Whittaker, J.M., Müller, R.D., 2013. The breakup of East Gondwana: assimilating constraints from Cretaceous ocean basins around India into a best-fit tectonic model. J. Geophys. Res. Solid Earth 118, 808–822.
Gibbs, A.D., 1984. Structural evolution of extensional basin margins. J. Geol. Soc. Lond. 141, 609–620.
Glorie, S., De Grave, J., Delvaux, D., Buslov, M.M., Zhimulev, F.I., Vanhaecke, F., Elburg, M.A., Van den haute, P., 2012. Tectonic history of the Irtysh shear zone (NE Kazakhstan): new constraints from zircon U/Pb dating, apatite fission track dating and palaeostress analysis. J. Asian Earth Sci. 45, 138–149.
Gombos Jr., A.M., Powell, W.G., Norton, I.O., 1995. The tectonic evolution of western India and its impact on hydrocarbon occurrences: an overview. Tectonophysics 96, 119–129.
Goswami, T., Gogoi, M., Mahanta, B.N., Mukherjee, S., Saikia, H., Shaikh, M., Kalita, P., Baral, U., Sarmah, R., 2022. Brittle tectonics in the western Arunachal frontal fold belt, India: change in stress regime from pre-collisional extension to collisional compression. Geol. J. https://doi.org/10.1002/gj.4393.
Gregory, L.C., Meert, J.G., Bingen, B., Pandit, M.K., Torsvic, T.H., 2009. Paleomagnetism and geochronology of the Malani igneous suite, NW India: implications for the configuration of Rodinia and the assembly of Gondwana. Precambrian Res. 170, 13–26.
Gudmundsson, A., Friese, N., Galindo, I., Philipp, S.L., 2008. Dike-induced reverse faulting in a graben. Geology 36, 123–126.
Heidbach, O., Rajabi, M., Reiter, K., Ziegler, M., 2016. World Stress Map 2016. GFZ Data Service.
Hossain, M.S., Ao, S., Mondal, T.K., Sen, A., Khan, M.S.H., Xiao, W., Zhang, P., 2022. Understanding the deformation structures and tectonics of the active orogenic fold-thrust belt: insights from the outer Indo-Burman ranges. Lithosphere 2022, 6058346.
Hughes, N.C., Myrow, P.M., McKenzie, N.R., Xiao, S., Banerjee, D.M., Stockli, D.F., Tang, Q., 2015. Age and implications of the phosphatic Birmania formation, Rajasthan, India. Precambrian Res. 267, 164–173.
Ikari, M.J., Saffer, D.M., Marone, C., 2009. Frictional and hydrologic properties of a major splay fault system, Nankai subduction zone. Geophys. Res. Lett. 36, L20313.

Irmak, T.S., 2013. Focal mechanisms of small-moderate earthquakes in Denizli Graben (SW Turkey). Earth Planets Space 65, 943–955.
Jani, C., Bhandari, S., Kothyari, G., Lakhote, A., Chauhan, G., Thakkar, M., 2022. Paleostress analysis and reconstruction of tectonic stress variations since Gondwana breakup in the Island Belt Fault Zone, Kutch basin, India. J. Asian Earth Sci., 105522
Ju, W., Wang, J., Fang, H., Gong, Y., Zhang, S., 2017. Paleostress reconstructions andstress regimes in the Nanchuan region of Sichuan Basin, South China: implications for hydrocarbon exploration. Geosci. J. 21, 553–564.
Kale, R.C., Ravi, K., 2022. Influence of thermal gradient and canister corrosion on the hydration of compacted Barmer bentonite. Ann. Nucl. Energy 166, 108727. https://doi.org/10.1016/j.anucene.2021.108727.
Kale, R.C., Ravi, K., 2023. Impact of iron corrosion on swell pressure of compacted Barmer bentonite induced with thermal history. Progress in Nuclear Energy 162, 104787.
Kapoor, S.P., Kapoor, A., 2016. Amalgamation of terrestrial heat flux map and sedimentary basins map will reduce the risk of exploration of hydrocarbons. Univers. J. Geosci. 4, 1–7.
Kar, N.R., Mani, D., Mukherjee, S., Dasgupta, S., Puniya, M.A., Kaushik, A.K., Biswas, M., Babu, E.V.S.S.K., 2022. Source rock properties and kerogen decomposition kinetics of Eocene shales from petroliferous Barmer basin, western Rajasthan, India. J. Nat. Gas Sci. Eng. 100, 104497.
Kaymakci, N., 2006. Kinematic development and paleostress analysis of the Denizli Basin (Western Turkey): implications of spatial variation of relative paleostress magnitudes and orientations. J. Asian Earth Sci. 27, 207–222.
Keary, P., Klepeis, K.A., Vine, F.J., 2013. Global Tectonics, third ed. Wiley Blackwell. 978-1-4051-0777-8.
Keller, E.A., Pinter, N., 2002. Active Tectonics. Earthquakes, Uplift and Landscape. Prentice Hall, New Jersey.
Kelly, M.J., Najman, Y., Mishra, P., Copley, A., Clarke, S., 2014. The potential record of far-field effects of the India-Asia collision: Barmer Basin, Rajasthan, India. In: Montomoli, C., Iaccarino, S., Groppo, C., Mosca, P., Rolfo, F., Carosi, R. (Eds.), Himalaya-Karakoram-Tibet Workshop, 29th (Lucca, Italy, 2014). Proc. J. Himal. Earth Sci. Spec., pp. 80–81
Kleinspehn, K.L., Pershing, J., Teyssier, C., 1989. Paleostress stratigraphy: a newtechnique for analyzing tectonic control on sedimentary-basin subsidence. Geology 17, 253–256.
Köküm, M., İnceöz, M., 2020. Paleostress analysis of the yeşilyurt-elazığ fault zone and its importance for the tectonic evolution, east Turkey. J. Struct. Geol. 138, 104093.
Koptev, A., Calais, E., Burov, E., Leroy, S., Gerya, T., 2015. Dual continental rift systems generated by plume-lithosphere interaction. Nat. Geosci. 8, 388–392.
Kothari, V., Naidu, B., Sunder, V.R., Dolson, J., Burley, S.D., Whiteley, N.P., Mohapatra, P., Ananthakrishnan, B., 2015. Discovery and Petroleum System of Barmer Basin. Search Discov, India, 110202, 2015.
Krishna, J., 2017. The Indian Mesozoic Chronicle - Sequence Stratigraphic Approach. Springer Geology, pp. 327–328, 978-981-10-2476-4.
Kulikowski, D., Amrouch, K., 2018. 4D modelling of fault reactivation using completepaleostress tensors from the Cooper–Eromanga Basin, Australia. Aust. J. Earth Sci. 65, 661–681.
Kumar, A., Shaikh, M.A., Singh, S., Singh, T., Mukherjee, S., Singh, S., 2022a. Active morphogenic faulting and paleostress analyses from the central Nahan Salient, NW Siwalik Himalaya. Int. J. Earth Sci. 111, 1251–1267.
Kumar, B., Verma, A.K., Bajpai, R.K., Singh, T.N., 2022b. Numerical analysis of heat dissipationthrough granite and clay in the multi-barrier system of a geological disposalfacility. Curr. Sci. 122 (No. 9), 1089–1093.
Kumar, A., 2023. Conceptualization of the recent change in groundwater quality of the shallow aquifer of the hydrocarbon-rich Barmer sedimentary basin, Rajasthan, India. Arabian Journal of Geosciences 16, 306.
Kumar, R., Hameed, A., Srivastava, P., 2023. Clay mineralogical evidence of near-equatorial Palaeocene–Eocene Thermal Maximum in Barmer Basin, India. Clay Minerals 1–22. https://doi.org/10.1180/clm.2023.19.
Kumar, N., Mann, S., Rana, S., Kumari, S., Yashpal, Ashwani, P., 2022c. Geochemistry of the neoproterozoic volcanic rocks of the nakora area of Malani igneous suite, Barmer district, western Rajasthan, India. Open J. Geol. 12, 91–110.
Kumar, N., Prakash, O., Singh, A.P., Tiwari, V.M., 2022d. Thermal Modification of the Northwest Indian Shield: as Evidenced by Integrated Geopotential Modelling. https://doi.org/10.2113/2022/8022620. Lithosphere, ID 8022620.
Lacazette, A., 2009. Paleostress analysis from image logs using pinnate joints as slip indicators. AAPG bulletin, 93(11), 1489-1501.Paleostress analysis from image logs using pinnate joints as slip indicators. AAPG (Am. Assoc. Pet. Geol.) Bull. 93, 1489–1501.
Lavier, L.L., Manatschal, G., 2006. A mechanism to thin the continental lithosphere at magma-poor margins. Nature 440, 324–328.
Lisle, R.J., 1989. Paleostress analysis from sheared dike sets. GSA Bulletin 101, 968–972.
Maheshwari, A., Sial, A.N., Mathur, S.C., 2002. Carbon isotope fluctuations through the neoproterozoic-lower cambrian Birmania basin, Rajasthan, India. Carbonates Evaporites 17, 53–59.
Mandal, A., Saha, A., Kumar, A., 2022. Structural analysis and seismic stratigraphy for delineation of Neoproterozoic-Cambrian petroleum system in central and eastern part of Bikaner–Nagaur basin, India. J. Pet. Explor. Prod. Technol. 12, 1709–1725.
Marrett, R.A., Allmendinger, R.W., 1990. Kinematic analysis of fault-slip data. J. Struct. Geol. 12, 973–986.
Maurya, D.M., Shaikh, M., Mukherjee, S., 2021. Comment on "structural attributes and paleostress analysis of quaternary landforms along the vigodi Fault (VF) in western Kachchh region. Quat. Int. 601, 143–147. https://doi.org/10.1016/j.quaint.2020.07.038. Quaternary International.
Merle, O., 2011. A simple continental rift classification. Tectonophysics 513, 88–95.
Mercier, J.L., Carey-Gailhardis, E., Sébrier, M., 1991. Palaeostress determinations from fault kinematics: application to the neotectonics of the Himalayas-Tibet and the Central Andes. Philos. Trans. R. Soc. London, Ser. A: Phys. Eng. Sci. 337, 41–52.
Mishra, D.C., 2011. Gravity and Magnetic Methods for Geological Studies: Principles, Integrated Explorations and Plate Tectonics. Hyderabad, BS, pp. 672–675.
Mishra, S., Kothyari, G.C., Dubey, R.K., Chauhan, G., 2020. Structural attributes and paleostress analysis of quaternary landforms along the vigodi Fault (VF) in western Kachchh region. Quat. Int. 599–600.
Misra, A.A., Bhattacharya, G., Mukherjee, S., Bose, N., 2014. Near N-S paleo-extension in the western Deccan region, India: does it link strike-slip tectonics with India-Seychelles rifting? Int. J. Earth Sci. 103, 1645–1680.
Misra, A.A., Mukherjee, S., 2015. Tectonic Inheritance in Continental Rifts and Passive Margins. Springerbriefs in Earth Sciences, Cham, Switzerland, ISBN 978-3-319-20576-2.
Misra, A.A., Mukherjee, S., 2017. Dyke –brittle shear relationships in the western deccan strike-slip zone around Mumbai (Maharashtra, India). In: Mukherjee, S., Misra, A.A., Calvès, G., Nemčok, M. (Eds.), Tectonics of the Deccan Large Igneous Province, vol. 445. Geological Society, London, Special Publications, pp. 269–295.
Misra, P.C., Singh, N.P., Sharma, D.C., Upadhyay, H., Kakroo, A.K., Saini, M.L., 1993. Lithostratigraphy of west Rajasthan basins. In: Oil and Natural Gas Commission Report. Keshava Deva Malaviya Institute of Petroleum Exploration, Dehradun.
Morgan, P., Baker, B.H.E., 1983. Introduction — processes of continental rifting. Tectonophysics 94, 1–10.
Morley, C.K., 1999. How successful are analogue models in addressing the influence of pre-existing fabrics on rift structure? J. Struct. Geol. 21, 1267–1274.
Morley, C.K., Gabdi, S., Seusutthiya, K., 2007. Fault superimposition and linkage resulting from stress changes during rifting: examples from 3D seismic data, Phitsanulok Basin, Thailand. J. Struct. Geol. 29, 646–663.
Morley, C.K., 2010. Stress re-orientation along zones of weak fabrics in rifts: an explanation for pure extension in 'oblique' rift segments. Earth Planet Sci. Lett. 297, 667–673.
Morley, C.K., 2016. The impact of multiple extension events, stress rotation and inherited fabrics on normal fault geometries and evolution in the Cenozoic rift basins of Thailand. In: Childs, C., Holdsworth, R.E., Jackson, C.A.-L., Manzocchi, T., Walsh, J. J., Yielding, G. (Eds.), The Geometry and Growth of Normal Faults, vol. 439. Geological Society, London, Special Publications, pp. 413–445.
Mukherjee, S., Koyi, H.A., 2010. Higher Himalayan Shear Zone, Sutlej Section: structural geology and extrusion mechanism by various combinations of simple shear, pure shear and channel flow in shifting modes. Int. J. Earth Sci. 99, 1267–1303.
Mukherjee, S., 2012. Tectonic implications and morphology of trapezoidal mica grains from the sutlej section of the higher himalayan shear zone, Indian himalaya. J. Geol. 120, 575–590.
Mukherjee, S., Mukherjee, B., Thiede, R., 2013. Geosciences of the himalaya Karakoram-tibet orogen. Int. J. Earth Sci. 102, 1757–1758.
Mukherjee, S., 2015. A review on out-of-sequence deformation in the Himalaya. In: Mukherjee, S., Carosi, R., van der Beek, P., Mukherjee, B.K., Robinson, D. (Eds.), Tectonics of the Himalaya, vol. 412. Geol. Soc. Lond. Spec. Publ, pp. 67–109.
Mukherjee, S., Dole, G., Yatheesh, V., Kale, V., 2020. Tectonics of the deccan trap: focus on Indian geoscientists' contribution in the last four years. In: Banerjee, D.M., Dasgupta, S., Jain, A.K., Bajpai, S. (Eds.), Glimpse of Geoscience Researches in India. Proceedings of the Indian National Science Academy. Coordinators, vol. 86, pp. 237–244.
Naidu, B., Burley, D.S., Dolson, J., Farrimond, P., Sunder, V., Kothari, V., Mohapatra, P., et al., 2017. Hydrocarbon generation and migration modeling in the Barmer Basin of Western Rajasthan, India: lessons for exploration in rift basins with late stage inversion, uplift and tilting. In: AbuAli, M., Moretti, I., Nordgård Bolås, H., et al. (Eds.), Petroleum Systems Analysis. Memoir: American Association of Petroleum Geologists114, pp. 61–94.
Nemčok, M., 2016. Rift and Passive Margins - Structural Architecture, Thermal Regimes, and Petroleum Systems. Cambridge University Press., New York, 9781107025837.
Nemčok, M., Lisle, R.J., 1995. A stress inversion procedure for polyphase fault/slip data sets. J. Struct. Geol. 17, 1445–1453.
Pandey, D.K., Bhadu, B., 2010. Inter-basinal correlation of Paleogene sediments of Jaisalmer and Barmer Basins, western India: an approach by sequence stratigraphy. In: 8th. Biennial International Conference and Exhibition on Petroleum Geophysics. Hyderabad, Society of Petroleum Geophysicists.
Pandey, D.K., Pandey, A., Whattam, S.A., 2019. Relict subduction initiation along a passive margin in the northwest Indian Ocean. Nat. Commun. 10, 2248.
Pandey, O.P., Agrawal, P.K., 2000. Thermal regime, hydrocarbon maturation and geodynamic events along the western margin of India since late Cretaceous. J. Geodyn. 30, 439–459.
Pandit, M.K., Shekhawat, L.S., Ferreira, V.P., Sial, A.N., Bohra, S.K., 1999. Trondhjemite and granodiorite assemblage from west of Barmer: probable basement from Malani magmatism in western India. J. Geol. Soc. India 53, 89–96.
Pareek, H.S., 1981. Petrochemistry and petrogenesis of the Malani igneous suite, India: summary. GSA Bulletin 92, 67–70.
Parsons, T., Thompson, G.A., 1993. Does magmatism influence low-angle normal faulting? Geology 21, 247–250.
Pascal, C., 2022. Paleostress Inversion Techniques – Methods and Applications for Tectonics. Elsevier, Netherlands, pp. 61–122, 978-012-811910-5.
Passchier, C.W., Trouw, R.A.J., 2005. Microtectonics. Springer, Berlin, pp. 111–158. -10 3-540-64003-7.
Petit, J.P., 1987. Criteria for the sense of movement on fault surfaces in brittle rocks. J. Struct. Geol. 9, 597–608.
Philippon, M., Willingshofer, E., Sokoutis, D., Corti, G., Sani, F., Bonini, M., Cloetingh, S., 2014. Slip re-orientation in oblique rifts. Geology 43, 147–150.

Ping, G., Liu, X., Li, M., Zhang, X., Gao, Y., Wang, S., Liu, X., 2022. Using seismic data and slip tendency to estimate paleostress: a case study from Xicaogu area of Bohai Bay basin, China. Front. Earth Sci. 10, 812874 https://doi.org/10.3389/feart.2022.812874.
Plummer, P.S., 1996. The Amirante ridge/trough complex: response to rotational transform rift/drift between Seychelles and Madagascar. Terra. Nova 8, 34–47.
Pollard, D.D., Saltzer, D., Rubin, A.M., 1993. Stress inversion methods: are they based on faulty assumptions? J. Struct. Geol. 15, 1045–1054.
Pooranchandra Rao, S.B., Singh, S.B., Prasanna Lakshmi, K.J., 2003. Palaeomagnetic dating of sankara dyke swarm in the Malani igneous suite, western Rajasthan, India. Curr. Sci. 85, 1486–1492.
Reeves, C.V., 2013. The global tectonics of the Indian Ocean and its relevance to India's western margin. J. Geophys. 34, 87–94.
Reeves, C.V., 2014. The position of Madagascar within Gondwana and its movements during Gondwana dispersal. J. Afr. Earth Sci. 94, 45–57.
Reeves, C.V., Teasdale, J.P., Mahanjane, E.S., 2016. Insight into the eastern margin of Africa from a new tectonic model of the Indian ocean. Geol. Soc. Lond. Spec. Publ. 431, 299–322.
Reeves, C.V., 2018. The development of the East African margin during Jurassic and Lower Cretaceous times: a perspective from global tectonics. Petrol. Geosci. 24, 41–56.
Roy, A.B., 2001. Neoproterozoic crustal evolution of north western Indian shield: implications on break-up and assembly of Supercontinents. Gondwana Res. 4, 289–306.
Roy, A.B., 2003. Geological and geophysical manifestations of the Réunion Plume–Indian lithosphere interactions— evidence from northwest India. Gondwana Res. 6, 487–500.
Saha, C., Konar, S., Bora, A.K., Kumar, P., Dhanasetty, A., Majumdar, P., Shankar, P., 2021. Multidisciplinary Approach in Tight Oil Appraisal: A Case Study from Barmer Basin, India, Adapted from Oral Presentation in - 2018. In: AAPG International Conference and Exhibition. https://doi.org/10.1306/11173Saha2018. Cape Town.
Scheiber, T., Viola, G., 2018. Complex bedrock fracture patterns: a multipronged approach to resolve their evolution in space and time. Tectonics 37, 1030–1062.
Scholz, C.H., 1987. Wear and gouge formation in brittle faulting. Geology 15, 493–495.
Scholz, C.H., 2002. The Mechanics of Earthquakes and Faulting, second ed. Cambridge University Press, Cambridge, pp. 97–165. 9781316681473.
Schumacher, M.E., 2002. Upper Rhine Graben: role of preexisting structures during rift evolution. Tectonics 21 (1), 1006.
Sen, S., Kundan, A., Kalpande, V., Kumar, M., 2019. The present-day state of tectonic stress in the offshore Kutch-Saurashtra Basin, India. Mar. Petrol. Geol. 102, 751–758.
Sengör, A.M.C., Burke, K., 1978. Relative timing of rifting and volcanism on Earth and its tectonic implications. Geophys. Res. Lett. 5, 419–421.
Sharma, K.K., 2005. Malani magmatism: an extensional lithospheric tectonic origin. In: Foulger, G.R., Natland, J.H., Presnall, D.C., Anderson, D.L. (Eds.), Plates, Plumes, and Paradigms, vol. 388. Geol. Soc. Am. Spec. Pap, pp. 463–476.
Sharma, K.K., 2007. K-T magmatism and basin tectonism in western Rajasthan, India: results from extensional tectonics and not from Reunion plume activity. In: Foulger, G.R., Jurdy, D.M. (Eds.), Plates, Plumes, and Planetary Processes, vol. 430. Geol. Soc. Am. Spec. Pap, pp. 775–784.
Shaikh, M.A., Maurya, D.M., Mukherjee, S., Vanik, N.P., PadmalalA, Chamyal, L.S., 2020. Tectonic evolution of the intra-uplift Vigodi-Gugriana-Khirasra-Netra Fault System in the seismically active Kachchh rift basin, India: implications for the western continental margin of the Indian plate. J. Struct. Geol. 140, 104124.
Shan, Y., Ni, Y., Liang, X., 2023. Palaeostress analysis using fault-slip data from the Xiangdong tungsten deposit in the central south China continent: evolution of intraplate stress in the Middle Mesozoic. J. Struct. Geol. 170, 104831.
Shipton, Z.K., Evans, J.P., Thompson, L.B., 2005. The geometry and thickness of deformation-band fault core and its influence on sealing characteristics of deformation-band fault zones. In: Sorkhabi, R., Tsuji, Y. (Eds.), Faults, Fluid Flow, and Petroleum Traps: AAPG Memoir 85, pp. 181–195.
Sibson, R.H., Robert, F., Poulsen, K.H., 1988. High angle reverse faults, fluid-pressure cycling, and mesothermal lgold-quartz deposits. Geology 16, 551–555.
Siddiqui, S., Soldati, M., 2014. Appraisal of active tectonics using DEM-based hypsometric integral and trend surface analysis in Emilia-Romagna Apennines, northern Italy. Turk. J. Earth Sci. 23, 277–292.
Simón, J.L., 2019. Forty years of paleostress analysis: has it attained maturity? J. Struct. Geol. 125, 124–133.
Singh, A.K., Tewari, P.K., 2011. Infracambrian hydrocarbon systems and emerging hydrocarbon potential in Bikaner-Nagaur and Jaisalmer basins (Miajlarsub-basin), Rajasthan, India. In: Geo India: South Asian Geoscience Conference and Exhibition, 10324, 2nd (Greater Noida, New Delhi, India, 2011). Search Discov. 2011.
Singh, H.K., Garg, G.C., Chandrasekharam, D., Trupti, G., Singh, B., 2014. Physicochemical evolution of the thermal springs over the Siwana Ring Complex, western Rajasthan. J. Geol. Soc. India 84, 668–674.
Singh, P.K., Rajak, P.K., Singh, M.P., Singh, V.K., Naik, A.S., Singh, A.K., 2016. Peat swamps at Giral lignite field of Barmer basin, Rajasthan, Western India: understanding the evolution through petrological modelling. Int. J. Coal Sci. Technol. 3, 148–164.
Singh, S., Ghosh, A., 2019. Surfacemotions and continental deformation in the Indian plate and the India-Eurasia collision zone. J. Geophys. Res. Solid Earth 124, 12141–12170.
Singh, V.P., Singh, B.D., Mathews, R.P., Singh, A., Mendhe, V.A., Mishra, S., Banerjee, M., 2022. Paleodepositional and hydrocarbon source-rock characteristics of the sonari succession (Paleocene), Barmer basin, NW India: implications from petrography and geochemistry. Nat. Resour. Res. https://doi.org/10.1007/s11053-022-10079-y.
Sinha, D.K., 2022. Reappraisal of 75 Years of exploration for atomic minerals in India and the way forward. J. Geol. Soc. India 98, 1029–1041. https://doi.org/10.1007/s12594-022-2121-z.
Sippel, J., Saintot, A., Heeremans, M., Scheck-Wenderoth, M., 2010. Paleostress field reconstruction in the Oslo region. Mar. Petrol. Geol. 27, 682–708.
Sisodia, M.S., Singh, U.K., Lashkari, G., Shukla, P.N., Shukla, A.D., Bhandari, N., 2005. Mineralogy and trace element chemistry of the Siliceous Earth of Barmer basin, Rajasthan: evidence for a volcanic origin. J. Earth Syst. Sci. 114 (No. 2), 111–124.
Sisodia, M.S., 2011. Malanirhyolite: highly eroded complex crater. Curr. Sci. 101, 946–951.
Smith, W.H.F., Sandwell, D., 1997. Measured and Estimated Seafloor Topography (Version 4.2), vol. 1. World Data Center A for Marine Geology and Geophysics research publicationRP poster 34" x 53.
Storey, M., Mahoney, J.J., Saunders, A.D., Duncan, R.A., Kelley, S.P., Coffin, M.F., 1995. Timing of hot-spot related volcanism and the breakup of Madagascar and India. Science 267, 852–855.
Srivastava, P., Kumar, S., Pal, T.K., Bajpai, R.K., Kaushik, C.P., 2022. Swelling clay based buffer component of engineered barrier system of waste disposal facilities. Deep Geol. Disposal, BARC Newsletter (380), 79–81.
Strahler, A.N., 1952. Hypsometric (area-altitude) analysis of erosional topography. Geol. Soc. Am. Bull. 63, 1117–1142.
Styron, R., Pagani, M., 2020. The GEM global active faults database. Earthq. Spectra 36 (S1), 160–180.
Thybo, H., Nielsen, C.A., 2009. Magma-compensated crustal thinning in continental rift zones. Nature 457, 873–876.
Tibaldi, A., Bonali, F.L., PasquaréMariotto, F., Corti, N., Russo, E., Einarsson, P., Hjartardóttir, Á.R., 2020. Rifting kinematics produced by magmatic and tectonic stresses in the north volcanic zone of Iceland. Front. Earth Sci. 8, 174.
Titus, S.J., Fossen, H., Pedersen, R.B., Vigneresse, J.L., Tikoff, B., 2002. Pull-apart formation and strike-slip partitioning in an obliquely divergent setting, Leka Ophiolite, Norway. Tectonophysics 354, 101–119.
Torsvik, T.H., Carter, L.M., Ashwal, L.D., Bhushan, S.K., Pandit, M.K., Jamtveit, B., 2001. Rodinia redefined or obscured: palaeomagnetism of the Malani igneous suite (NW India). Precambrian Res. 108, 319–333.
Torsvik, T.H., Amundsen, H., Hartz, E.H., Corfu, F., Kusznir, N., Gaina, C., Doubrovine, P. V., Steinberger, B., Ashwal, L.D., Jamtveit, B., 2013. A precambrian microcontinent in the Indian ocean. Nat. Geosci. 6, 223–227.
Tripathy, V., Saha, D., 2013. Plate margin paleostress variations and intracontinental deformationsin the evolution of the Cuddapah basin through Proterozoic. Precambrian Res. 235, 107–130.
Torabi, A., Johannessen, M.U., Ellingsen, T.S.S., 2019. Fault core thickness: insights from siliciclastic and carbonate rocks. Geofluids, 2918673.
Turcotte, D.L., Emerman, S.H., 1983. Mechanisms of active and passive rifting. In: Morgan, P., Baker, B.H. (Eds.), Processes of Continental Rifting, vol. 19. Tectonophysics, pp. 39–50.
URL-1: https://www.dghindia.gov.in/(Accessed on 2-April-2022).
URL-2: https://www.worldofchemicals.com/media/cairn-oil-gas-baker-hughes-to-produce-geothermal-energy-in-rajasthan-india/7751.html (Accessed on 4-April-2023).
URL-3:Bureau Gravimétrique International (BGI)/International Association of Geodesy: http://bgi.omp.obs-mip.fr/data-products/Gravity-Databases/Land-Gravity-data (Accessed on 9-November-2021).
URL-4. https://www.sciencephoto.com/media/159933/view/indian-ocean-topographical-map. (Accessed 4 May 2022).
van Hinsbergen, D.J.J., Lippert, P.C., Dupont-Nivet, G., McQuarrie, N., Doubrovine, P.V., Spakman, W., Torsvik, T.H., 2012. Greater India basin hypothesis and a two-stage cenozoic collision between India and asia. Proc. Natl. Acad. Sci. USA 109, 7659–7664.
van Hinsbergen, D.J.J., Steinberger, B., Cuilmette, C., et al., 2021. A record of plume – induced plate rotation triggering subduction initiation. Nat. Geosci. 14, 626–630.
Vanik, N., Shaikh, M.A., Mukherjee, S., Maurya, D.M., Chamyal, L.S., 2018. Post-Deccan Trap stress reorientation under transpression: evidence from fault-slip analysis from SW Saurashtra, Western India. J. Geodyn. 121, 9–19.
van der Zee, W., Urai, J.L., 2005. Processes ofnormal fault evolution in a siliciclastic sequence: a case study from Miri, Sarawak, Malaysia. J. Struct. Geol. 27, 2281–2300.
van der Zee, W., Wibberley, C.A.J., Urai, J., 2008. The influence of layering and pre-existing joints on the development of internal structure in normal fault zones: the Lodeve basin, France. In: Wibberley, C.A.J., Kurz, W., Imber, J., Holdsworth, R.E., Collettini, C. (Eds.), The Internal Structure of Fault Zones: Implications for Mechanical and Fluid-Flow Properties, vol. 299. The Geological Society of London, pp. 57–74.
van Wijk, J.W., van der Meer, R., Cloetingh, S.A.P.L., 2004. Crustal thickening in an extensional regime: application to the mid-Norwegian Vøring margin. Tectonophysics 387, 217–228.
Vijayan, A., Sheth, H., Sharma, K.K., 2015. Tectonic significance of dykes in the Sarnu-Dandali alkaline complex, Rajasthan, northwestern Deccan Traps. Geosci. Front. 7, 783–791.
Wallace, R.E., 1951. Geometry of shearing stress and relation to faulting. J. Geol. 59, 118–130.
Wang, W., Spencer, C., Pandit, M.K., Wu, Y.-B., Zhao, J.-H., Zheng, J.-P., Xia, X.-P., Lu, G.-M., 2023. Crustal evolution and tectonomagmatic history of the Indian Shield at the periphery of supercontinents. Geochem. Cosmochim. Acta 341, 90–104.
Watts, A.B., 2001. Isostasy and the origin of geological features in the continents and oceans. In: Isostasy and Flexure of the Lithosphere. Cambridge University Press, New York, ISBN 0 521 62272 7, pp. 285–300.
Whitney, D.L., Teyssier, C., Rey, P., Buck, W.R., 2013. Continental and oceanic core complexes. Geol. Soc. Am. Bull. 125, 273–298.

Withjack, M.O., Jamison, W.R., 1986. Deformation produced by oblique rifting. Tectonophysics 126, 99–124.
Withjack, M.O., Schlische, R.W., Olsen, P.E., 1998. Diachronous rifting, drifting, and inversion on the passive margin of central eastern North America: an analog for other passive margins. Am. Assoc. Petrol. Geol. Bull. 82, 817–835.
Wright, T.J., Ayele, A., Ferguson, D., Kidane, T., Vye-Brown, C., 2016. Magmatic rifting and active volcanism: introduction. In: Wright, T.J., Ayele, A., Ferguson, D.J., Kidane, T., Vye-Brown, C. (Eds.), Magmatic Rifting and Active Volcanism, vol. 420. Geol. Soc. Lond. Spec. Publ., pp. 1–9
Yamaji, A., 2003. Are the solutions of stress inversion correct? Visualization of their reliability and the separation of stresses from heterogeneous fault-slip data. J. Struct. Geol. 25, 241–252.
Yamaji, A., Tomita, S., Otsubo, M., 2005. Bedding tilt test for paleostress analysis. J. Struct. Geol. 27, 161–170.
Yamaji, A., Otsubo, M., Sato, K., 2006. Paleostress analysis using the Hough transform for separating stresses from heterogeneous fault-slip data. J. Struct. Geol. 28, 980–990.
Yamaji, A., Sato, K., Tonai, S., 2010. Stochastic modeling for the stress inversion of vein orientations: paleostress analysis of Pliocene epithermal veins in southwestern Kyushu, Japan. J. Struct. Geol. 32, 1137–1146.
Yatheesh, V., 2019. Structure and Tectonics of the Continental Margins of India and the Adjacent Deep Ocean Basins: Current Status of Knowledge and Some Unresolved Problems. IUGS, pp. 586–608.
Yin, A., Taylor, M.H., 2008. Non-Andersonian conjugate strike-slip faults: observations, theory, and tectonic implications. IOP Conf. Ser. Earth Environ. Sci. 2, 012026.
Yin, Z.M., Ranalli, G., 1992. Critical stress difference, fault orientation and slip direction in anisotropic rocks under non-Andersonian stress systems. J. Struct. Geol. 237–244.
Zain Eldeen, U., Delvaux, D., Jacobs, P., 2002. Tectonic Evolution in the Wadi Araba Segment of the Dead Sea Rift, South-West Jordan, vol. 2. EGU Stephan Mueller Special Publication Series, pp. 1–19.
Žalohar, J., Vrabec, M., 2007. Paleostress analysis of heterogeneous fault-slip data: the Gauss method. J. Struct. Geol. 29, 1798–1810.
Žalohar, J., 2018. The Ω-Theory: the New Physics of Earthquakes. Elsevier, Amsterdam.
Ziegler, P.A., Cloetingh, S., 2004. Dynamic processes controlling evolution of rifted basins. Earth Sci. Rev. 64, 1–50.